

---

Theses and Dissertations

---

Fall 2011

# Studies on the mechanisms of solid state and solution instability of drugs

Zhixin Zong  
*University of Iowa*

Copyright 2011 Zhixin Zong

This dissertation is available at Iowa Research Online: <http://ir.uiowa.edu/etd/2795>

---

## Recommended Citation

Zong, Zhixin. "Studies on the mechanisms of solid state and solution instability of drugs." PhD (Doctor of Philosophy) thesis, University of Iowa, 2011.  
<http://ir.uiowa.edu/etd/2795>.

---

Follow this and additional works at: <http://ir.uiowa.edu/etd>

 Part of the [Pharmacy and Pharmaceutical Sciences Commons](#)

STUDIES ON THE MECHANISMS OF SOLID STATE AND SOLUTION  
INSTABILITY OF DRUGS

by  
Zhixin Zong

An Abstract

Of a thesis submitted in partial fulfillment  
of the requirements for the Doctor of  
Philosophy degree in Pharmacy  
in the Graduate College of  
The University of Iowa

December 2011

Thesis Supervisor: Professor Lee E. Kirsch

## ABSTRACT

The overarching objective of this thesis is to demonstrate a systematic approach for addressing the instability issues associated with low limit degradants by developing quantitative degradation models that incorporate key instability determinants into predictive equations.

Chlorhexidine was used as model compound in aqueous solution to demonstrate the application of the predictive models to issues of formulation design and manufacturing. Chlorhexidine degrades to p-chloroaniline, a well-established toxicant, by various pH-dependent pathways. In acidic conditions, the direct formation of p-chloroaniline from chlorhexidine is the major pathway whereas the indirect formation of p-chloroaniline via p-chlorophenylurea is the main alkaline pathway. Rate laws and mechanisms for each pathway were presented. Shelf life predictions equations for chlorhexidine formulations were derived based on the kinetics of p-chloroaniline appearance as a function of formulation strength, solution pH, bulk chlorhexidine purity and storage temperature. The pH range for optimal shelf-life was 5.0 to 5.5. Simple extraction procedures used during formulation preparation were identified to improve bulk chlorhexidine purity and thereby extend product shelf-life.

Gabapentin degrades directly to gabapentin-lactam in the solid-state. The established limit on gabapentin-lactam in gabapentin pharmaceutical formulations is <0.5% w/w thus gabapentin instability was studied as a model compound for solid state formulation applications. Mechanical stress associated with drug product manufacturing in unit operations such as milling increased the subsequent lactamization rate upon storage due to increased gabapentin crystal disorder. The effect of environment moisture was to decrease the rate of gabapentin-lactam formation due to competitive recovery of gabapentin crystallinity which was accelerated by humidity. A degradation model that combined both physical and chemical instability pathways including autocatalytic

branching, spontaneous intra-molecular cyclization and moisture-induced physical transformation steps was shown to be consistent with lactamization kinetics as a function of both environmental (temperature and humidity) and manufacturing-related effects. This kinetic model was used to predict the shelf-life of gabapentin tablets prepared under various exemplary manufacturing conditions thereby demonstrating the ability of the model to link manufacturing variation and shelf-life stability in for solid-state drug formulations.

Abstract Approved: \_\_\_\_\_  
Thesis Supervisor  
\_\_\_\_\_  
Title and Department  
\_\_\_\_\_  
Date

STUDIES ON THE MECHANISMS OF SOLID STATE AND SOLUTION  
INSTABILITY OF DRUGS

by  
Zhixin Zong

A thesis submitted in partial fulfillment  
of the requirements for the Doctor of  
Philosophy degree in Pharmacy  
in the Graduate College of  
The University of Iowa

December 2011

Thesis Supervisor: Professor Lee E. Kirsch

Copyright by  
ZHIXIN ZONG  
2011  
All Rights Reserved

Graduate College  
The University of Iowa  
Iowa City, Iowa

CERTIFICATE OF APPROVAL

PH.D. THESIS

This is to certify that the Ph.D. thesis of

Zhixin Zong

has been approved by the Examining Committee  
for the thesis requirement for the Doctor of Philosophy  
degree in Pharmacy at the December 2011 graduation.

Thesis Committee: \_\_\_\_\_  
Lee E. Kirsch, Thesis Supervisor

\_\_\_\_\_  
Douglas R. Flanagan

\_\_\_\_\_  
Mickey L. Wells

\_\_\_\_\_  
Aliasger K. Salem

\_\_\_\_\_  
Lei Geng

## ACKNOWLEDGMENTS

I wish to sincerely thank Professor Lee E. Kirsch for his wise and thoughtful support and guidance, his tolerance. He is the finest teacher I have known.

I have learned much from the pharmaceuticals faculty, staff. In particular, I appreciate Dr Flanagan, Dr Wells, Dr Salem, Dr Geng for serving on my thesis committee. Sincere thanks to Dr Wurster and Dr Donovan for serving on my comprehensive exam.

I thank all my labmates, classmates and friends, Lairi, Madhu, Salil, Jiang, Radaduen, Hoa, Greg, Hefei, Dong, Dongmei, Yi and too many names to mention.

I thank my family and friends for their support.

I'm grateful to the National Institute for Pharmaceutical Technology and Education (NIPTE) and the U.S. Food and Drug Administration (FDA) for providing funds for part of my research.



## TABLE OF CONTENTS

LIST OF TABLES .....	v
LIST OF FIGURES .....	vi
CHAPTER	
I INTRODUCTION .....	1
II KINETICS AND MECHANISMS OF CHLORHEXIDINE HYDROLYSIS .....	6
Introduction.....	6
Materials and Methods .....	7
Materials .....	7
Stability-indicating Assay Development .....	7
Kinetics of CHD Hydrolysis .....	8
Effect of pH and Buffers .....	9
Model Fitting.....	9
Results and Discussion .....	10
Identification of Degradation Products .....	10
Degradation Scheme in Acidic Conditions .....	12
Degradation Scheme in Alkaline Conditions .....	14
Effect of pH .....	15
Proposed Mechanisms .....	17
Conclusion .....	18
III EFFECTS OF CHLORHEXIDINE FORMULATION AND PREPARATION ON SHELF-LIFE .....	38
Introduction.....	38
Materials and Methods .....	39
Materials .....	39
Stability-indicating Assay Method .....	40
Preparation of Test Formulations .....	40
Evaluation and Purification of Bulk CHD Solutions .....	41
Results.....	41
Discussion.....	42
Development of a PCA Prediction Model.....	42
Model Validation.....	46
Assessment of Factors Affecting Formulation Stability .....	46
Purification of CHD Bulk Solution .....	47
Conclusion .....	48
IV THE STABILIZING EFFECT OF MOISTURE ON THE SOLID- STATE DEGRADATION OF GABAPENTIN .....	59
Introduction.....	59
Materials and Methods .....	61
Chromatographic Methods .....	62
Surface Area Measurement .....	63

	TGA and DSC .....	63
	Powder X-ray Diffraction.....	63
	Solid-state NMR.....	64
	Solid State Degradation.....	64
	Solution Degradation.....	65
	Results.....	65
	Discussion.....	67
	Effects of Milling .....	68
	Effects of Moisture.....	69
	Conclusion.....	71
V	KINETIC MODEL FOR SOLID-STATE DEGRADATION OF GABAPENTIN.....	84
	Introduction.....	84
	Materials and Methods .....	85
	X-Ray Powder Diffraction .....	86
	Chromatographic Methods.....	86
	Milling Stress.....	86
	Degradation Kinetics .....	87
	Long-term Stability Studies.....	87
	Results.....	88
	Discussion.....	90
	Model Development.....	90
	Gabapentin Degradation Kinetics.....	93
	Quantitative Effect of Milling Duration on Lactamization Kinetics.....	94
	Quantitative Effect of Temperature on Lactamization Kinetics.....	94
	Quantitative Effect of Humidity on Lactamization Kinetics.....	95
	Validation of Model .....	96
	Conclusion.....	97
	APPENDIX	
A	WINNONLIN MODEL FOR CHD ACIDIC HYDROLYSIS .....	107
B	WINNONLIN MODEL FOR CHD ALKALINE HYDROLYSIS.....	110
C	WINNONLIN MODEL USED TO ESTIMATE EFFECT OF MILLING ON GABA LACTAMIZATION .....	112
	REFERENCES .....	115

## LIST OF TABLES

Table II-1.	CHD and hydrolysis intermediates and products.....	19
Table II-2.	Reaction conditions and estimated rate constants (90.0 °C) for acidic CHD degradation pathways.....	20
Table II-3.	Reaction conditions and estimated rate constants (90.0 °C) for neutral and alkaline CHD degradation pathways.....	21
Table III-1.	PCA levels in 20% CHD digluconate solutions from various sources.....	49
Table III-2.	CHD recovery and PCA removal after exposure to adsorptive materials.....	50
Table IV-1.	The accuracy of HPLC method.....	73
Table IV-2.	Specific surface area, initial gaba-L concentration and lactamization rate.....	74
Table IV-3.	Gaba-L recovery in saturated salt solutions.....	75

## LIST OF FIGURES

Figure II-1.	Possible CHD degradation products resulting from formation and breakdown of hydrolytic tetrahedral intermediate.....	22
Figure II-2.	Representative HPLC chromatogram of a synthetic mixture of CHD and possible degradation products.....	23
Figure II-3.	Representative chromatogram of CHD reaction mixture in acidic conditions (pH 1.0, 90.0 °C, 5 hours).....	24
Figure II-4.	Representative chromatogram of CHD reaction mixture in alkaline conditions (pH 8.6, 90.0 °C, 24 hours).....	25
Figure II-5.	Concentration time profiles of CHD and its degradation products under acidic conditions (pH 1.0, 90.0 °C) .....	26
Figure II-6.	Proposed CHD degradation scheme in acidic conditions.....	27
Figure II-7.	Concentration time profiles for CHD and degradation intermediates under acidic conditions (pH 1.0, 90.0 °C).. .....	28
Figure II-8.	Proposed CHD degradation scheme in alkaline conditions.....	29
Figure II-9.	Typical concentration time profiles of CHD degradation under alkaline conditions (pH 8.1, 90.0 °C) .....	30
Figure II-10.	Typical concentration time profiles of PCPU degradation under alkaline conditions (pH 8.1, 90.0°C).. .....	31
Figure II-11.	PH rate profiles for rate constants ( $k_A$ , $k_D$ and $k_E$ ) estimated from concentration time profiles obtained under acidic conditions. ....	32
Figure II-12.	PH rate profiles for rate constants ( $k_B$ , $k_F$ ) estimated from concentration time profiles obtained under alkaline conditions. ....	33
Figure II-13.	Proposed mechanisms for the hydrolytic formation of PCA/PBG-AU (pathway A) and NH <sub>3</sub> /PBG-APU (pathway D) under acidic conditions.....	34
Figure II-14.	Proposed mechanism for the hydrolytic formation of PCA/PBG-CA from APU moiety (pathway E) under acidic conditions.....	35
Figure II-15.	Proposed mechanism for the hydrolytic formation of PCPU/PBG-G (pathway B) under alkaline conditions. ....	36
Figure II-16.	Proposed mechanism for the hydrolytic formation of PCA from PCPU (pathway F) under alkaline conditions.....	37
Figure III-1.	Simplified PCA formation scheme in acidic CHD solutions.....	51
Figure III-2.	Simplified PCA formation scheme in alkaline CHD solutions. ....	52

Figure III-3.	Representative concentration time profiles in acidic conditions at 70°C, 80°C and 90 °C.....	53
Figure III-4.	Representative concentration time profiles in alkaline condition at 70°C, 80°C and 90 °C.....	54
Figure III-5.	PCA appearance in 1.0% CHD formulations (pH 5.9) at 25°C and 40 °C.....	55
Figure III-6.	Correlation between formation of PCA and loss of CHD in acidic and alkaline conditions at 70°C, 80°C, and 90 °C.....	56
Figure III-7.	Predicted critical PCA formation time from CHD digluconate solutions as function of pH at 25°C.....	57
Figure III-8.	Predicted critical PCA formation time (T <sub>c</sub> ) for CHD digluconate solution as function of formulation strength at pH 5.2 and 25°C.....	58
Figure IV-1.	Lactamization of gabapentin.....	76
Figure IV-2.	Representative HPLC chromatograms showing peaks for gabapentin and gaba-L.....	77
Figure IV-3.	XRD patterns of unmilled and milled gabapentin samples.....	78
Figure IV-4.	Solid State NMR spectrum of unmilled and milled gabapentin samples.....	79
Figure IV-5.	Gaba-L formation from 60 minutes milled gabapentin sample at 50 °C and different relative humidity.....	80
Figure IV-6.	Lactamization rate (mole%/day at 5%RH and 50 °C) for gabapentin samples as a function of the measured specific surface area.....	81
Figure IV-7.	XRD patterns of moisture treated milled gabapentin sample and gabapentin monohydrate.....	82
Figure IV-8.	Gaba-L formation from moisture pretreated gabapentin sample.....	83
Figure V-1.	Typical gaba-L formation time profile from mechanically-stressed gabapentin Form II sample (60 min milled at speed setting 5) stored at 40 °C and 5%RH.....	98
Figure V-2.	Proposed solid-state gabapentin degradation model.....	99
Figure V-3.	Effects of milling duration on gaba-L formation.....	100
Figure V-4.	Gaba-L formation from milled gabapentin samples (60 min at speed setting 5) stored at various relative humidity and 40 °C.....	101
Figure V-5.	XRD patterns of milled gabapentin sample (60 min at speed setting 7) stored at 25°C and various RH.....	102

Figure V-6.	Gaba-L formation from milled gabapentin samples (60 min at speed setting 5) stored at 5%RH and various temperatures.....	103
Figure V-7.	Gaba-L formation and prediction based on different models .....	104
Figure V-8.	Arrhenius plots for the estimated rate constants .....	105
Figure V-9.	Observed and predicted long term gaba-L formation from gabapentin tablets.....	106

## CHAPTER I

### INTRODUCTION

Drug product performance is determined by critical quality attributes such as stability, safety, bioavailability, and product utility which, in turn, are dependent on the underlying physical chemical, biophysical and biochemical properties of the drug and the product components such as solubility, particle size and distribution, surface properties, purity, partition coefficient, permeability, propensity to undergo chemical and physical transitions, etc.

Stability is the ability of product and its components to resist physical, chemical and biological properties changes due to time-dependent and environmental stresses. The chemical and physical stabilities of the active pharmaceutical ingredient (API) are important and sometimes critical product quality issues. The chemical changes of API, the changes in physical state or form of API and other performance attributes of drug product (e.g. dissolution, particulate changes, surface changes) can significant impact product efficacy and safety.

In terms of chemical instability, loss of API potency is frequently the focus of product quality considerations. Historically the loss of 5 percent label potency would be considered significant quality change by regulatory agencies(1) and the time that elapses for the drug potency drops to 95 percent at storage conditions might be the main factor used to determine the shelf life. However if the drug degrades to toxic degradant, the accumulation of this degradant in pharmaceutical product may supplant API potency loss as a critical instability criteria. In these situations, the stability limit may be much lower than the typical potency limit of the API.(1) Two examples of APIs with potential toxic degradation products that limit their shelf-life are the subject of this thesis: namely chlorhexidine which degrades to p-chloroaniline and gabapentin which degrades to gabapentin-lactam.

In general, drug substances (and other formulation components) are susceptible to various chemical degradation pathways including but not limited to hydrolysis, oxidation, photo-degradation, interactions with excipients and packaging materials. Identification and a thorough understanding of the chemistry of important degradation pathways is essential for predicting chemical instability, defining optimized storage conditions, designing and optimizing drug products and processes and establishing pharmaceutical product quality assurance.

The physical instability of the API during manufacturing of the drug substance, drug product and during storage is also an important factor that may affect the biopharmaceutical and pharmaceutical properties of the drug product and ultimately product quality. For example, the physical state of a drug substance may dissolution which, in turn, may affect the bioavailability of the product. In addition, the physical state of the API may influence its susceptibility to covalent changes associated with chemical stability. For example, amorphous drug substances are typically more prone to chemical instability than crystalline form. Physical changes can be induced by many factors such as mechanical impact, temperature changes, and environmental moisture levels.

To study the stability of a drug product, it is necessary to develop a stability-indicating assay which is capable of distinguishing and quantifying the API in the presence of degradants, process impurities, excipients or other potential impurities, and can quantitatively detect the changes of the active ingredient with time. (1, 2) The limit of toxic degradant is generally very low, therefore development of an assay method that is capable of separating the degradant from parent drug and detecting low level of impurities quantitatively can be a challenge.

Frequently stability-related measurements are also critical for understanding and controlling product quality. For example, chemical instability may be related to exposure to water, reactive gases such as oxygen, or specific environment conditions such as pH. Thus design of measurement methods and the development of control specifications on



such properties as residual moisture, headspace gas content or pH may all be essential for establishing product quality.

Since the physical state or form of the API may be related to its susceptibility to chemical (covalent) changes, measurements for physical state properties of API may be useful in predicting and controlling chemical instability.

The determination of degradation scheme and kinetics is essential for rational design of pharmaceutical product and its manufacturing processes. However, defining the degradation pathways and rate laws can be challenging for drugs with low limit of degradants. At shelf-life condition, degradation kinetics may be relatively slow wherein limit level of critical degradant accumulates over months. To study these phenomena in a useful and timely way requires experimentation utilizing accelerated conditions, for example severe exposure to temperature, pH extremes, mechanical stress, light, oxidizing or other reactive contaminants, reactive gases (oxygen or water), etc. Moreover at low degradant level, the concentrations of reaction intermediates may be even lower, thereby further challenge in analytical methods both in terms of intermediate detection and identification.

For our studies, we have selected two model compounds that are currently used therapeutically and are known to be chemically unstable wherein a critical quality attribute is the appearance of low levels of a toxic degradant. The two model compounds are chlorhexidine and gabapentin. Chlorhexidine is typically used in aqueous solution and/or semisolid formulation and its shelf-life is limited by the appearance of 3 ppm of p-chloroaniline. Gabapentin is typically formulated as an oral solid dosage form and its shelf-life is limited by 0.4% of gabapentin-lactam.

The overarching objective of our studies was to demonstrate a systematic approach for addressing the instability issues associated with low limit degradants by developing quantitative degradation models that incorporate key instability determinants into predictive equations. In the case of chlorhexidine, we sought to demonstrate the

application of the predictive model to issues of formulation design and manufacturing. In the case of gabapentin, the degradation model was used to establish a link between manufacturing-related variables and chemical instability during storage.

To pursue our chlorhexidine research objective we sought to develop and apply a fundamental understand of the aqueous degradation pathways and kinetics of aqueous chlorhexidine solutions and to apply that understanding to issues associated with formulation design and preparation.

In Chapter II we present studies which describe the acid and alkaline chlorhexidine degradation schemes, pH-dependent rate laws for each degradation pathway and propose reasonable mechanisms of degradation. In Chapter III we apply this understanding to practical formulation design issues that impact shelf-life based on a simplified model for the appearance of p-chloroaniline under initial conditions. We also address temperature effects and present possible approaches to improving drug substance quality as a part of formulation preparation.

The overall objectives of our gabapentin studies used to investigate the role of manufacturing-related mechanical stress on the solid state chemical instability. These investigations were undertaken by developing degradation models that combined both physical and chemical instability pathways and incorporated environmental and manufacturing-related effect into the rate laws for individual steps in the combined physical/chemical degradation scheme and into the initial degradation conditions. Our research was part of a multi-institutional project sponsored by the National Institute for Pharmaceutical Technology and Education that attempted to demonstrate methods for evaluating stability considerations into pharmaceutical product development using Quality by Design (QbD) as defined in FDA guidance Q8, 9, 10, and 11.

Quality by Design (QbD) is “A systematic approach to development that begins with predefined objectives and emphasizes product and process understanding and process control, based on sound science and quality risk management”(3) Implement of

QbD offers the possibility of improving product quality through science and technology. The current practice of pharmaceutical manufacturing is achieving quality by inspection. QbD will help to build quality into design. A thorough understanding of the degradation mechanism and the relationship between stability and material attributes and process parameters can be used to define in design space models that correlate to the stability considerations, and it is essential part of pharmaceutical quality assurance, helps build quality early in development.

In Chapter IV, we present evidence that mechanical stress induces physical changes that result in increased rates of gabapentin-lactam formation. The effect of environment moisture was to decrease the rate of gabapentin-lactam formation. We present evidence that this phenomenon was attributable to a competitive stabilizing physical transformation of mechanically stressed gabapentin.

In Chapter V, we build a complete quantitative solid-state degradation model for gabapentin-lactam formation that incorporates both the effects of mechanical stress and the effects of storage temperature and moisture on degradation kinetics and demonstrate the utility of this model in predicting shelf-life in gabapentin tablets that were prepared under conditions of variable manufacturing stress.

## CHAPTER II

### KINETICS AND MECHANISMS OF CHLORHEXIDINE HYDROLYSIS

#### Introduction

Chlorhexidine (CHD) is a cationic bisbiguanide with germicidal activity against bacteria, yeasts, and molds. The combination of high level of antibacterial activity, low mammalian toxicity, and a strong affinity for binding to skin and mucous membranes renders CHD as potentially useful anti-infective agent especially in the treatment of severe caries and ophthalmic infections.(4, 5)

The stability of CHD is limited by the appearance of its primary degradation product p-chloroaniline (PCA). All chloroaniline isomers are hematotoxic, but PCA possesses additional toxicities. PCA is rapidly absorbed and metabolized, and the reactive metabolites of PCA bind covalently to hemoglobin and liver and kidney proteins. PCA has demonstrated nephro- and hepato- toxicity.(6) PCA is also carcinogenic and has been associated with the induction of unusual and rare cancers.(7, 8) PCA is possibly genotoxic.(9) Because of its toxicity, the USP limit for the level PCA in CHD mouth rinse is less than 3 ppm.(10) This limit restricts the safe use of CHD especially in products containing high CHD concentrations.

Because the usefulness of CHD is limited by its hydrolytic degradation, a thorough understanding of the degradation pathways, rate laws and mechanisms is essential for rational product design development and manufacture. The studies presented herein attempt to provide that understanding. This chapter presents a detailed description of the kinetic and mechanisms of CHD hydrolysis. Chapter III will apply this understanding to predict the effects of formulation design on shelf-life storage; in addition we describe an approach to improve shelf-life by modification of formulation preparation.

The instability of CHD in autoclaving (11) and antacid suspensions (12) has been reported. A possible degradation scheme for CHD hydrolysis has been proposed to involve the direct formation of PCA (13) (pathway A in Figure II-1) and the parallel formation of (p-chlorophenyl)urea (PCPU) or (p-chlorophenyl)guanidine (PCPG), followed by the sequential hydrolysis of these intermediates to PCA (14) (pathways B and C in Figure II-1). The hydrolysis of CHD was reported to most likely to proceed via pathways B and C, instead of the direct formation of PCA from CHD.(14) The kinetics and mechanisms of degradation have not been reported. In addition, the effects of pH on PCA formation have not been reported.

The objectives of the studies presented herein were to determine the pH-dependent CHD degradation scheme, to determine the rate laws and to propose reasonable mechanisms for CHD hydrolysis in aqueous solutions.

### Materials and Methods

#### Materials

CHD digluconate solutions (20% USP) were obtained from Spectrum Chemicals (New Brunswick, NJ, US). CHD free base, PCA, (p-chlorophenyl)guanidine and (p-chlorophenyl)urea were obtained from Sigma-Aldrich (St Louis, MO, US). Sodium dihydrogen phosphate, o-phosphoric acid, acetic acid, formic acid, hydrochloric acid were obtained from Fisher Scientific (Fair Lawn, NJ, US). Organic solvents and water used to prepare mobile phases were HPLC grade (Fisher Scientific, Fair Lawn, NJ, US). All other chemicals were reagent grade and used as received.

#### Stability-indicating Assay Development

HPLC analyses were performed using a Thermo Separation HPLC system consisting of a SN4000 system controller, P4000 analytical pump, AS3000 auto-injector, UV3000 UV-VIS detector. Chromatographic data was analyzed and stored using PC1000 chromatography data system software. The column used for separating the degradation

products was a 4.6x25 cm C-18 column (Inertsil 5 $\mu$  ODS2, Varian). Mobile phase was prepared from a formic acid solution(0.1 M) which was adjusted to a pH value of 3.0 with ammonium hydroxide, mixed with acetonitrile (60:40 v/v), and filtered with a 0.2 micron filter. The analytic wavelength was 239 nm which is associated with the UV absorption of aromatic ring. An isocratic method was developed with a flow rate of 0.5 mL/minute, a run time of 30 minutes and auto injector temperature of 4 °C.

Forced degradation studies of CHD (0.10 mM) in acidic (0.100 M HCl) and alkaline (0.100 M HEPES, pH 8.5) solutions were conducted at 90.0 °C for 5 and 24 hours, respectively, to identify degradation products and demonstrate stability-indicating capabilities of the HPLC method. A mixture containing authentic CHD, PCA, PCPU and PCPG was prepared and used to determine retention values and peak resolution.

An LC-MS system was used to identify degradation products and intermediates. The mass spectrometry used was an HP/Agilent 1100 LC/MSD system consisting of 1100 Benchtop Mass Selective Detector, 1327A Auto-sampler, 1312A Binary Pump. For mass spectrometry, an electrospray ionization (ESI) was used in positive ion mode. The same column and mobile phase were used as the HPLC with UV detection.

#### Kinetics of CHD Hydrolysis

A series of reaction mixtures containing 0.10 mM CHD were prepared in the pH range of 0.5-9.0 using hydrochloric acid, sodium hydroxide, acetate, phosphate, HEPES buffers at a constant ionic strength of 0.500 M adjusted with sodium chloride. Reaction mixture aliquots were placed in Type II borosilicate glass vials, sealed with Teflon-coated butyl rubber stoppers and stored in a 90.0 °C water bath. The water bath was enclosed to prevent the exposure to light which is known to cause photolytic degradation of CHD.(15, 16) Aliquots were periodically removed, cold quenched (4 °C) and analyzed by HPLC.

To determine whether oxidative pathways were involved in CHD degradation in the absence of light, a CHD solution (0.10 mM) in 0.100 M hydrochloric acid was prepared and filled into glass vials, one of which was sparged with inert gas for 15 minutes, and sealed in an inert environment. Another reaction mixture vial was sealed in air. These reaction mixtures were stored together at 90.0 °C in a light-protected water bath. Aliquots of both reactions mixtures were periodically removed, cold quenched and assayed by HPLC.

A series of reaction mixtures containing 0.10 mM PCPU, PCPG or PCA were prepared using the same buffers as were used to prepare CHD degradation mixtures. Reaction mixture aliquots were placed in Type II borosilicate glass vials, sealed with Teflon-coated butyl rubber stoppers and stored at 90.0 °C in a light-protected water bath. Aliquots were periodically removed, cold quenched (4 °C) and analyzed by HPLC.

#### Effect of pH and Buffers

CHD digluconate solutions were prepared in the pH range of 0.5-9.0 using hydrochloride, sodium hydroxide, acetate, phosphate or HEPES buffers with various buffer concentrations (0.010 -0.200 M) and a constant ionic strength of 0.50 M. The experimental conditions are listed in the Tables 1 and 2. These solutions were stored in glass vials and subjected to thermal stress in 90.0 °C water bath. Aliquots were periodically removed, cold quenched (4 °C) and analyzed by HPLC. The pH values of reaction mixtures were measured at reaction temperature at the beginning and end of reaction.

#### Model Fitting

WinNonlin software (v. 4.1, Pharsight) was used to do all non-linear data fitting.

## Results and Discussion

### Identification of Degradation Products

The ability of the HPLC method to separate the reported degradation products of CHD was demonstrated by analysis of a synthetic mixture prepared by dissolving authentic samples of CHD, PCPG, PCPU and PCA in water. The retention volumes were 5.6, 7.4, 10.2, 16.0 mL for PCPG, CHD, PCPU and PCA, respectively (Figure II-2). A solution of CHD prepared at pH 1.0 and stored at 90.0 °C was subjected to HPLC analysis after 5 hours. Six major peaks were observed (Figure II-3) with retention volumes of 4.8, 5.8, 7.4, 11.5, 13.8 and 16.0 mL; peaks were tentatively labeled A1, A2, A3, A4, A5 and A6, respectively. Peak A3 and Peak A6 corresponded to CHD and PCA based on comparison to retention volumes of authentic standards. No significant peak was observed at a retention volume corresponding to PCPU (10.2 mL). Peak A2 had a retention volume of 5.8mL which is similar to PCPG (5.6 mL). However spiking the reaction mixture sample with authentic PCPG demonstrated that peak A2 was not PCPG.

Degradation products were identified by comparing the theoretical mass of predicted products to the mass observed by LC-MS analysis, and results are listed in Table 1. The mass of peak A3 (505) was consistent with the theoretical mass of CHD. CHD possesses two (p-chlorophenyl)biguanide groups (PBG), therefore degradation products were anticipated to possess one or zero intact PBG residues. The molecule weight of peak A1 (395) was consistent with a structure wherein one PBG residue was intact and PCA was lost from the other PBG group giving rise to an amidinourea group (AU). Peaks A4 and A5 did not correspond to any of the peaks observed in the synthetic mixtures prepared from reported CHD degradation products. Peak A4 had a molecular weight (506) consistent with the substitution of an oxygen for nitrogen. One of C=N bonds in PBG residue can get protonated and converted to C=O bond forming N-amidino-N'-(p-chlorophenyl)urea or N-[(p-chlorophenyl)amidino]urea. But N-amidino-N'-(p-chlorophenyl)urea (APU) is the major intermediate depending on the further



breakdown. The molecular mass of peak A5 (507) was consistent with a molecular structure wherein both PBG residues have been hydrolyzed to APU residues. PCPG and PCPU were not detected in the acidic degradation samples of CHD.

In CHD solutions degraded under alkaline condition (pH 8.5, HEPES buffer), four major peaks were observed with retention volumes of 6.5, 7.4, 10.2, and 16.0 mL corresponding to peaks labeled B1, B2, B3 and B4 in Figure II-4. The retention volumes of peaks B2 and B4 were consistent with CHD and PCA, respectively. Peak B3 with a retention volume of 10.2 mL which was consistent with the retention volume of authentic sample of PCPU. The peak B1 did not correspond to any of the peaks observed in acidic reaction mixture or the synthetic mixtures prepared from reported CHD degradation products. The mass of peak B3 (171) was consistent with the theoretical mass of PCPU. The mass of peak B1 (353) was consistent with a structure wherein one PBG residue in CHD was intact and PCPU was lost from the other PBG group giving a rise to a guanidine group (G).

In reaction mixtures prepared using PCPU or PCPG as substrates, the only degradation product observed was PCA in both acidic and alkaline conditions. There were no peaks arising from PCA solution even after thermal stress (90.0 °C, pH 1.0 or 8.5) for 5 days.

Calibration standards for the CHD, PCA, PCPU, PCPG were prepared in the range of 0.010-0.200 mM by using authentic analytical reagent grade of CHD free base, PCA, PCPG dissolved in mobile phase. The concentration of PBG-APU and APU-APU was estimated by using CHD calibration standards. The UV absorption coefficient of PBG-AU, PBG-CA, PBG-G were assumed to be half of CHD, and the concentrations of these compounds were estimated using calibration curve of CHD with an absorptivity equal to half of the value for CHD.

### Degradation Scheme in Acidic Conditions

First-order loss of CHD was observed over three half-lives at low pH (0.5-2.0). Moreover there was no detectable pH change which was consistent with first order kinetics. For reactions in the pH range 2.5 to 6.0, initial rate conditions (substrate loss less than 10%) were used to estimate rate constants. The overall degradation kinetics under these conditions was assumed to be first-order.

PCPG and PCPU were reported degradation products of CHD (14, 15), however neither compound was observed in the acidic reaction mixtures (Figure II-3). In order to confirm that their absence was not due to their instability under the reaction conditions, a study was conducted at 90.0 °C and pH 1.0 using either PCPG or PCPU as substrate. The half-lives for PCPG and PCPU loss were 170 and 9.2 hours, respectively, whereas the half life for CHD loss was 2.9 hours. Since the HPLC system was shown to be capable at detecting PCPG and PCPU, and both of these compounds were greater than three-fold more stable than CHD, these potential degradation products would have been detected if they were present during CHD degradation. They were not detected and therefore are not acidic degradation products of CHD.

Typical concentration time profiles for the loss of CHD, the appearance and loss of PBG-APU and PBG-CA and appearance of PCA from a reaction initiated with CHD in acidic conditions are shown in Figure II-5. No difference was observed in these concentration time profiles in the presence or absence of atmospheric oxygen. Therefore, oxidation does not appear to play a role under the conditions studied herein.

The precursor-successor relationships between the six compounds observed in acidic CHD degradation mixtures can be deduced based on their chemical identity and stepwise degradation pathways. As depicted in the scheme shown in Figure II-6, the three primary pathways for CHD degradation in acidic conditions would include: the hydrolytic conversion of a PBG residue to AU with concurrent generation of PCA (pathway A); hydrolysis of a PBG residue to a APU residue concurrent with loss of

ammonium (pathway D); hydrolysis of a APU residue to carbamic acid with concurrent formation of PCA (pathway E).

The kinetics of CHD degradation in accordance with the acidic scheme (Figure II-6) can be defined by a model composed of a series of differential equations that describe the rate of appearance and loss of all substrates, intermediates and products (Equations II-1- II-8) via three chemically distinct pathways (A, D, and E) with corresponding first order rate constants labeled  $k_A$ ,  $k_D$  and  $k_E$ . The values for  $k_A$ ,  $k_D$ ,  $k_E$  were estimated by simultaneously fitting the model equations to concentration time profiles for CHD, PCA, PBG-AU, PBG-APU, PBG-CA and APU-APU. WinNonlin software (v. 4.1, Pharsight) was used to do data fitting. (Appendix A) Agreement between model-predicted concentration time profiles and observed data (Figure II-7) demonstrated the suitability of degradation scheme and model to describe the kinetics of the acidic degradation of CHD.

$$\frac{d[CHD]}{dt} = -2(k_A + k_D)[CHD] \quad \text{Equation II-1}$$

$$\frac{d[PBG-APU]}{dt} = 2k_D[CHD] - (k_A + k_D + k_E)[PBG-APU] \quad \text{Equation II-2}$$

$$\frac{d[APU-APU]}{dt} = k_D[APU-APU] - 2k_E[PAG-APU] \quad \text{Equation II-3}$$

$$\frac{d[PBG-AU]}{dt} = 2k_A[CHD] - (k_A + k_D)[PBG-AU] \quad \text{Equation II-4}$$

$$\frac{d[APU-AU]}{dt} = k_A[PBG-APU] + k_D[PBG-APU] - k_E[APU-AU] \quad \text{Equation II-5}$$

$$\frac{d[PBG-CA]}{dt} = k_E[PBG-APU] - (k_A + k_D)[PBG-CA] \quad \text{Equation II-6}$$

$$\frac{d[APU-CA]}{dt} = 2k_E[APU-APU] + k_D[PBG-CA] - k_E[APU-CA] \quad \text{Equation II-7}$$

$$\frac{d[PCA]}{dt} = k_A(2[CHD] + [PBG-AU] + [PBG-CA] + [PBG-APU]) + k_E(2[APU-APU] + [PBG-APU] + [APU-AU] + [APU-CA]) \quad \text{Equation II-8}$$

### Degradation Scheme in Alkaline Conditions

Under alkaline conditions, first-order loss of CHD was observed over three half-lives. No detectable pH change was observed which was consistent with first order kinetics. PCPU was not observed to be present in acidic reaction mixtures, but was present in alkaline conditions as a major intermediate in CHD hydrolysis (Figure II-4). Therefore, in contrast to the CHD degradation in acidic conditions, pathway B (Figure II-1) is the major pathway for CHD degradation in alkaline conditions.

To determine if the direct formation of PCA from CHD (pathway A) occurs in alkaline conditions, an area under curve (AUC) analysis (17, 18) was conducted. A reaction was initiated with 0.10 mM CHD, and the area-under-concentration time profile (AUC) for PBG-G was 7.69 mM·hr (pH 8.1, 90.0 °C). If the reaction was initiated from 0.10 mM PBG-G, the predicted AUC for the loss of PBG-G would be 7.64 mM·hr. Because these two AUC values are essentially identical, no significant parallel loss of CHD was observed. Therefore the CHD degradation in alkaline conditions occurs exclusively by pathway B wherein the two PBG residues in CHD are cleaved to form PCPU and guanidine (G). Subsequently PBG-G degrades by pathway B to form PCPU which is further degraded giving rise to PCA (Figure II-8).

The kinetics of CHD degradation in alkaline conditions occurs according to the scheme depicted in Figure II-8 which can be defined by a model composed of a series of differential equations (Equations II-9 –12) describing pathways B and F with first order rate constants labeled  $k_B$ ,  $k_F$ .

$$\frac{d[CHD]}{dt} = -2k_B[CHD] \quad \text{Equation II-9}$$

$$\frac{d[PBG-G]}{dt} = 2k_B[CHD] - k_B[PBG-G] \quad \text{Equation II-10}$$

$$\frac{d[PCPU]}{dt} = k_B(2[CHD] + [PBG-G]) - k_F[PCPU] \quad \text{Equation II-11}$$

$$\frac{d[PCA]}{dt} = k_F[PCPU] \quad \text{Equation II-12}$$

Typical concentration time profiles for the loss of CHD, the appearance and loss of PCPU and PBG-G and appearance of PCA from a reaction initiated with CHD are shown in Figure II-9. The reactions initiated with PCPU under alkaline conditions were also conducted, and the typical concentration profile is shown in Figure II-10. WinNonlin software (v.4.1) was used to do nonlinear regressions (Appendix B). The values for  $k_B$ , were estimated by simultaneously fitting the model equations to concentration time profiles for CHD, PBG-G and PCPU, and values of  $k_F$  were estimated by fitting the model equations to concentration time profile for reactions initiated with PCPU. Agreement between model-predicted concentration time profiles and observed data demonstrated the suitability of degradation scheme and model to describe the kinetics of the alkaline degradation CHD.

### Effect of pH

The rate constants for the primary pathways in acidic conditions ( $k_A$ ,  $k_D$ ,  $k_E$ ) and alkaline conditions ( $k_B$ ,  $k_F$ ) were estimated at reaction pH values in the ranges 0.5 to 3.2 and 6 to 8.5, respectively. Buffers (acetate, phosphate and HEPES) were observed to increase the hydrolysis rate. The rate constants estimated in these systems were plotted versus buffer concentration to obtain rate constants at zero buffer concentrations ( $k_A$ ) (Tables 2 and 3). The logarithm of the  $k_A$  values for each primary pathway was plotted versus pH to generate pH rate profiles for each pathway.

For pathway A and D, a slope of -1 was observed at  $\text{pH} \geq 2$  with a slight downward bend as the pH values approach 1 (Figure II-11). This pH rate profile is

consistent with specific acid catalyzed hydrolysis of an unprotonated substrate (or the kinetically –equivalent mechanism including solvent attack of a protonated substrate). The reported pKa's of CHD are 2 and 11, and the lower value is consistent with observed inflection in the pH rate profile. The dominant species of PBG moiety at pH 2-11 is monopronated form (PBGH<sup>+</sup>). The rate laws consistent with the pH rate profiles for path A and D are given by Equations II-13 and II-14.

$$k_{\Delta,A} = k_{H,A} a_H f_{PBGH^+} \quad \text{Equation II-13}$$

$$k_{\Delta,D} = k_{H,D} a_H f_{PBGH^+} \quad \text{Equation II-14}$$

The estimates for  $k_{H,A}$  and  $k_{H,D}$  (90.0°C ) were 1.467 and 0.363 M<sup>-1</sup> hr<sup>-1</sup>. For pathway E, no pH dependence was observed. This implies solvent attack or spontaneous degradation of substrate. The rate law can be described by Equation II-15.

$$k_{\Delta,E} = k_{s,E} \quad \text{Equation II-15}$$

For pathway B in alkaline conditions, a slope of 1 was observed at pH >7 (Figure II-12). This pH rate profile is consistent with specific base catalysis hydrolysis of a protonated substrate (or the kinetically equivalent mechanism including solvent attack of an unprotonated substrate). The rate law is given by Equation II-16.

$$k_{\Delta,B} = k_{OH,B} a_{OH} f_{PBGH^+} \quad \text{Equation II-16}$$

The estimated value for  $k_{OH}$  (90.0 °C) is 10889 M<sup>-1</sup> hr<sup>-1</sup>. For the loss of PCPU (pathway F), there was no apparent dependence between rate constant and pH (i.e. the slope of the pH-rate profile was about 0). This implies solvent attack or spontaneous degradation of substrate. The rate law is described by Equation II-17.

$$k_{\Delta,F} = k_{s,F} \quad \text{Equation II-17}$$

### Proposed Mechanisms

In aqueous solution, (p-chlorophenyl)biguanide has been reported to have two pKa values at about 11 and 2. Therefore in the pH range of 2 to 11, both of the biguanide residues in CHD will be mostly monoprotonated. In very acidic aqueous solutions (pH < 2), biguanide residues are diprotonated. Based on the tautomeric structure of biguanide, (19) the positive charges are predicted to be distributed between all the nitrogen and carbon atoms in the biguanide moiety. Solvent attack on an electron deficient carbon would lead to a tetrahedral intermediate with potential leaving groups including PCA and ammonia, giving rise to PBG-AU or PBG-APU, respectively. The similarity in pH rate profiles for pathways A and D imply that the composition of the rate-determining transition state for each of the parallel pathways is the same (e.g. diprotonated substrate). This observation is consistent with a shared tetrahedral intermediate with multiple parallel pathways for rate-determining breakdown leading to different products. The relative facility of the partitioning of the proposed tetrahedral intermediate between the potential products is given by the pH-independent ratio of the rate constants ( $k_A:k_B \approx 4$ ). Thus tetrahedral intermediate breakdown leading to the expulsion of PCA is much more facile than expulsion of ammonia which is consistent with the greater basicity or nucleophilicity of ammonia relative to the aromatic amine in PCA. The possible mechanisms for pathway A and D are presented in Figure II-13. A possible related scheme for pathway E (Figure II-14) would involve solvent attack on the APU moiety to form a tetrahedral intermediate, followed by expulsion of PCA.

At alkaline pHs (pH values between 7 and about 10), biguanide residues in CHD would be monoprotonated. Nucleophilic attack of hydroxide ions on electron-deficient carbons would lead to the formation of neutral tetrahedral intermediates. Because of its strong basicity, the guanidine group in the tetrahedral intermediate is easily protonated and giving rise exclusively to PCPU. This mechanism is shown in Figure II-15. The unsaturated carbon in PCPU can be also attacked by hydroxide ions to form a tetrahedral

intermediate which is able to degrade to PCA and carbamic acid in aqueous solutions (Figure II-16).

### Conclusion

In acidic conditions, CHD degrades by two major pathways, one at which leads to direct formation of PCA and the other indirect formation of PCA via the formation of the intermediate PBG-APU with loss of ammonia. The preferred product (PCA) is the best leaving group (weakest base).

In alkaline conditions, CHD degrades by a different single pathway leading indirectly to PCA. Partitioning of degradation products from a tetrahedral intermediate under alkaline conditions appears to be due to leaving-group protonation of the strongest base.

PCA appearance is determined by a pH-dependent pathway, and the rate constants are pH-dependent. The degradation model described herein is used in Chapter III to evaluate effects of formulation design on shelf-life.



Table II-1. CHD and hydrolysis intermediates and products

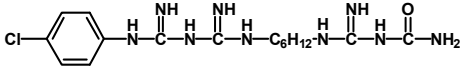
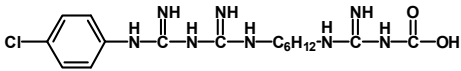
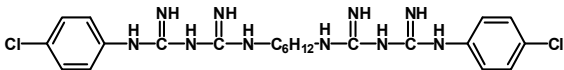
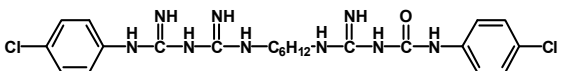
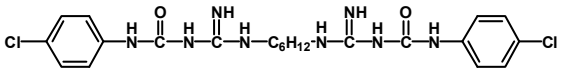
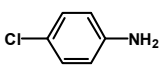
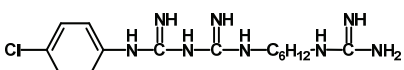
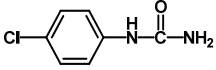
Peak #	Label used in degradation scheme	MW	Proposed Structure
A1	PBG-AU	395	
A2	PBG-CA	396	
A3, B2	CHD (PBG-PBG)	505	
A4	PBG-APU	506	
A5	APU-APU	507	
A6, B4	PCA	127	
B1	PBG-G	352	
B3	PCPU	171	

Table II-2. Reaction conditions and estimated rate constants (90.0 °C) for acidic CHD degradation pathways.

pH	Buffer	Buffer Conc. (M)	$k_A$ (hr <sup>-1</sup> )	Std Dev (hr <sup>-1</sup> )	$k_D$ (hr <sup>-1</sup> )	Std Dev (hr <sup>-1</sup> )	$k_E$ (hr <sup>-1</sup> )	Std Dev (hr <sup>-1</sup> )
0.62	HCl	0.240	$1.41 \times 10^{-1}$	$4.81 \times 10^{-3}$	$3.52 \times 10^{-2}$	$1.81 \times 10^{-3}$	0.501	0.051
1.09	HCl	0.090	$9.51 \times 10^{-2}$	$4.12 \times 10^{-3}$	$2.34 \times 10^{-2}$	$1.33 \times 10^{-3}$	0.550	0.043
1.64	HCl	0.023	$3.72 \times 10^{-2}$	$1.21 \times 10^{-3}$	$9.20 \times 10^{-3}$	$5.20 \times 10^{-4}$	0.488	0.042
2.13	HCl	0.007	$1.10 \times 10^{-2}$	$4.64 \times 10^{-4}$	$2.73 \times 10^{-3}$	$2.39 \times 10^{-4}$	0.467	0.044
2.64	Phosphate	0.010	$5.60 \times 10^{-3}$	$3.31 \times 10^{-4}$	$1.41 \times 10^{-3}$	$1.32 \times 10^{-4}$	0.491	0.063
		0.050	$7.80 \times 10^{-3}$	$4.24 \times 10^{-4}$	$2.04 \times 10^{-3}$	$3.31 \times 10^{-4}$	0.511	0.057
		0.100	$1.00 \times 10^{-2}$	$6.21 \times 10^{-4}$	$2.52 \times 10^{-3}$	$5.18 \times 10^{-4}$	0.510	0.056
3.20	Phosphate	0.010	$9.80 \times 10^{-4}$	$5.52 \times 10^{-5}$	$2.39 \times 10^{-4}$	$2.51 \times 10^{-5}$	0.492	0.061
		0.050	$1.05 \times 10^{-3}$	$7.81 \times 10^{-5}$	$2.61 \times 10^{-4}$	$3.57 \times 10^{-5}$	0.505	0.054
		0.100	$1.18 \times 10^{-3}$	$8.69 \times 10^{-5}$	$2.90 \times 10^{-4}$	$5.21 \times 10^{-5}$	0.532	0.079
4.11	acetate	0.010	$2.28 \times 10^{-4}$	$2.31 \times 10^{-6}$	$5.51 \times 10^{-5}$	$3.46 \times 10^{-6}$		
		0.050	$4.60 \times 10^{-4}$	$5.22 \times 10^{-6}$	$9.02 \times 10^{-5}$	$2.53 \times 10^{-6}$		
		0.100	$9.78 \times 10^{-4}$	$4.51 \times 10^{-6}$	$1.48 \times 10^{-4}$	$6.07 \times 10^{-6}$		
5.24	acetate	0.010	$3.63 \times 10^{-5}$	$1.53 \times 10^{-6}$	$5.41 \times 10^{-6}$	$7.47 \times 10^{-7}$		
		0.050	$3.69 \times 10^{-5}$	$8.52 \times 10^{-7}$	$5.49 \times 10^{-6}$	$4.32 \times 10^{-7}$		
		0.100	$3.75 \times 10^{-5}$	$7.84 \times 10^{-7}$	$5.52 \times 10^{-6}$	$3.10 \times 10^{-7}$		

Table II-3. Reaction conditions and estimated rate constants (90.0 °C) for neutral and alkaline CHD degradation pathways.

pH	Buffer	Buffer Conc. (M)	$k_B$ (hr <sup>-1</sup> )	Std Dev (hr <sup>-1</sup> )	$k_F$ (hr <sup>-1</sup> )	Std Dev (hr <sup>-1</sup> )
6.20	phosphate	0.010	$4.70 \times 10^{-4}$	$1.02 \times 10^{-4}$	$5.13 \times 10^{-2}$	$9.60 \times 10^{-4}$
		0.050	$5.90 \times 10^{-4}$	$1.18 \times 10^{-4}$	$5.50 \times 10^{-2}$	$5.60 \times 10^{-4}$
		0.100	$9.50 \times 10^{-4}$	$2.03 \times 10^{-4}$	$5.94 \times 10^{-2}$	$7.04 \times 10^{-4}$
7.03	Phosphate	0.010	$1.32 \times 10^{-3}$	$1.41 \times 10^{-4}$	$5.24 \times 10^{-2}$	$1.42 \times 10^{-3}$
		0.050	$2.45 \times 10^{-3}$	$2.53 \times 10^{-4}$	$5.64 \times 10^{-2}$	$1.01 \times 10^{-3}$
		0.100	$3.71 \times 10^{-3}$	$4.04 \times 10^{-4}$	$6.04 \times 10^{-2}$	$1.08 \times 10^{-3}$
7.68	Phosphate	0.050	$3.20 \times 10^{-3}$	$3.51 \times 10^{-4}$	$5.01 \times 10^{-2}$	$1.28 \times 10^{-3}$
		0.100	$3.35 \times 10^{-3}$	$3.10 \times 10^{-4}$	$5.19 \times 10^{-2}$	$1.11 \times 10^{-3}$
		0.200	$3.66 \times 10^{-3}$	$2.24 \times 10^{-4}$	$5.38 \times 10^{-2}$	$1.40 \times 10^{-3}$
8.10	HEPES	0.050	$1.32 \times 10^{-2}$	$2.03 \times 10^{-4}$	$4.88 \times 10^{-2}$	$1.92 \times 10^{-3}$
		0.100	$1.42 \times 10^{-2}$	$1.08 \times 10^{-3}$	$4.99 \times 10^{-2}$	$2.03 \times 10^{-3}$
		0.200	$1.51 \times 10^{-2}$	$1.27 \times 10^{-3}$	$5.16 \times 10^{-2}$	$1.15 \times 10^{-3}$
8.50	HEPES	0.050	$3.40 \times 10^{-2}$	$1.62 \times 10^{-3}$	$5.24 \times 10^{-2}$	$1.08 \times 10^{-3}$
		0.100	$3.90 \times 10^{-2}$	$2.59 \times 10^{-3}$	$5.40 \times 10^{-2}$	$1.17 \times 10^{-3}$
		0.200	$4.55 \times 10^{-2}$	$2.67 \times 10^{-3}$	$5.54 \times 10^{-2}$	$1.58 \times 10^{-3}$

Figure II-1. Possible CHD degradation products resulting from formation and breakdown of hydrolytic tetrahedral intermediate.

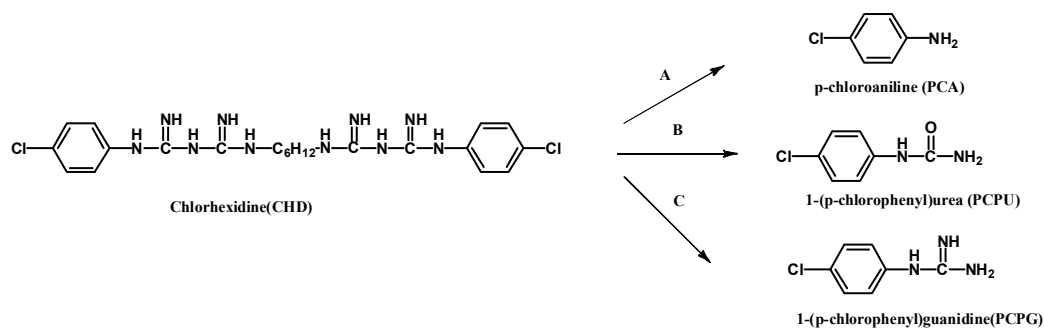


Figure II-2. Representative HPLC chromatogram of a synthetic mixture of CHD and possible degradation products.

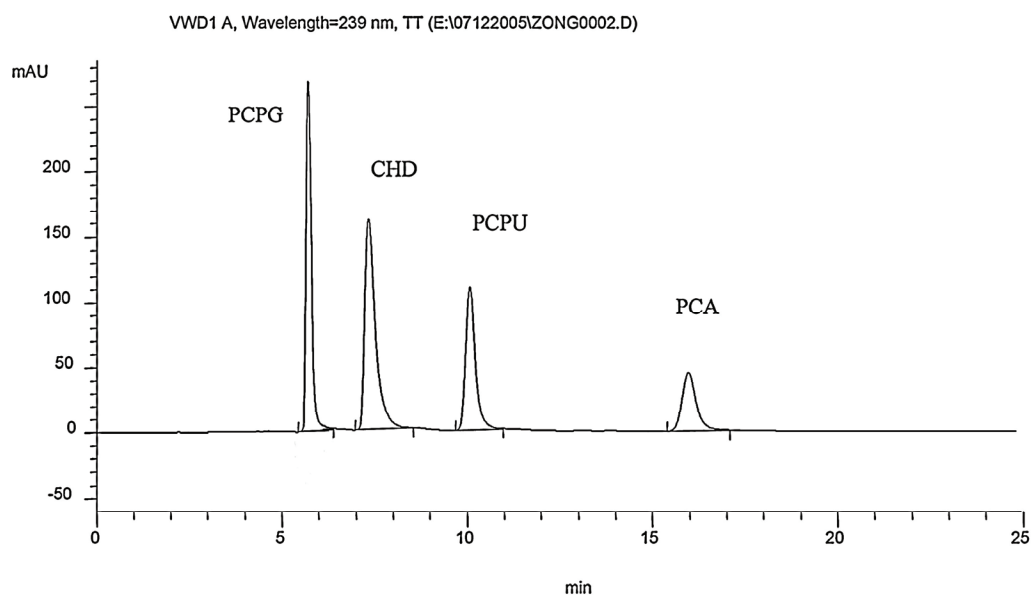


Figure II-3. Representative chromatogram of CHD reaction mixture in acidic conditions (pH 1.0, 90.0 °C, 5 hours). Peak labels refer the compounds identified in Table II-1.

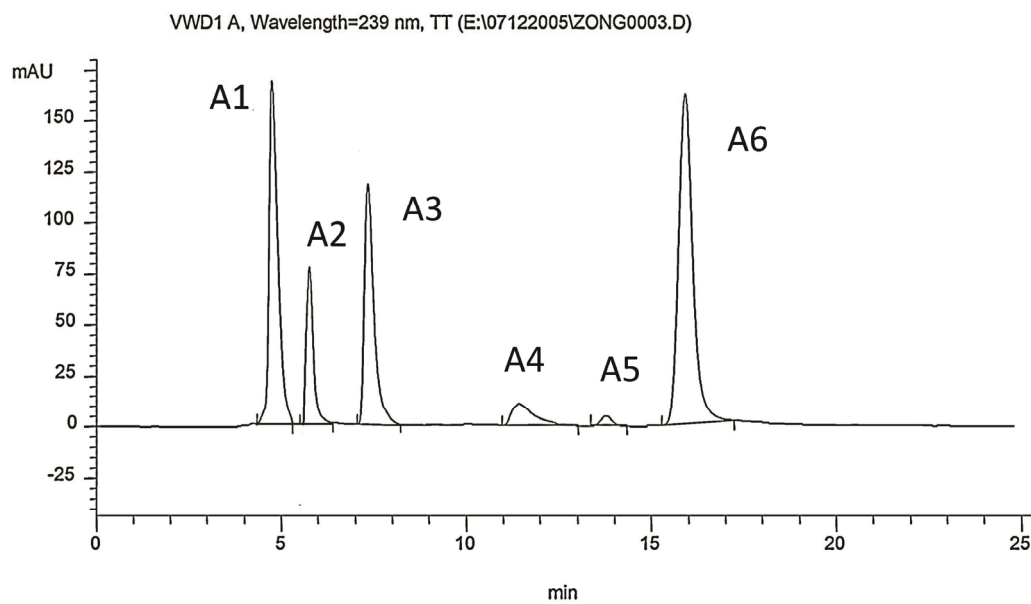


Figure II-4. Representative chromatogram of CHD reaction mixture in alkaline conditions (pH 8.6, 90.0 °C, 24 hours). Peak labels refer the compounds identified in Table II-1.

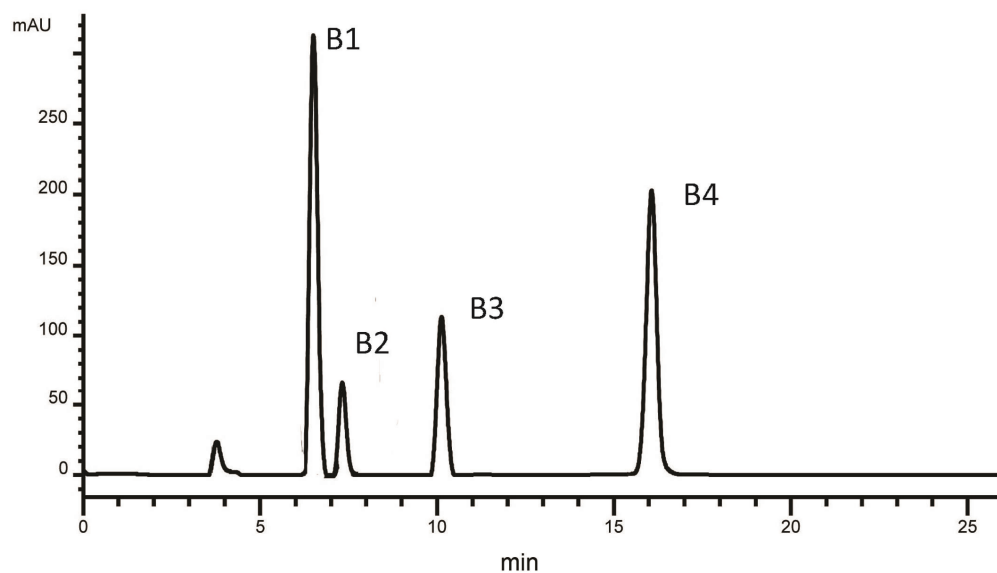


Figure II-5. Concentration time profiles of CHD and its degradation products under acidic conditions (pH 1.0, 90.0 °C). *Open triangle* under air headspace, *open circle* solution was purged and sealed with helium.

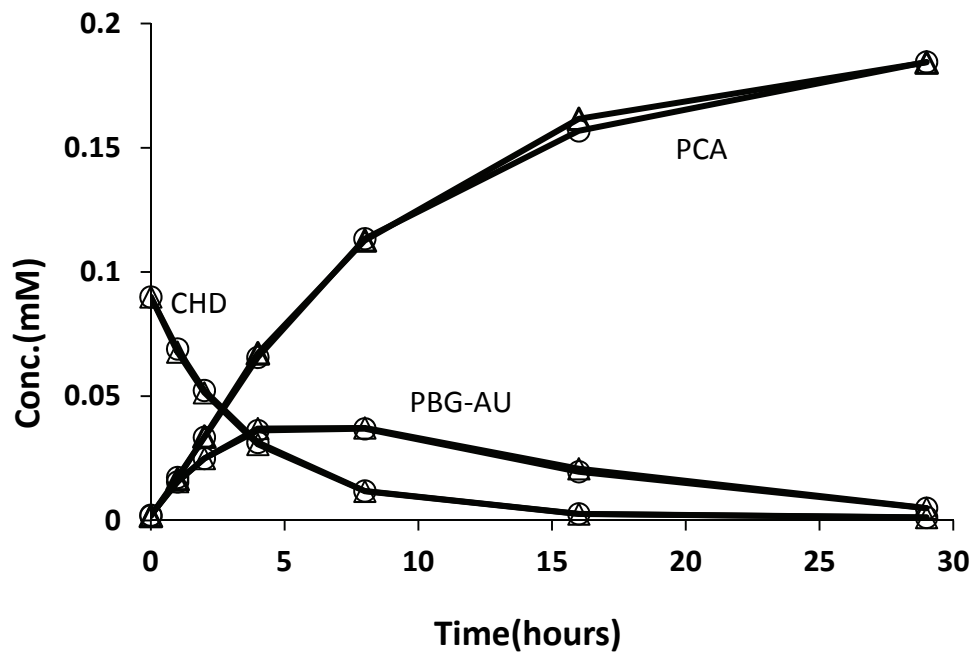




Figure II-6. Proposed CHD degradation scheme in acidic conditions.

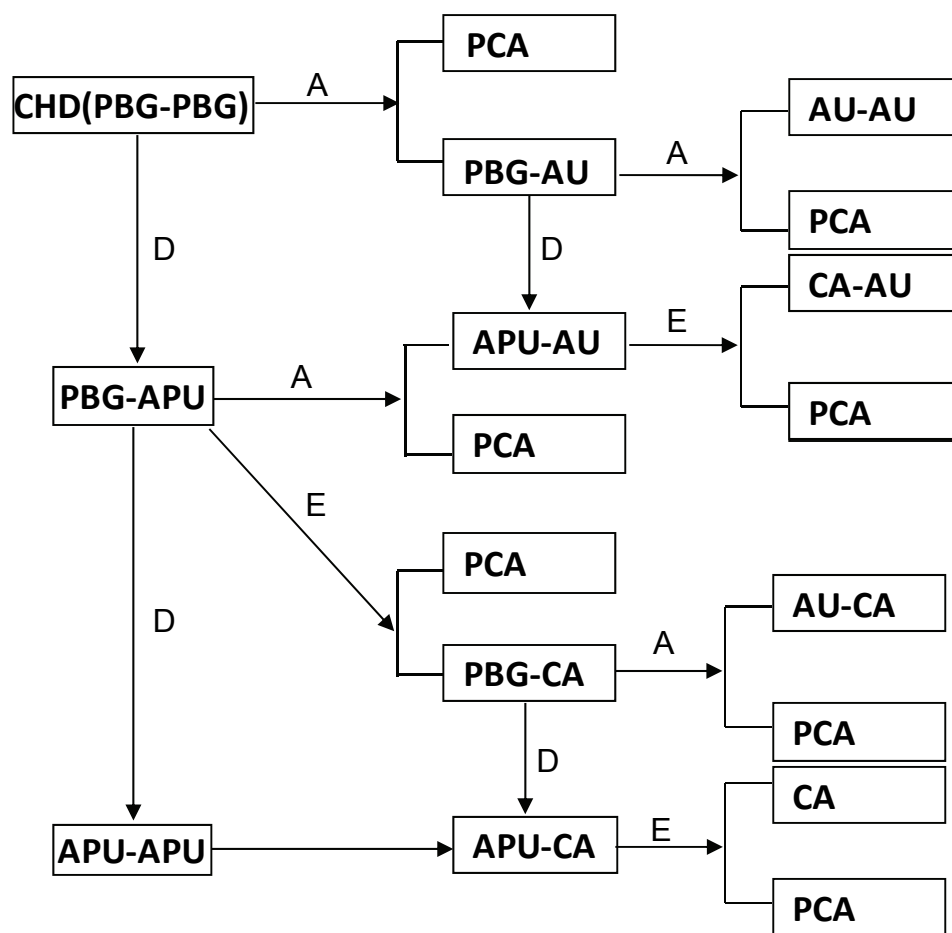


Figure II-7. Concentration time profiles for CHD and degradation intermediates under acidic conditions (pH 1.0, 90.0 °C). Symbols are observed results; lines are predicted using least square estimated parameters based on proposed model.

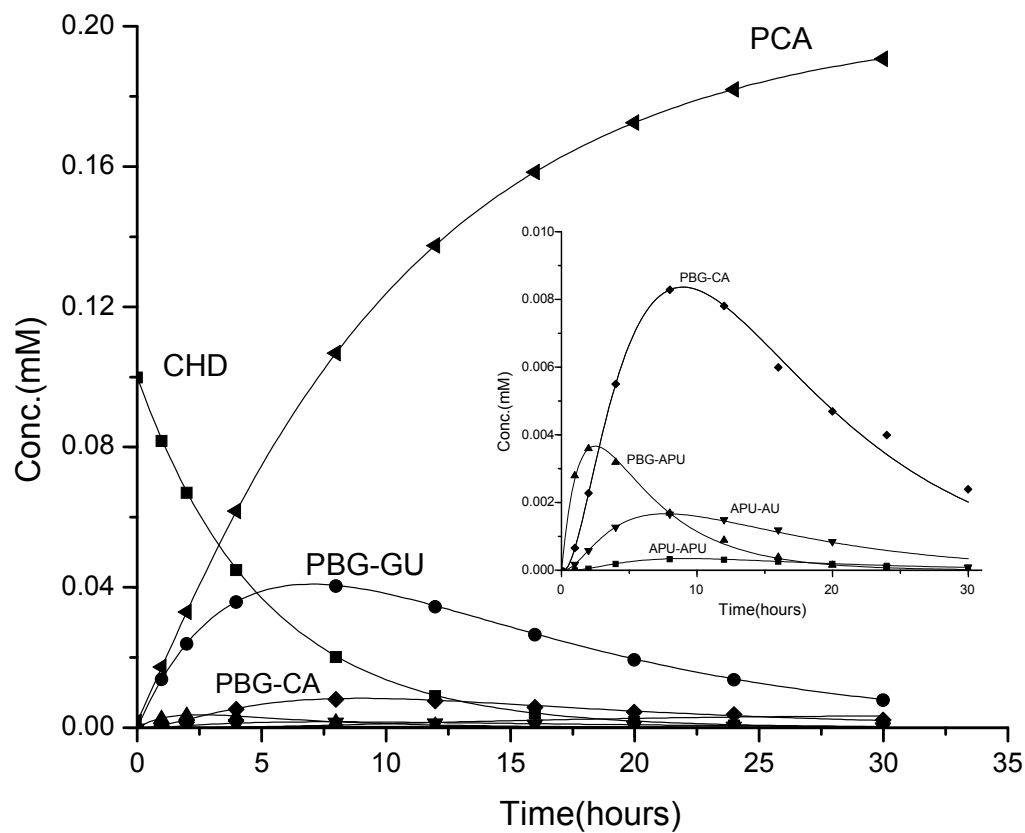


Figure II-8. Proposed CHD degradation scheme in alkaline conditions.

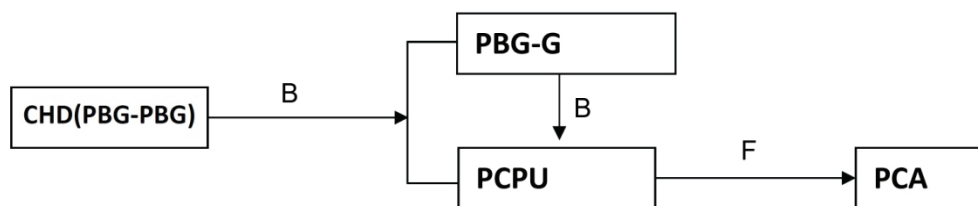


Figure II-9. Typical concentration time profiles of CHD degradation under alkaline conditions (pH 8.1, 90.0 °C). Symbols are observed results; lines are predicted using least square estimated parameters based on proposed model.

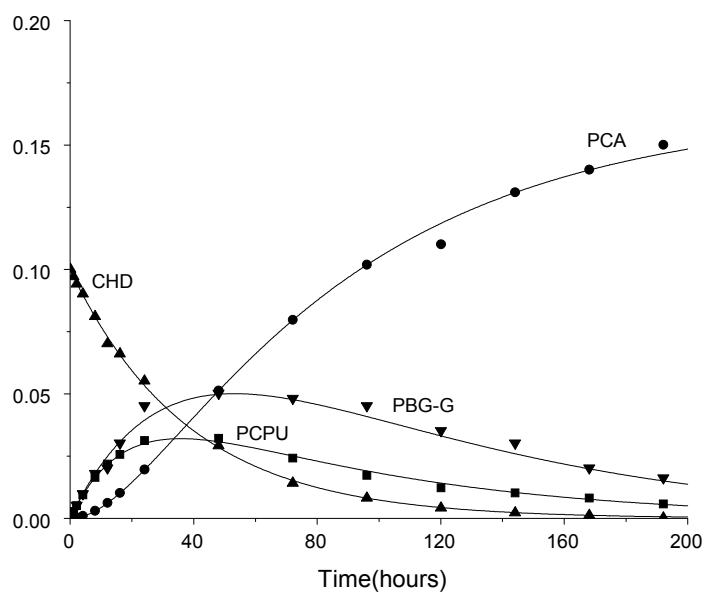


Figure II-10. Typical concentration time profiles of PCPU degradation under alkaline conditions (pH 8.1, 90.0°C). Symbols are observed results; lines are predicted using least square estimated parameters based on proposed model.

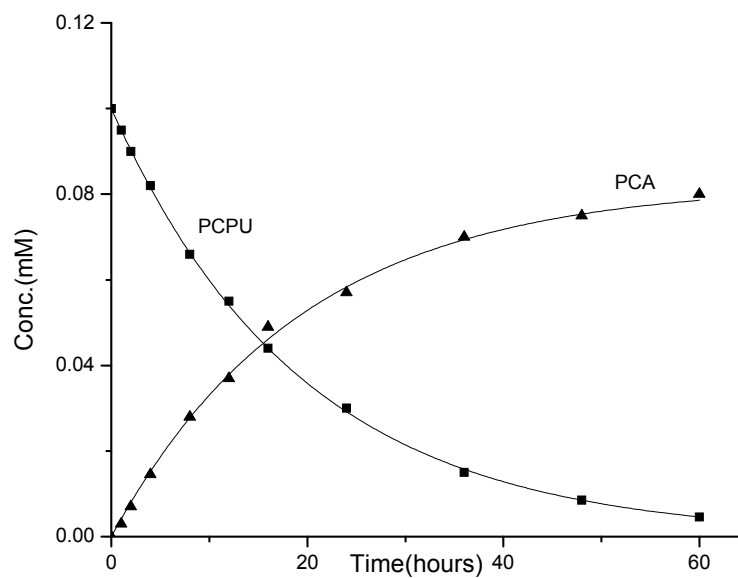


Figure II-11. PH rate profiles for rate constants ( $k_A$ ,  $k_D$  and  $k_E$ ) estimated from concentration time profiles obtained under acidic conditions.

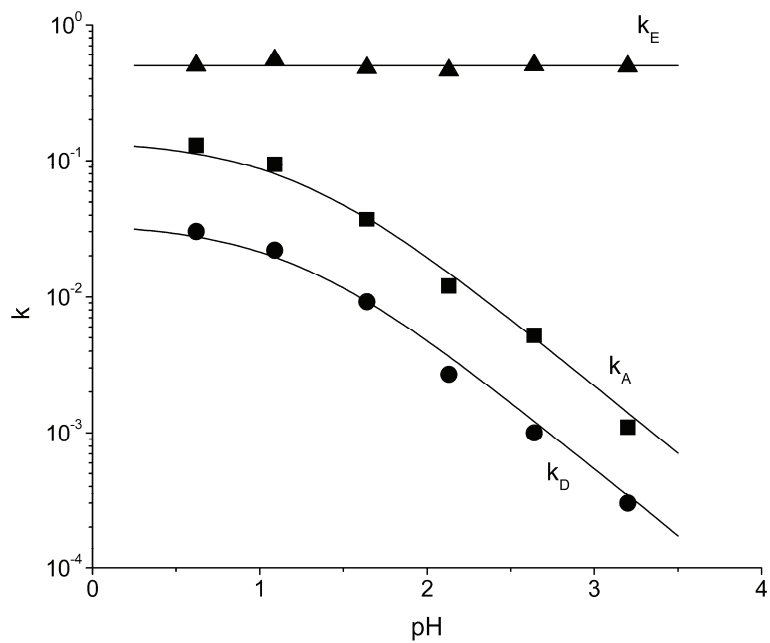


Figure II-12. PH rate profiles for rate constants ( $k_B$ ,  $k_F$ ) estimated from concentration time profiles obtained under alkaline conditions.

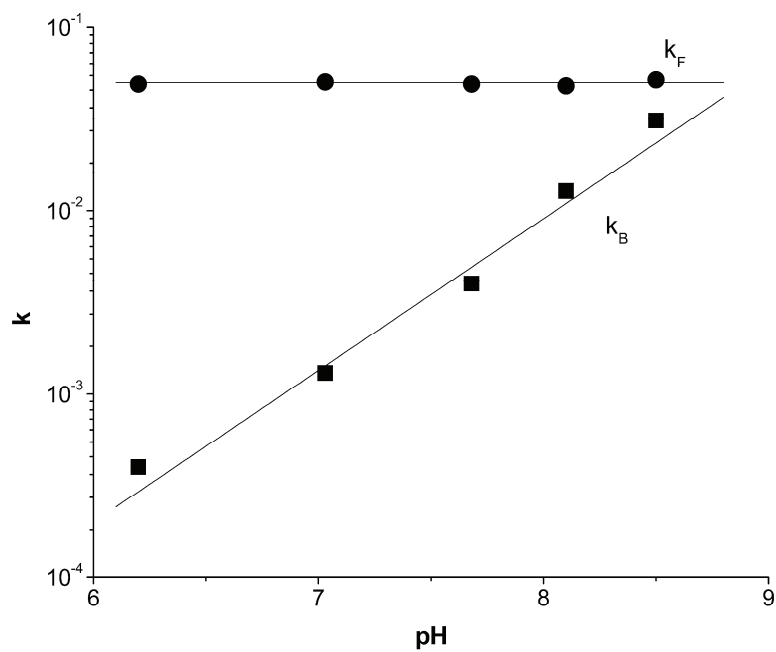


Figure II-13. Proposed mechanisms for the hydrolytic formation of PCA/PBG-AU (pathway A) and  $\text{NH}_3$ /PBG-APU (pathway D) under acidic conditions.

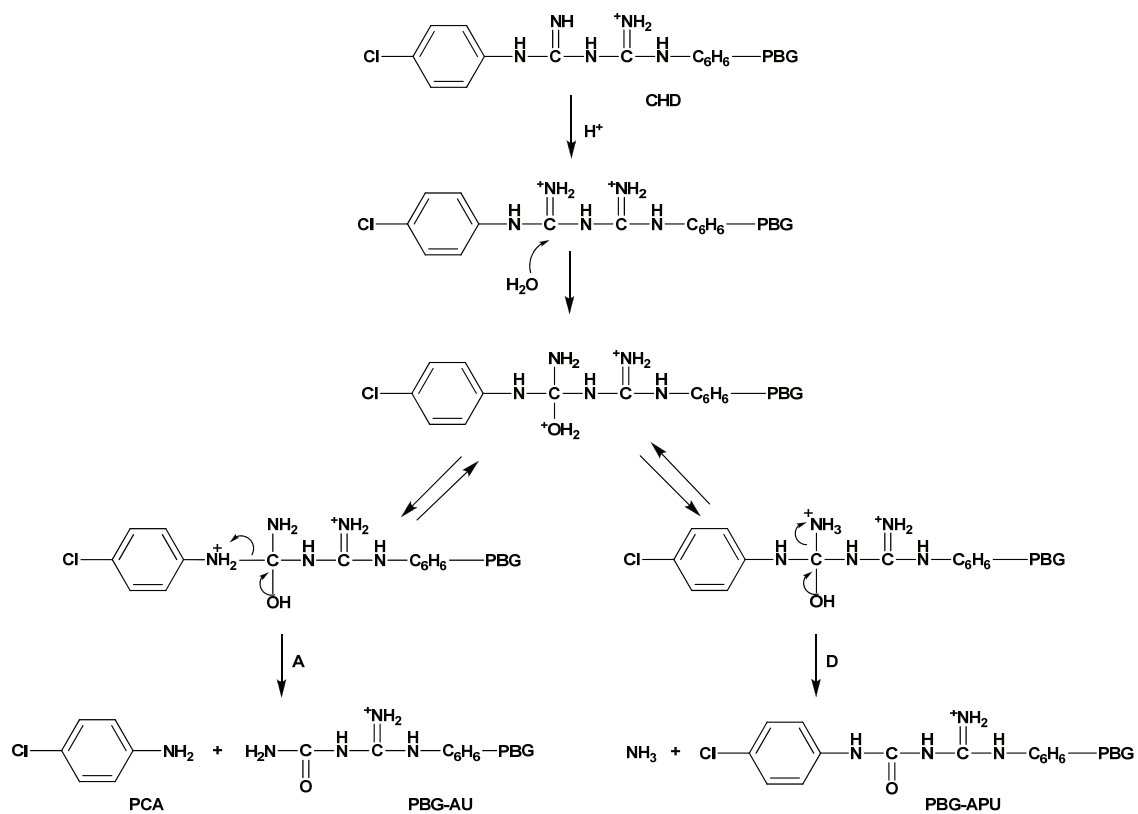




Figure II-14. Proposed mechanism for the hydrolytic formation of PCA/PBG-CA from APU moiety (pathway E) under acidic conditions.

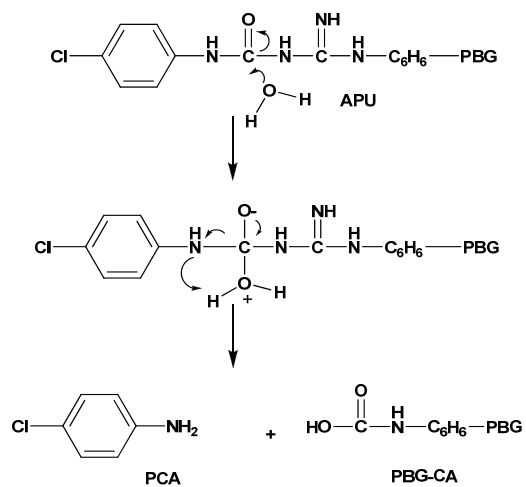


Figure II-15. Proposed mechanism for the hydrolytic formation of PCPU/PBG-G (pathway B) under alkaline conditions.

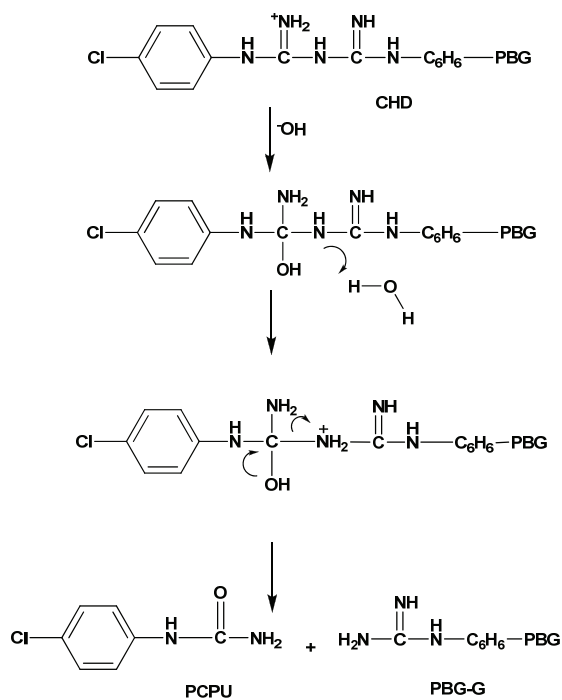
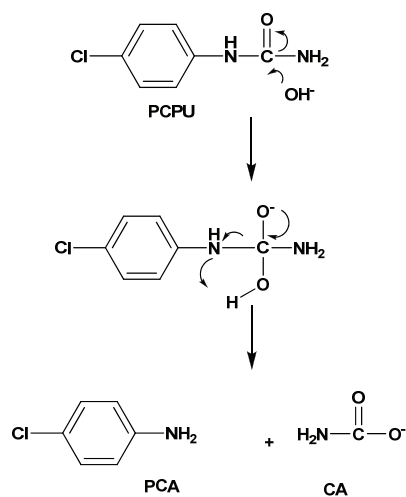


Figure II-16. Proposed mechanism for the hydrolytic formation of PCA from PCPU (pathway F) under alkaline conditions.



## CHAPTER III

### EFFECTS OF CHLORHEXIDINE FORMULATION AND PREPARATION ON SHELF-LIFE

#### Introduction

Chlorhexidine (CHD) is a broad spectrum antimicrobial agent against gram positive/negative bacteria and fungi. This cationic biguanide has substantivity: its antibacterial action is maintained for a long period because of its ability to interact electrostaticly with anionic substrates, such as glycoproteins, and phospholipids membranes associated with root canal walls and dentinal tubuli.(20-22) CHD is typically non-irritating to periapical tissues even at high concentrations.(23) These characteristics are desired for a large number of medical and dental applications.(24-27) CHD is used as a mouthwash at concentration of 0.1-0.2% for dental cares, and its use in more concentrated formulations (1-2%) has been advocated for treatment of severe caries.(28-31)

P-chloroaniline (PCA), the primary degradation product of CHD, is a known carcinogen with additional nephro and hepato toxicity.(32) The formation of PCA limits the usefulness of CHD, e.g. the United State Pharmacopeia limit for PCA in CHD mouth rinse is 3 ppm.(33)

In Chapter II, we have investigated the kinetics of PCA formation as a function of pH. CHD is a symmetric molecule containing two p-chlorophenylbiguanide groups (PBG), both of which degrade to PCA in a pH dependent manner. On a molecular basis, each completely degraded CHD molecule generates two PCA molecules. In acidic conditions, the degradation follows stepwise scheme: direct hydrolysis of one PBG moiety to form PCA or N-Amidino-N'-(p-chlorophenyl)urea (APU) moiety. The second PBG residue can also hydrolyze to PCA or APU. Moreover the APU residues are also capable of hydrolyzing to release PCA. In acidic conditions the direct formation of PCA

from PBG (Pathway A) is the major pathway. A simplified scheme for the PCA formation in acidic conditions can be depicted in Figure III-1. In alkaline conditions, the degradation follows a different stepwise pathway: hydrolysis of one PBG to form (p-chlorophenyl)urea (PCPU)(pathway B), then sequential hydrolysis of PCPU to release PCA (pathway F). This pathway occurs for both PBG residues in CHD. The simplified scheme is depicted in Figure III-2.

The objective of the present study in this chapter was to use our understanding of pH-dependent CHD degradation pathways and kinetics to address the practical problems of predicting and minimizing the rate of PCA formation in CHD preparations. Toward this end the following specific aims were addressed and are reported herein:

- Development of a simplified degradation model for PCA generation;
- Validation of an instability prediction method using representative CHD formulations;
- Determination of the effects of temperature on the rate of PCA formation;
- Assessment of the effect of formulation and storage conditions on shelf-life;
- Evaluation of the usefulness of adsorptive materials for removing PCA from CHD bulk solutions.

### Materials and Methods

#### Materials

CHD digluconate solutions (20%, USP grade) were obtained from Alfa Asar (Ward Hill, MA), Gallipot ( St. Paul, MN), Letco (Decatur, AL), MP Biomedicals (Solon, OH), PCCA (Houston, TX), Spectrum (Gardena, CA), Sigma (St Louis, MO). CHD free base, PCA, Amberlite CG-50, Amberlite IRA-67, IRA-400(Cl), IR-120H, molecular sieves 13x, 8-12 mess, Amberlite CG-400, Dowex 50WX8-200 and Amberlite XAD-4 were obtained from Sigma-Aldrich ( St Louis, MO, US); veegum was from Spectrum(Gardena, CA); Rexyn 300 was from Fisher Scientific( Pittsburgh, PA, US),

activated charcoal was from Gulf Bio-Systems (Dallas, TX, US). All chemicals were reagent grade or higher and used as received. Organic solvents used were HPLC grade from Fisher Scientific. All water used was HPLC grade.

#### Stability-indicating Assay Method

The stability-indicating HPLC method has been reported in the previous manuscript. The liquid chromatography system was equipped with a 239-nm detector (SpectrumSystem UV2000) and a 4.6×25-cm C-18 column (Inertsil 5u ODS2, Varian) at room temperature. The LC system also contained a pump (SpectrumSystem P4000), an autosampler (SpectrumSystem AS3000) and system controller (SpectrumSystem SN 4000). PC1000 software was used to control the HPLC system. Formic acid solution (0.1 M) was adjusted to pH 3.0 with ammonium hydroxide. Then a mixture of this solution and acetonitrile with a ratio (v/v) of 60:40 was used as mobile phases. The flow rate was set as 1.0 mL/min. The analytical wavelength was 239 nm.

#### Preparation of Test Formulations

Solutions (0.10 mM) of CHD in 0.100 M hydrochloric acid (pH 1.0) and 0.100 M HEPES buffer (pH 8.1) were prepared at a constant ionic strength of 0.200M using sodium chloride. Degradation studies were conducted at 70.0, 80.0 and 90.0 °C in water baths. The solutions were protected from exposure to light. Aliquots were periodically removed and analyzed immediately by HPLC for CHD, PCA and major intermediates.

CHD formulations (1.0% CHD) were prepared using 20% CHD bulk solution (Spectrum, Gardena, CA), and USP water with 2.0% HPMC, 1.4% raspberry flavor and 0.4% aspartame. These 1.0% CHD formulations were stored under 25 and 40 °C, protected from light. Aliquots of samples were removed at 0, 2, 4, 8, 12, 16, 32 weeks, and were analyzed by HPLC immediately for the PCA and CHD concentrations. The concentration time profile for the appearance of PCA was used to demonstrate the

validity of the degradation model based on comparisons of observed and model-predicted concentrations.

### Evaluation and Purification of Bulk CHD Solutions

Bulk CHD digluconate solutions (20%, USP grade) from various sources were diluted using mobile phase to appropriate PCA concentration range (0.01-0.20 mM). Triplicate samples were analyzed by HPLC to determine the PCA concentrations. These results were used to assess effect of the initial PCA concentration on the quality and stability of final CHD formulation especially at high dose.

Different adsorptive materials were used to evaluate their ability to remove PCA from the bulk CHD digluconate solution. An aliquot of each adsorbent (1.0 g) was added to 20.0 mL bulk CHD solution, and then the mixture was stirred for 1 hour. The mixtures were filtered through 0.45 micron glass filters and the filtrates were analyzed for CHD and PCA recovery by comparing the pre- and post- adsorbent treated concentrations.

### Results

CHD solutions (0.10 mM) prepared at pH values 1.0 and 8.1 and constant ionic strength ( $\mu = 0.200\text{M}$ ) were degraded at 70.0, 80.0, and 90.0 °C. The loss of CHD, appearance of PCA, the appearance and loss of major intermediates were measured by HPLC. Exemplary concentration time profiles are depicted in Figures III-3 and III-4. The loss of CHD under acidic condition increased dramatically with temperature (Figure III-3a), and the corresponding rate of PCA appearance increased with temperature (Figure III-3b). The appearance and loss of the major intermediate PBG-AU are depicted in Figure III-3c wherein the peak time decreased with increasing temperature in the range 70.0 - 90.0 °C.

The loss of CHD under alkaline condition also increased with temperature (Figure III-4a), and the corresponding lag time in the appearance of PCA decreased with

temperature (Figure III-4b). The peak time of major intermediate PCPU also changes with temperature (Figure III-4c).

At lower temperature (25 and 40 °C) and weakly acidic conditions, the degradation rate were sufficiently slow that PCA appearance rather CHD loss is a meaningful measurement of instability. The initial rate of PCA appearance in CHD formulations was determined (Figure III-5). The initial level of PCA in the formulation was 2 ppm due to the amount of PCA present in the bulk CHD solution used to prepare the formulation. The PCA levels increased to 20 ppm in 12 weeks and 11 ppm in 36 weeks at 40 and 25 °C, respectively.

The levels of PCA were determined in 20% CHD digluconate solutions (USP) obtained from various suppliers. The dates of analysis were within the expiry for all bulk solutions. The results of our assay were shown in Table III-1. Samples were assayed in triplicate and the mean and relative standard deviations are reported. The PCA levels varied from 40 to 240 ppm.

Twelve adsorbents and ion exchange resins were used to evaluate their utility in removing PCA from bulk CHD digluconate solutions. The results for CHD recovery and PCA loss after exposure to each adsorptive material for 1 hour varied from 41 to 100% and 0 to 100% (Table III-2), respectively. Eight adsorbents removed more than 80% of the PCA present in the bulk CHD solutions. Four of those adsorbents allowed nearly 80% recovery of CHD. Dowex 50WX8-200 and activated charcoal removed 100% of the PCA while retaining 79% and 86% of the CHD.

## Discussion

### Development of a PCA Prediction Model

Although the generation of PCA in CHD is complex in both acidic and alkaline solutions, the major degradation pathways can be depicted by relatively simple schemes. In acidic conditions, PCA is formed directly from CHD and also from CHD degradation



intermediates (Figure III-1). In alkaline conditions PCA is not formed directly from CHD but from CHD degradation intermediates (e.g. PCPU) (Figure III-2). The degradation rates can be described by Equations III-1–III-3 for acidic conditions and Equations III-4–III-7 for alkaline conditions. In the neutral and weak acidic pH range (e.g. pH range from 5 to 7), both acidic and alkaline pathways contribute to PCA formation.

$$\frac{d[CHD]}{dt} = -2k_A[CHD] \quad \text{Equation III-1}$$

$$\frac{d[I]}{dt} = 2k_A[CHD] - k[I] \quad \text{Equation III-2}$$

$$\frac{d[PCA]}{dt} = 2k_A[CHD] + k_A[I] \quad \text{Equation III-3}$$

$$\frac{d[CHD]}{dt} = -2k_B[CHD] \quad \text{Equation III-4}$$

$$\frac{d[I]}{dt} = 2k_B[CHD] - k_B[I] \quad \text{Equation III-5}$$

$$\frac{d[PCPU]}{dt} = 2k_B[CHD] + k_B[I] - k_F[PCPU] \quad \text{Equation III-6}$$

$$\frac{d[PCA]}{dt} = k_F[PCPU] \quad \text{Equation III-7}$$

The correlation between loss of CHD and appearance of PCA in acidic and alkaline CHD solutions at different temperatures demonstrated that the degradation pathways were pH-dependent but not temperature dependent although the rates associated with each pathway increased with increasing temperature (Figure III-6). Concentration time profiles for substrate, intermediates and products were used simultaneously to estimate rate constants associated with schemes shown in Figure III-1 and 2 by nonlinear regression method (WinNonlin, V. 4.1). Examples of the model

predicted and observed concentration time profiles at pH values 1.0 and 8.1 are shown in Figures III-3 and III-4.

Typically the shelf-life for a drug is determined by the time associated with the degradation of 5-10% of the drug substrate. However for products like CHD with toxic degradants, the USP limit concentration of these degradants in the product determines the shelf-life. PCA limit in CHD oral rinse solution is 3 ppm which is equivalent to 0.03% degradation from a 0.10% CHD product or 0.003% from a 1.0 % CHD formulation. Therefore, for the purposes of shelf-life determination, the complexities of PCA formation can be reduced by imposing initial rate conditions wherein the substrate loss is less than 10%, and the concentrations of most CHD degradation intermediates are kinetically insignificant.

Based on Equations III-1–III-3 for acidic conditions and Equations III-4–III-7 for alkaline conditions, the simplified model equation for the prediction of PCA at acidic and alkaline conditions is given by Equation III-8.

$$[PCA]_t = 2[CHD]_0 \times (1 - e^{-kt}) \quad \text{Equation III-8}$$

Where,  $[PCA]_t$  is the PCA level at time t,  $[CHD]_0$  is the initial level of CHD. For acidic conditions, k is the pH-dependent rate constant  $k_A$  (Figure III-1); for alkaline conditions, k is the pH-dependent rate constant  $k_B$  (Figure III-2). For weakly acidic and neutral conditions, both acidic and alkaline pathways contribute to the PCA formation, thus k is the sum of  $k_A$  and  $k_B$ .

The effects of pH on rate constants  $k_A$  and  $k_B$  have been previously discussed in Chapter II. The pH rate profile for  $k_A$  demonstrates that this pathway is subject to specific acid catalysis and the rate constant is proportional to the hydronium concentration. Conversely, the pH rate profile for  $k_B$  demonstrated first order dependence on hydroxide ion concentration, or specific base catalysis. The rate constants  $k_A$  and  $k_B$  can be

described by Equations III-9 and III-10. In pH range from 2 to 10, PBG is monoprotated and the fraction of monoprotated form ( $f_{PBGH^+}$ ) is approximately 1.

$$k_A = k_{H,A} a_H f_{PBGH^+} \quad \text{Equation III-9}$$

$$k_B = k_{OH,B} a_{OH} f_{PBGH^+} \quad \text{Equation III-10}$$

The effects of temperature on the values of  $k_A$  and  $k_B$  is described by Arrhenius relationship wherein the activation energies and pre-exponential constants for the second-order rate constants associated with specific acid and specific base catalysis ( $k_{H,A}$  and  $k_{OH,B}$ , respectively) are 20.0 and 21.6 kcal/mol, and  $1.61 \times 10^{12}$  and  $1.10 \times 10^{17} \text{ M}^{-1} \text{ h}^{-1}$ , respectively.

The combined effect of pH and temperature results in the following predictive equations for  $k_A$  and  $k_B$  (Equations III-11 and III-12).

$$k_A = 1.61 \times 10^{12} \times \exp\left(\frac{-10063}{T}\right) \times a_H \quad \text{Equation III-11}$$

$$k_B = 1.10 \times 10^{17} \times \exp\left(\frac{-10870}{T}\right) \times a_{OH} \quad \text{Equation III-12}$$

A prediction model for the appearance of PCA in aqueous CHD preparation can be derived by combining Equations III-8, III-11 and III-12. The critical time ( $t_c$ ) can be defined as the duration of storage at a specific temperature and pH conditions whereupon the PCA level reaches the limit. Equation III-13 was derived to estimate this critical time.

$$t_c = \frac{1}{k} \ln\left[\frac{2[CHD]_0}{505} / \left(\frac{2[CHD]_0}{505} - \frac{[PCA]_{limit} - [PCA]_0}{127}\right)\right] \quad \text{Equation III-13}$$

Where,  $[CHD]_0$  is the concentration (percent) of CHD in the formulation;  $[PCA]_0$  is the initial PCA level (percent) in formulation, and  $k$  is the sum of  $k_A$  and  $k_B$ . Molecular weights of CHD and PCA (505 and 127, respectively) were used in the equation to convert weight to molar concentrations.

### Model Validation

A series of studies were conducted using aqueous formulations composed 1.0% CHD, 2.0% HPMC, 1.4% raspberry flavor, 0.4% aspartame and USP water. The predicted PCA concentrations were determined using Equation III-8 wherein the values of the rate constant  $k$  were estimated as function of pH and temperature using Equations III-11 and III-12. The predicted values were compared to the observed appearance of PCA over 9 months at 25 °C and 3 months at 40 °C (Figure III-5), the R-square values were 0.99 and 0.98, respectively. Agreement between model-predicted and observed PCA levels demonstrates the ability of the model to accurately predict CHD instability at pharmaceutically-relevant storage conditions.

### Assessment of Factors Affecting Formulation Stability

The effect of pH on shelf-life was examined by calculating the critical product failure time ( $t_c$ ) at 25 °C for a series of formulations containing 1.0 to 0.1 % CHD (Figure III-7). The pH value of maximum stability was determined to be 5.2, and the predicted shelf-life varied with the concentration of CHD in the formulation. At pH 5.2, the predicted shelf-life of 0.1, 0.2, 0.5 and 1.0% CHD is about 14.5, 7.2, 2.9, and 1.4 years, assuming that the formulation contains no PCA at the beginning of storage.

However, PCA is typically present in bulk CHD solutions commonly used to prepare CHD formulations. For example, we analyzed the PCA content of commercially available USP grade 20% CHD digluconate solutions. The results (Table III-1) illustrate that PCA levels varied between 40 to 240 ppm, which would result in initial PCA levels in a formulation prepared at 0.10% CHD of 0.1 to 1.2 ppm, and 1 to 12 ppm for 1.0% CHD formulation. Therefore, the initial PCA level at the beginning of product storage is a critical determinant of shelf-life, especially for higher concentration formulations.

The magnitude of the effects of bulk CHD purity and CHD formulation strength are depicted in Figure III-8 which relates shelf-life to formulation strength at the optimal

pH condition (pH 5.2) for various initial levels of PCA in the formulation. For a 1.0% CHD formulation, the effect of an initial PCA at 1 ppm level is to decrease the critical time to reach USP limit (3 ppm) by 0.48 years from 1.4 years if there is no PCA at the beginning of product storage. Therefore control of the initial level of PCA in the bulk CHD solution, in combination with pH and temperature, is critical for optimizing CHD formulation shelf-life.

### Purification of CHD Bulk Solution

Shelf-life optimization for CHD formulation depends on combination of controlling formulation factors such as formulation strength, pH and optimizing storage conditions by using controlled room temperature or refrigeration. As illustrated in Figure III-8 and discussed above, another essential factor in optimizing the shelf-life is to minimize the initial concentration of PCA in the formulation using “clean” bulk CHD preparation or by removing PCA from the bulk solution during the preparation of the formulation. Toward this end, we investigated the potential usefulness of various adsorbents to quickly remove PCA from bulk CHD solutions while maintaining the active pharmaceutical ingredient concentration. Our trials were conducted by suspending 1.0 gram of various adsorptive materials in 20.0 mL of 20% CHD digluconate solution. These mixtures were gently agitated for 1 hour and then filtered using 0.45 micron glass filters. Both the resultant PCA and CHD concentrations were measured by HPLC and the percent recovery for CHD and percent removal of PCA were calculated by comparison of treated and untreated control samples (Table III-2). The most promising result was obtained using Amberlite IRA-120H, the PCA level decreased from 93 ppm to 1.8ppm, and the CHD level decreased from 20.1% to 19.7%. With Dowex 50WX8-200 and activated charcoal, PCA was also effectively removed with little loss of CHD. These results suggest that the extemporaneous removal of PCA from bulk CHD solutions may

be possible with the design, evaluation and validation of a simple extraction procedure used during formulation preparation.

### Conclusion

The shelf-life of CHD formulations can be predicted based on a model that accounts for the kinetics of PCA appearance as a function of formulation strength, solution pH, bulk CHD purity, and storage temperature. The critical product failure time is limited by the USP limit of 3 ppm PCA. The pH range for optimal shelf-life is 5.0 to 5.5. The absence of PCA in bulk CHD solution used to prepare formulation is critical, especially when the formulation CHD concentration is more than 0.5%. Simple extraction procedure may be possible used to remove PCA from bulk CHD solution while keep maintain the API potency.

Table III-1. PCA levels in 20% CHD digluconate solutions from various sources.

Supplier	Lot#	PCA level as received ( $\mu\text{g/mL}$ )	RSD (%)
Spectrum	X00789	40.1	2.10
Gallipot	405204	62.1	1.87
Spectrum	TR1420	68.5	1.10
Letco	4170503	70.1	1.75
PCCA	C105220	77.4	1.29
Sigma	093K1056	93.2	0.76
Alfa Asar	A13P11	146.6	2.86
MP	9764C	238.3	0.67

Table III-2. CHD recovery and PCA removal after exposure to adsorptive materials.

Adsorbent	Supplier	Lot#	CHD recovery (%)	PCA removal (%)
Control (untreated)	n/a		100.0	0.0
Molecular sieves	Acros	A0198863401	94.7	4.0
Amberlite IRA-67	Aldrich	11731KC	99.6	13.4
Veegum	Spectrum	GA044	61.3	65.2
Amberlite CG-50	Fluka	454529/1	81.2	68.6
Amberlite CG-400	Sigma	99C-0146	81.1	79.7
Rexyn 300	Fisher	850608	56.7	80.5
Amberlite IRA-400(Cl)	Aldrich	04503CC	50.9	83.9
Dowex 1X8-100	Aldrich	05006JV	41.1	88.7
Amberlite IR-120H	Aldrich	05904MC	98.0	98.1
Amberlite XAD-4	Supelco	00971141	49.6	98.5
Dowex 50WX8-200	Sigma	68H0618	79.1	100.0
SuperChar	Gulf Bio-Systems	G812R	85.6	100.0



Figure III-1. Simplified PCA formation scheme in acidic CHD solutions.

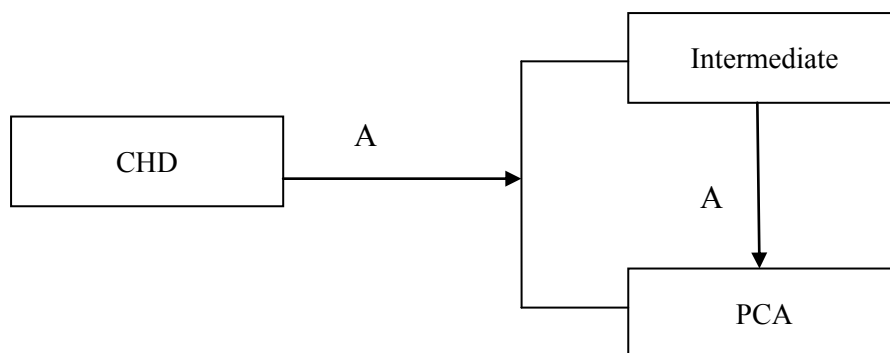


Figure III-2. Simplified PCA formation scheme in alkaline CHD solutions.

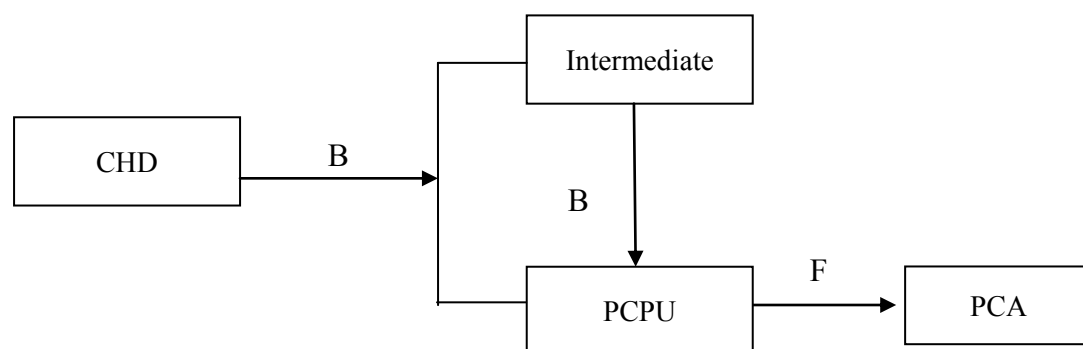
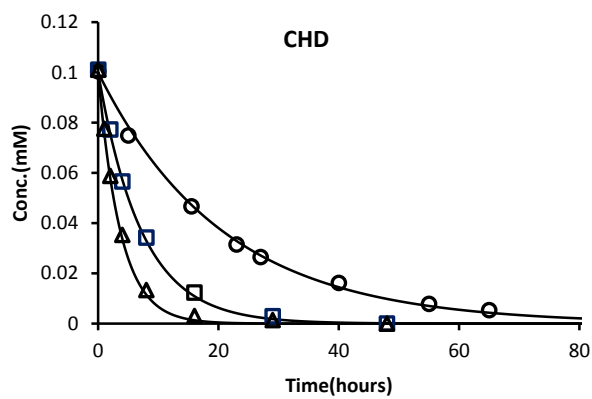
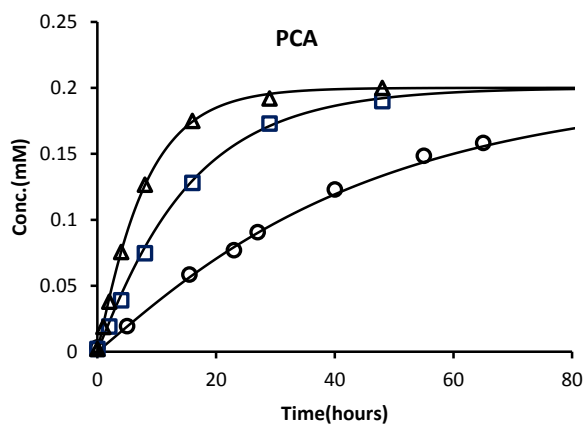


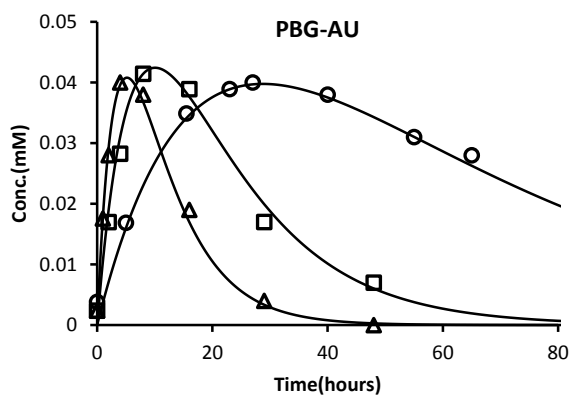
Figure III-3. Representative concentration time profiles in acidic conditions at 70°C (○), 80°C (□) and 90 °C (Δ). (a) CHD; (b) PCA; (c) PBG-AU.



(a)

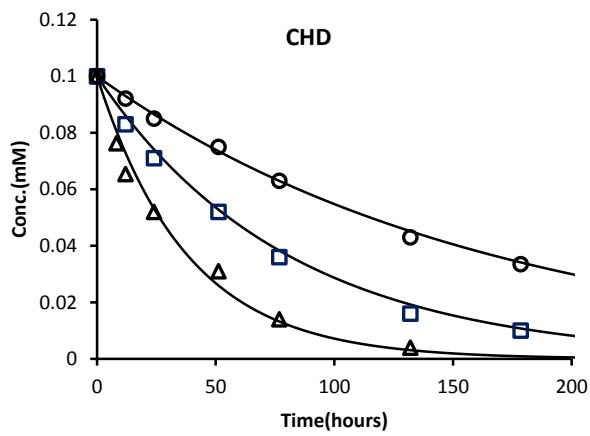


(b)

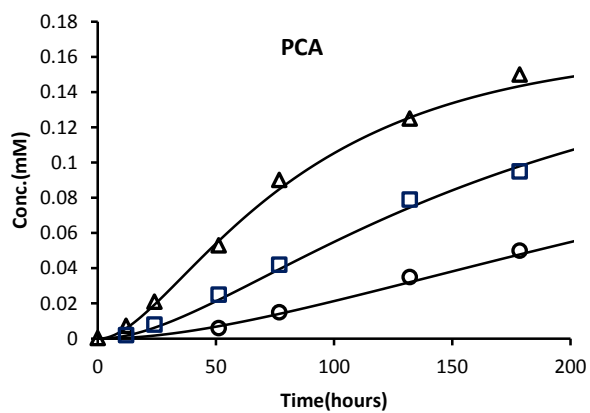


(c)

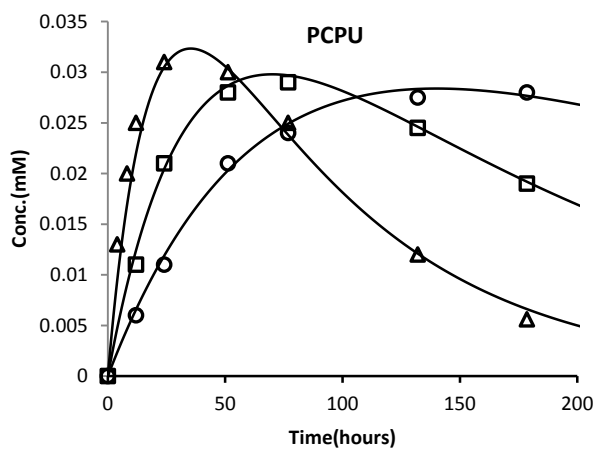
Figure III-4. Representative concentration time profiles in alkaline condition at 70°C (○), 80°C (□) and 90 °C (Δ). (a) CHD; (b) PCA); (c) PCPU.



(a)



(b)



(c)

Figure III-5. PCA appearance in 1.0% CHD formulations (pH 5.9) at 25°C (□) and 40 °C (○). Straight lines were predicted data based on the prediction model equations.

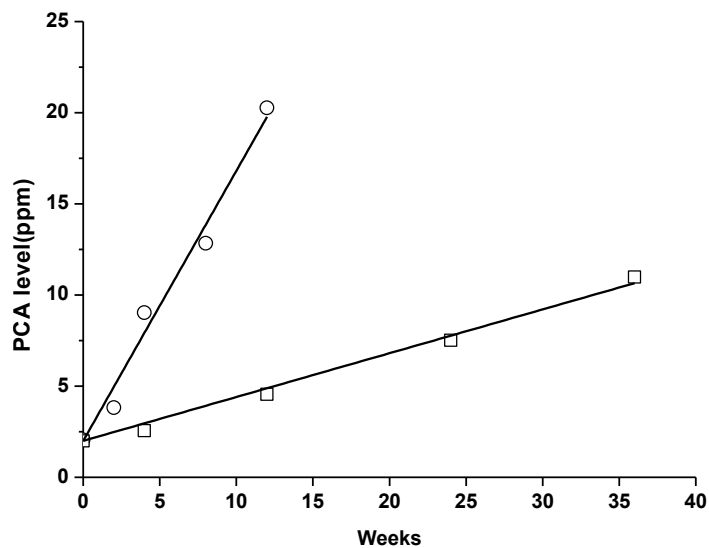


Figure III-6. Correlation between formation of PCA and loss of CHD in acidic and alkaline conditions at 70°C, 80°C, and 90 °C.

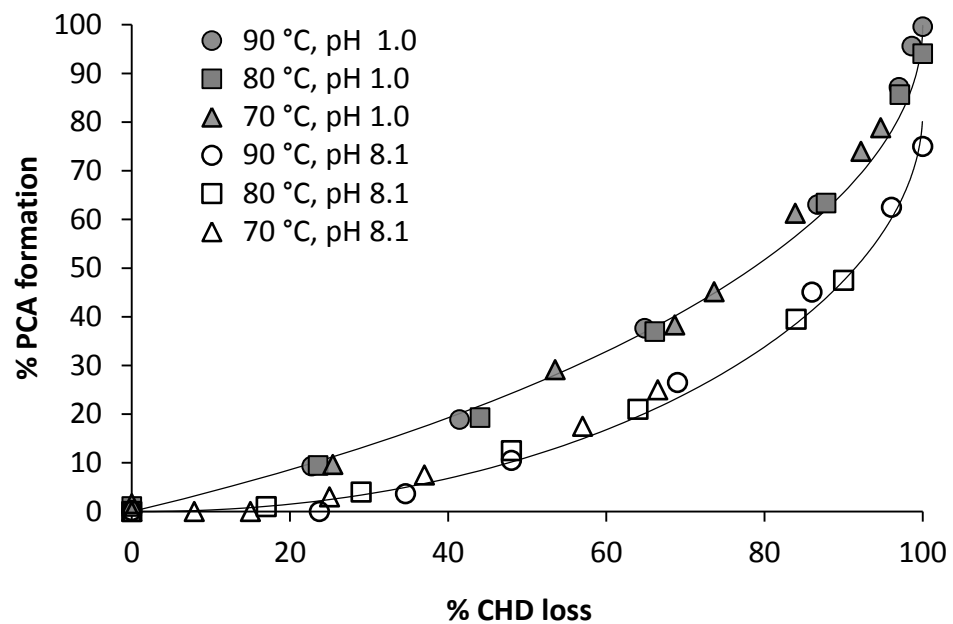


Figure III-7. Predicted critical PCA formation time from CHD digluconate solutions as function of pH at 25°C.

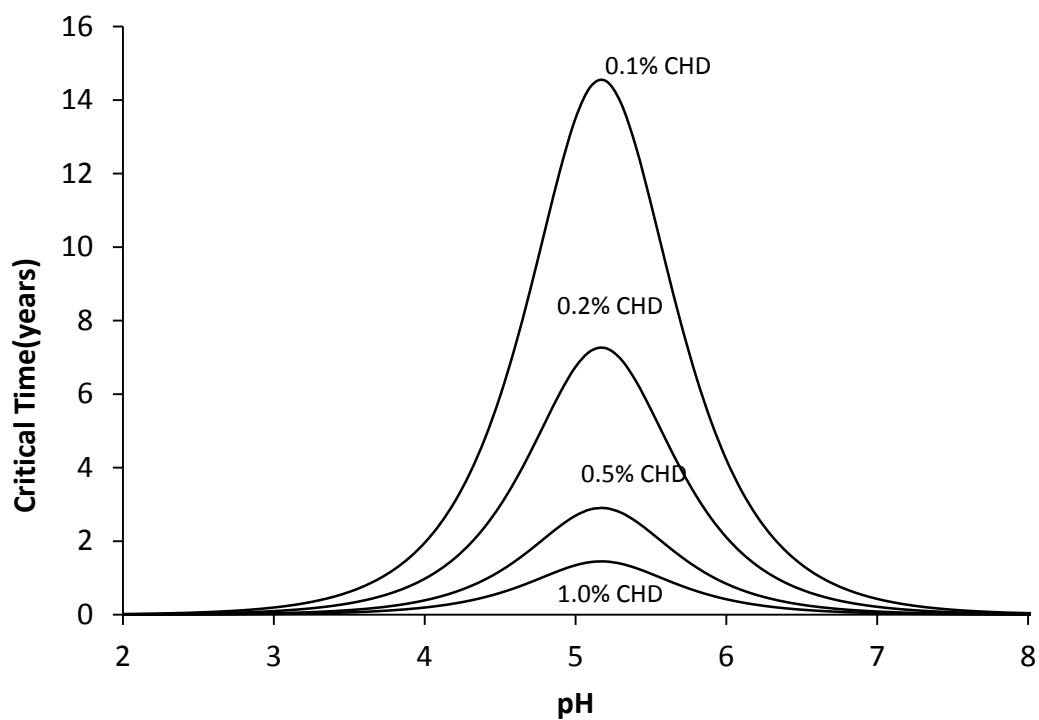
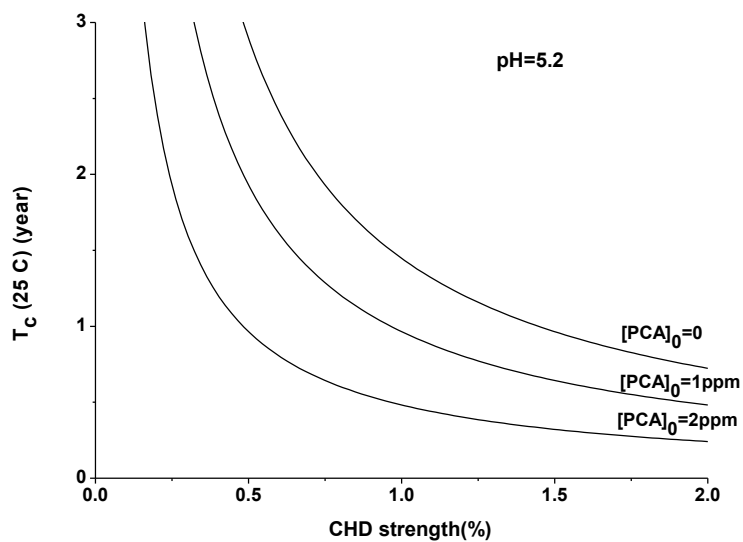


Figure III-8. Predicted critical PCA formation time ( $T_c$ ) for CHD digluconate solution as function of formulation strength at pH 5.2 and 25°C.





CHAPTER IV  
THE STABILIZING EFFECT OF MOISTURE ON THE SOLID-STATE  
DEGRADATION OF GABAPENTIN

Introduction

The research reported in this chapter and Chapter V was part of a multi-institutional project entitled *Development of Quality by Design (QbD) Guidance Elements on Design Specifications Across Scales with Stability Considerations* that encompassed fundamental physical chemical properties investigations; laboratory- and pilot-scale unit operations studies, and process simulation model development efforts conducted by researchers from eight universities over 30 months. The overarching objectives of the project were to investigate approaches to apply QbD principles and model-building technologies to incorporate solid oral drug product stability and scale-up issues into manufacturing quality assurance. A model compound was chosen for this project based on its known propensity to undergo physical and chemical transformations and its current use as a solid oral drug product. The report in this chapter is one of the fundamental physical chemical properties investigations and on the linkage between physical and chemical instability of the model compound.

Gabapentin is a GABA analogue used for the treatment of epilepsy and neuropathic pain. This  $\gamma$ -amino acid has been reported to exist as three polymorphs and a monohydrate and the crystal structures of all of these forms have been reported.(34-36) The commercial drug substance is Form II ( $\alpha$ -gabapentin). Form III ( $\beta$ -gabapentin) has been crystallized from a saturated ethanol solution with heat (60 °C).(36) The Form IV ( $\gamma$ -polymorph) was similarly prepared but at room temperature. Interestingly, Form III is reportedly unique in that intramolecular hydrogen bonding occurs between the amine and carboxylic acid groups whereas only intermolecular hydrogen bonding has been

associated with the crystalline structures of Form II and Form IV between these groups in the  $\alpha$  and  $\beta$ -forms . Form I is the hydrate.(36)

The interconversion between the polymorphic forms has been reported to occur by thermal treatment and milling.(37-39) In the latter case, the presence of various excipients has been reported to induce differences in the polymorphic composition of co-milled gabapentin.(39)

In solution, gabapentin can exist in four ionic forms: cationic, zwitterionic, neutral and anionic species. The carboxylate and amine pKa values have been reported to be 3.7 and 10, respectively.(40-42)

Three studies have been reported on the kinetics and mechanisms of gabapentin instability at elevated temperatures in aqueous solution.(40-42) Gabapentin degrades by intramolecular cyclization to form a five-membered lactam by nucleophilic attack of the alkyl amine on the carboxylate carbonyl followed by dehydration (Figure IV-1). This lactamization reaction is pH-dependent with minimum rate at pH 5.5-6 and is buffer catalyzed. It has been hypothesized that the reactive form is the neutral species which is in equilibrium with the predominant zwitterionic form and requires proton transfer from the amine to the carboxylate.

In lyophilized samples of gabapentin in the presence of various excipients (PVP K30, calcium sulfate, HP- $\beta$ -CD, SBE- $\beta$ -CD, mannitol, D-raffinose, trehalose and lactose), lactamization was studied upon storage at 50 °C and various relative humidity conditions (0, 45 and 75%).(43) The rate of lactamization was highest in the presence of cyclodextrins and PVP K30 and lowest in the neat sample. Lactose also appeared to increase lactamization. High humidity did not consistently increase lactamization rates. Accelerated lactamization in the presence of cyclodextrin (perhaps associated with the formation of inclusion complexes) have been reported in aqueous solution as well as solid-state.(40, 43)

Minimizing lactamization is a critical product quality attribute in that gabapentin lactam has been reported to be 20-fold more toxic.(41) Thus the USP limit on lactam is less than 0.4 %. A number of patents have been issued for stable solid and liquid formulations and manufacturing processes to achieve this target.(44-51) The stability of split and intact tablets have also been compared and found to be the same.(52, 53)

The key objective of the work presented here with respect to the overarching project goals was to 1) provide evidence for the linkage between manufacturing-stress induced physical change and subsequent chemical instability for the model compound, gabapentin, and 2) provide a rational explanation for the unexpected relation between chemical instability and atmospheric humidity during storage. The first objective was an essential requirement for the project's success whereas the latter objective was necessary first step in the development of a useful solid state drug degradation model.

#### Materials and Methods

Gabapentin was obtained from Hangzhou Starshine Pharmaceutical Co. Ltd (Hangzhou, China) and gabapentin lactam (gaba-L) was purchased from Sigma-Aldrich (St. Louis, MO).

Gabapentin is known to undergo intramolecular cyclization to form a lactam (gaba-L) with concomitant loss of water however the drug substance itself (crystalline Form II anhydrate) is resistant to chemical instability. In order to generate relatively unstable gabapentin and to evaluate the effects of manufacturing stress on chemical stability, approximately three grams of drug substance was placed in a 45 mL milling bowl with four hardened steel balls (15 mm) and milled in a planetary mill (Pulviserette 7, Planetary Micro Mill) for 15 to 60 minutes. Unmilled and milled gabapentin were stored at 50 °C, and the relative humidity ranged between 5 and 80% using storage chambers containing saturated salt solutions as described below. The unmilled and milled

samples were assayed for gabapentin and gaba-L by RP-HPLC and also subjected to PXRD, solid-state NMR and surface area analyses.

### Chromatographic Methods

Chemical instability measurements were made using two methods both of which involved detection of the % mole formation of gaba-L by chromatographic methods.

- 1) The level of gaba-L generated during milling was determined using samples taken before and after milling and measuring gaba-L levels by HPLC methods described below.
- 2) The susceptibility of process-stressed gabapentin to thermally induced chemical degradation was determined by storing an aliquot of milled gabapentin at 50 °C (5 % RH) for 24 hours. The initial rate of gaba-L formation (i.e. lactamization rate) was determined by measuring the time-dependent increase in % mole concentration of gaba-L in the thermally-treated solid after 24 hours storage.

Chromatographic analysis was carried using a high/low assay(54) wherein trace amounts of degradation product (gaba-L) were measured using high concentrations of parent gabapentin (~12 mg/mL) and gabapentin mass was measured at low concentrations (about 2.4 mg/mL). These two results were then used to compute the gaba-L content as a mole percentage (w/w) of total gabapentin (gabapentin plus gaba-L) . Calibration standards for the gaba-L and gabapentin were prepared in the range of 0.0005-0.005 mg/mL and 0.5 to 5 mg/mL, respectively. The HPLC system was a Thermo Spectrum System P4000 pump, AS3000 auto injector, and UV 6000 LP photodiode array detection system. The column was  $\mu$ Bondapak Cyano column 3.9x300mm. Isocratic analysis was conducted using a mobile phase composed of 95 parts buffer (10 mM  $\text{KH}_2\text{PO}_4$ /10 mM  $\text{K}_2\text{HPO}_4$ ) and 5 parts acetonitrile . Mobile phase was filtered through a 0.2 micron filter. Analysis was carried out using an analytical wavelength of 210 nm, flow rate of 1.0 mL/min and a 0.020 mL injection volume. Run times were 10 minutes. Retention volumes for gabapentin and gaba-L were 3.8 and 7.6 mL, respectively (Figure IV-2).

Calibration plots for gabapentin and gaba-L were linear at the range of 0.5-10 mg/mL and 0.5 -10  $\mu\text{g/mL}$ .

#### Surface Area Measurement

Milled and unmilled aliquots of gabapentin were evaluated by measuring the specific surface areas by nitrogen adsorption. To fractionate gabapentin into different particle sizes ranges, a 5 gram aliquot of gabapentin was placed in #35 sieve on top of a six sieves of various sizes. Then all sieves were loaded in a Vibratory 3-in Sieve Shaker (Model SS-5, Gibson Company, Inc, Worthington, OH). After shaking for 0.5 hour, powder particles were distributed into sieve fractions using the following sieves: #35 (500  $\mu$ ), #120 (125  $\mu$ ), #140 (106  $\mu$ ), #170 (90  $\mu$ ), #230 (63  $\mu$ ), #400 (38  $\mu$ ), #450 (32  $\mu$ ), #500 (27  $\mu$ ), and #635 (20  $\mu$ ).

Specific surface area was determined using a Quantasorb sorption system. Nitrogen was used as adsorbate gas, and helium was used as carrier gas. A five point BET analysis was conducted on the samples, and the specific surface area was calculated based on BET plot and weight of samples.

#### TGA and DSC

A thermo-gravimetric analyzer (TGA, Model Q50, TA Instruments, New Castle, DE) and a differential scanning calorimeter (DSC, Model 2920, TA Instruments) were connected to a thermal analysis operating system (Thermal Analyst 2000, TA Instruments). Approximately 2 to 6 mg of the sample, in a crimped aluminum pan or an open aluminum pan, was heated from room temperature to 250  $^{\circ}\text{C}$  at varying rates under nitrogen purge.

#### Powder X-ray Diffraction

XRD analysis was conducted as follows: samples were filled in a glass holder and exposed to Cu  $K\alpha$  radiation (45 kV x 40 mA) in a wide angle X-ray diffractometer

(model D5005, Bruker, Madison, WI) at ambient temperature. The instrument was operated in a step-scan mode, in  $0.05^\circ 2\theta$  increments, and counts were accumulated for 1.0 second at each step over the angular range of  $5^\circ$  to  $40^\circ 2\theta$ . Data analyses were performed with commercially available software (JADE, version 8.0, Materials Data Inc., Livermore, CA).

### Solid-state NMR

Solid state NMR spectra were acquired on a CMX spectrometer operating at 300 MHz for proton and 75 MHz for carbon. Samples were packed into a Revolution NMR 7 mm (o.d.) zirconia rotor. The spectra were acquired with cross polarization (CP) using a linear ramp on the proton channel during the CP period. The optimal contact time varied between samples, but was typically around 0.9 ms. Magic angle spinning (MAS) was done at a rate of 4.0 kHz. Proton spin-lattice relaxation data were acquired via saturation recovery. Spinning sidebands were eliminated from non-relaxation spectra via sideband suppression techniques.

### Solid State Degradation

To evaluate the susceptibility of gabapentin materials to thermally-induced degradation, an aliquot of gabapentin (approximately 15 mg) was weighed and placed in a USP type II glass vial, wrapped with aluminum foil, and then stored in desiccators containing anhydrous calcium sulfate (Drierite®) or saturated salt solutions to control the relative humidity at the following values (50 °C) 5 (Drierite), 30.5 (MgCl<sub>2</sub>), 46.9 (Mg[NO<sub>3</sub>]<sub>2</sub>), 74.4 (NaCl) and 81.2 (KCl) %RH at 50 °C for 24, 48, 72 and 96 hours.

Periodically a 1.0 mL aliquot of mobile phase was injected into a sample vial containing thermally-stress gabapentin by using a 25 G needle and 1.0 mL syringe. The vials were shaken until the sample dissolved. Solutions were assayed for gaba-L (high concentration) and diluted 5-fold (low concentration) with mobile phase for analysis of

gabapentin. The gaba-L concentration was calculated as a molar percentage of gabapentin.

### Solution Degradation

Gaba-L solutions (30mM) were prepared in pH 2 and 7 0.1M phosphate buffer and pH 8.5 0.1M borate buffer and stored in Type II glass vials, sealed with a teflon-faced butyl rubber stopper and crimp-secured with an aluminum seal. Vials were immersed in 80 °C water bath for 5 days. A 0.5 mL aliquot was taken by using 25 G needle and 1.0 mL syringe at different time points and subjected to HPLC assay for gabapentin and gaba-L.

### Results

Representative HPLC chromatograms for samples of gabapentin before and after thermal stress (50 °C, 5 % RH) for 24 hours are depicted in Figure IV-2. Retention volumes for gabapentin and lactam were 3.8 and 7.6 mL, respectively. Calibration plots for gabapentin and lactam were linear at the range of 0.5-10 mg/mL and 0.5 -10 µg/mL. Upon thermal stress (50 °C, 24 hours, 5% RH), no significant decrease in gabapentin peak area was observed for this sample, however the gaba-L peak area approximately doubled which illustrates the sensitivity of the HPLC method to very small changes in gaba-L concentration. The limit of detection (LOD) for gaba-L was determined by the signal-to-noise ratio of 3 to be 0.1 µg/mL, and the relative standard deviation for multiple analyses (6 sequential injections of a 0.1 µg/mL gaba-L solution) was 9.5%. The limit of quantification (LOQ) of gaba-L was determined by the signal-to-noise ratio of 10 was 0.5 µg/mL, and the RSD for 6 injections of 0.5 µg/mL gaba-L solution was 1.4% (Table IV-1).

Milling was used to induce manufacturing-type stress in gabapentin. The effects of milling were evaluated by surface area determination, PXRD, solid-state NMR and chemical instability. The specific area increased from 0.20 to 17.7 m<sup>2</sup>/g with milling

duration of 0 to 60 minutes (Table IV-2). Unmilled and milled gabapentin samples showed similar PXRD patterns (Figure IV-3) that were consistent with maintenance of Form II as the predominant polymorphic form, although the intensity of typical Form II XRD peaks at  $7.8^\circ$  and  $14.9^\circ$   $2\theta$  decreased with increased milling time. Solid state NMR spectra (Figure IV-4) showed no significant changes in the chemical shifts for milled and unmilled samples although again significant peak broadening was observed.

The effects of milling on chemical stability was measured in two ways: the change in gaba-L content before and after milling (“in-process lactam”) and the susceptibility of milled samples to further degradation (rate of lactimization at  $50^\circ\text{C}$ ). During the milling operation gaba-L levels increased from 0.007 mole % for unmilled gabapentin to 0.042, 0.095, 0.152 and 0.234 mole % during milling for 15, 30, 45 and 60 minutes, respectively.

Milled samples were subsequently thermally stressed at  $50^\circ\text{C}$  and 5 % RH and the initial rates of lactimization were measured after 24 hours. The lactimization rate increased with increased duration of milling. The lactimization rates were 500 times faster in samples of gabapentin milled for 60 minutes compared to the unmilled samples (Table IV-2). Moreover, increased rates of lactimization in the milled samples correlated to increased surface area, milling duration and in-process lactam levels.

An attempt was made to investigate the relationship between surface area and lactimization rate using both milled and unmilled gabapentin by separating an aliquot of gabapentin into sieve fractions and subjecting each fraction to thermal stress to determine the initial lactimization rate associated with unmilled gabapentin with different particle sizes. For the sieve fractions of unmilled gabapentin ranging in specific surface area from 0.1 to  $0.9\text{ m}^2/\text{g}$ , the lactimization rate increased with increasing surface area from about 0.007 to 0.015 mole%/day; and for 10 minutes milled gabapentin ranging in specific surface area from 4.2 to  $5.7\text{ m}^2/\text{g}$ , the lactimization rate increased from about 0.055 to 0.063 mole%/day (Table IV-2).



The rate of lactamization in milled samples exposed to different levels of atmospheric humidity at 50 °C gave rise to the most surprising results (Figure IV-5). The lactamization rate was greatest in the presence of the lowest humidity conditions and dramatically decreased with increasing humidity. In particular, milled gabapentin appeared to be much more stable at humidity levels greater than 31 % RH.

### Discussion

The measurement of lactamization rate was a useful method for determining gabapentin chemical instability. One potential complication in using gaba-L appearance rate as a measure of gabapentin instability is that gaba-L is demonstrably volatile at elevated temperatures. However the rate of evaporative loss of gaba-L was < 3%/day at 50 °C. Moreover when an aliquot of gaba-L was placed in a controlled humidity chamber (5, 31, 47, 74 or 81 % RH) and stored for 3 days at 50 °C, the percentage recovery was 99 to 102 % .Therefore gaba-L loss by vaporization during exposure to elevated temperatures was not expected to significantly affect the measured lactamization rate.

The lack of changes in PXRD patterns and solid state NMR chemical shifts between milled and unmilled samples that could be attributed to polymorphic transition suggests that the extent of any milling-induced form changes under the conditions used in our studies were sufficiently small as to avoid detection by these techniques. Additional NMR analysis on milled samples has demonstrated significant <sup>1</sup>H relaxation time changes; these results are presented in a separate manuscript. Moreover subsequent milling studies under more rigorous conditions have revealed polymorphic changes, and a separate manuscript has been prepared to discuss these results. Moreover, Lin et al. has reported polymorphic changes detected by FTIR upon more rigorous milling conditions in the presence and absence of co-milled excipients.(37)

### Effects of Milling

Duration of milling clearly impacted both the generation of gaba-L during this unit operation and also affected the susceptibility of the milled material for further degradation by intramolecular cyclization to form gaba-L. The effects of milling could be due to the dramatic increase in surface area associated with particle size reduction. Alternatively crystal disorder associated with the milling stresses could also be a major factor in the increased lactamization rate.

An attempt was made to investigate the relationship between surface area and lactamization rate by separating aliquots of milled and unmilled gabapentin into sieve fractions and subjecting each sieve fraction to thermal stress to determine the dependence of lactamization rate on particle size. The magnitude of the effects of particle size and lactamization rate were compared for aliquots of gabapentin that were milled for 15, 30, 45 and 60 minutes and for sieve fractions obtained from an unmilled aliquot of gabapentin or an aliquot milled for 10 minutes.

For sieved and unsieved aliquots, particle size differences were measured by specific surface area. The lactamization rates are compared to the measured specific surface areas of all aliquot in Figure IV-6. A least squares correlation line for each group was estimated to illustrate the magnitude of the apparent correlation between lactamization rate and specific surface area. The slope of this correlation line was five times greater for the milled unsieved aliquots than either the sieve fractions obtained from milled or unmilled aliquot. This observation suggests that the effect of milling could not be explained solely by the increase in surface area with increased milling time but was more likely due to increased regions of crystal disorder caused by the milling stresses.

### Effects of Moisture

The effect of moisture on the solid state stability of milled gabapentin was unexpected. At high humidity ( $\geq 74$  % RH and 50 °C), the rate of lactimization was essential zero whereas at low humidity (5 % RH and 50 °C) the initial rate of lactamization for the same aliquot of milled gabapentin was about 0.7 mole%/day. This apparent stabilizing effect of humidity on gabapentin degradation could be explained by a number of phenomena including: 1) loss of lactam during humidity-facilitated vaporization, 2) decreased rate of lactamization due to mass law effect, 3) decreased rate of lactamization due to formation of stable gabapentin hydrate, 4) decreased rate of lactamization due to competitive crystal defect annealing process that is facilitated by surface adsorbed moisture. We have attempted to investigate each of these possibilities.

If the rate of lactamization was same or greater in humid conditions than in a dry atmosphere then it is conceivable that the observed rate decrease under humid conditions was due to loss of gaba-L by vaporization and subsequent dissolution of gaseous gaba-L into the saturated salt solution. This explanation is unlikely because although gaba-L is volatile, the rate of gaba-L loss by TGA is much slower than the rate of lactamization under dry conditions. Moreover there was no apparent increase in gaba-L mass loss in the presence of saturated salt solutions and the detected amount of gaba-L in the saturated salt solutions used to humidify the storage chamber was  $\leq 5\%$  of the amount of gaba-L present in the solid-state (Table IV-3).

Intramolecular lactamization of gabapentin is a dehydration reaction resulting in the stoichiometric formation of gaba-L and water. Therefore, if the reaction is reversible, then the presence of surface-adsorbed water could decrease the lactamization rate by mass law effect. This hypothesis was tested using two experiments. Firstly, an aliquot of milled gaba-L powder was subjected to elevated temperature (50 °C) and humidity conditions (31 to 81 % RH) for three days, and the gaba-L mass balance and the appearance of gabapentin was determined by HPLC. Secondly, an attempt was made to

hydrolyze gaba-L at 80 °C for 5 days in aqueous buffered solutions at pH values of 2.2, 7.0 and 8.5. No detectable loss of gaba-L or appearance of gabapentin was observed in solution or solid-state. Therefore the decrease in lactamization rate of gabapentin under high humidity conditions could not be explained by mass law effect because the reaction does not appear to be reversible even under these more rigorous conditions. It should be noted parenthetically that several patents (55-57) have disclosed a synthetic process for gabapentin involving the hydrolysis of gaba-L in the presence of 50% hydrochloric acid by refluxing at 108 °C for 6 hours.

Formation of stable hydrate form at high humidity is another possible reason. An aliquot of gabapentin sample was milled for 60 minutes to generate high level of crystal defects, and then the sample was stored at 81% RH and room temperature for 1 day. From the XRD pattern, there was no detectable gabapentin hydrate peaks (Figure IV-7) found, but the lactamization rate was significantly decreased. Therefore, formation of stable hydrate form is not likely the cause for the stabilizing effect.

Another explanation for the stabilizing effect of moisture on the chemical degradation of gabapentin is that high humidity conditions facilitate the “self-healing” of crystal defects generated by milling. Thus at high humidity, milling-damaged crystals are able of recovering or at least transitioning to a form of gabapentin that is incapable of spontaneous dehydration. And if the recovery (or termination) process is kinetically competitive with lactamization then a decrease in the apparent lactamization rate will be observed.

Although altered crystalline forms due to manufacturing stress are consistent with the changes observed in PXRD and SSNMR data and with the evaluation of the relationships between surface area and lactamization rate for milled and unmilled gabapentin, the direct detection of specific form transitions was not observed and therefore recovery or “self-healing” could not be directly observed. This inability to obtain direct empirical evidence was primarily due to the detection limits of the physical

characterization methods employed and the small extent of milling-induced form changes under the conditions used in this study. Subsequent characterization efforts using additional ssNMR methods (e.g. relaxation times) and PXRD after much more rigorous milling are presented in future manuscripts. These studies showed additional evidence of physical transformation during milling (as has been previously reported in the literature (38) and evidence of accelerated reformation of the stable polymorphic form (Form II) upon exposure to high humidity.

Our hypothesis that humidity promotes the recovery of milling-induced crystal disorder predicts that milled gabapentin subjected to high humidity for a short period of time and then subjected to thermal stress under dry conditions would show significantly decreased rates of lactamization when compared to a control sample of milled gabapentin that had not been exposed to high humidity. This experiment was conducted and the results are presented in Figure IV-8. The lactamization rate for the aliquot that was exposed to 81% RH for 24 hours prior to being exposed to dry heat for an additional 72 hours was much lower than the control sample which was not exposed to high humidity. This result is consistent with the hypothesis that high atmosphere moisture facilitates the recovery of manufacturing-induced crystal defects thereby stabilizing gabapentin. Moreover these results are also inconsistent with gaba-L vaporization or mass law effect hypotheses both of which would have predicted comparable rates of lactamization for the humidified and control samples.

### Conclusion

Gabapentin has been shown to be susceptible to milling-induced chemical instability that can be attributed to the formation of crystal defects that lead to increased rates of lactamization. Moreover, these defects can be annealed by exposure to high atmospheric moisture which stabilizes the milling-damaged drug substance. Additional studies are underway to develop quantitative solid-state degradation model that

incorporates the effects of manufacturing (crystal damage and in-process lactamization) with the effects of co-milled excipients and the environment effects of storage (humidity and temperature) on the kinetics of lactamization. The overarching research objective is to use gabapentin as a prototype drug substance to investigate the relationship between manufacturing variation and drug stability.

Table IV-1. The accuracy of HPLC method.

Sample ID	Sample weight(mg)	Gabapentin detected		Gaba-L added		Gaba-L detected		Detected added gaba-L	
		Weight(mg)	Recovery%	Weight(mg)	Mole%	Weight(mg)	Mole %	Mole%	Recovery%
o1	14.51	14.34	98.82	0.000	0.000	1.056	0.008	n/a	n/a
o2	12.43	12.41	99.81	0.000	0.000	0.761	0.007	n/a	n/a
o3	11.99	11.86	98.91	0.000	0.000	0.765	0.007	n/a	n/a
A1	11.42	11.40	99.81	1.021	0.010	1.813	0.018	0.010	103.30
A2	13.30	13.47	101.25	1.021	0.008	1.919	0.016	0.008	100.18
A3	11.06	11.22	101.49	1.021	0.010	1.830	0.018	0.011	106.11
B1	11.93	12.11	101.50	2.553	0.024	3.343	0.031	0.023	99.40
B2	13.49	13.41	99.37	2.553	0.021	3.591	0.030	0.022	105.73
B3	13.41	13.51	100.72	2.553	0.021	3.477	0.029	0.021	101.00
C1	14.4	13.96	96.96	5.106	0.041	5.971	0.048	0.040	98.74
C2	11.81	12.01	101.68	5.106	0.048	6.193	0.058	0.050	105.63
C3	14.28	13.96	97.74	5.106	0.041	6.179	0.049	0.042	102.82
D1	12.11	12.05	99.52	10.212	0.095	11.063	0.102	0.095	100.47
D2	12.34	12.33	99.94	10.212	0.092	10.882	0.099	0.091	98.52
D3	12.48	12.60	100.99	10.212	0.090	11.098	0.098	0.091	100.45
E1	12.92	12.68	98.16	25.53	0.224	26.045	0.229	0.222	98.70
E2	11.98	12.03	100.39	25.53	0.237	26.136	0.242	0.235	99.23
E3	11.17	11.15	99.80	25.53	0.255	26.259	0.263	0.255	99.94
F1	10.86	11.13	102.51	51.06	0.510	51.439	0.514	0.506	99.28
F2	13.48	13.45	99.79	51.06	0.422	52.273	0.432	0.425	100.61
F3	10.72	10.80	100.78	51.06	0.525	51.826	0.533	0.526	100.08
G1	12.58	12.49	99.28	127.65	1.129	127.370	1.127	1.119	99.13
G2	11.20	11.26	100.51	127.65	1.251	128.290	1.258	1.250	99.90
G3	13.04	12.91	99.02	127.65	1.093	127.901	1.095	1.088	99.51

Table IV-2. Specific surface area, initial gaba-L concentration and lactamization rate.

milling time (minute)	Sieve fraction (sieve mesh size, microns)	Specific surface area(m <sup>2</sup> /g)	Initial gaba-L (mole %)	lactamization rate (mole%/day)*
0	125	0.1	0.0037	0.007
0	106	0.3	0.0064	0.013
0	90	0.4	0.0096	0.006
0	63	0.6	0.0057	0.013
0	38	0.9	0.0117	0.015
10	32	4.2	0.055	0.242
10	27	4.7	0.050	0.245
10	20	4.9	0.057	0.248
10	<20	5.4	0.063	0.250
0		0.2	0.007	0.002
15		5.7	0.042	0.355
30		12.1	0.095	0.632
45		16.2	0.152	0.842
60		17.7	0.234	0.954

\*Lactamization rate was measured at 5%RH and 50 °C.



Table IV-3. Gaba-L recovery in saturated salt solutions.

Powders	RH	Saturated salt solution	Total Gaba-L mole%	% Gaba-L recovered After 96 hours at 50 °C	
				In solid	In saturated solution
Milled gabapentin	31%	MgCl <sub>2</sub>	1.49	98.14	0.93
	47%	Mg(NO <sub>3</sub> ) <sub>2</sub>	1.27	98.82	0.78
	74%	NaCl	1.04	95.61	3.92
	81%	KCl	1.02	95.54	3.57
Milled Gaba-L	31%	MgCl <sub>2</sub>	100.00	99.78	0.19
	47%	Mg(NO <sub>3</sub> ) <sub>2</sub>	100.00	99.96	0.02
	74%	NaCl	100.00	99.90	0.08
	81%	KCl	100.00	99.87	0.12

Figure IV-1. Lactamization of gabapentin.

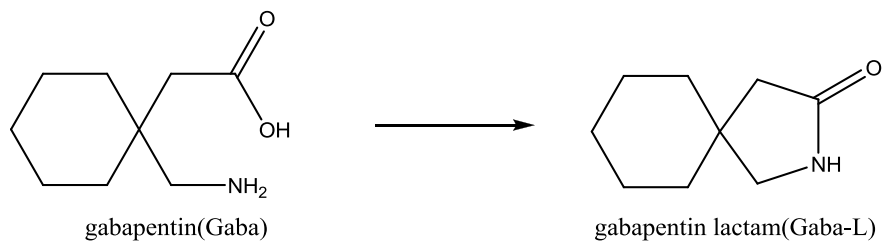


Figure IV-2. Representative HPLC chromatograms showing peaks for gabapentin and gaba-L. Thermal stress condition was 50 °C in a sealed vial for 1 day.

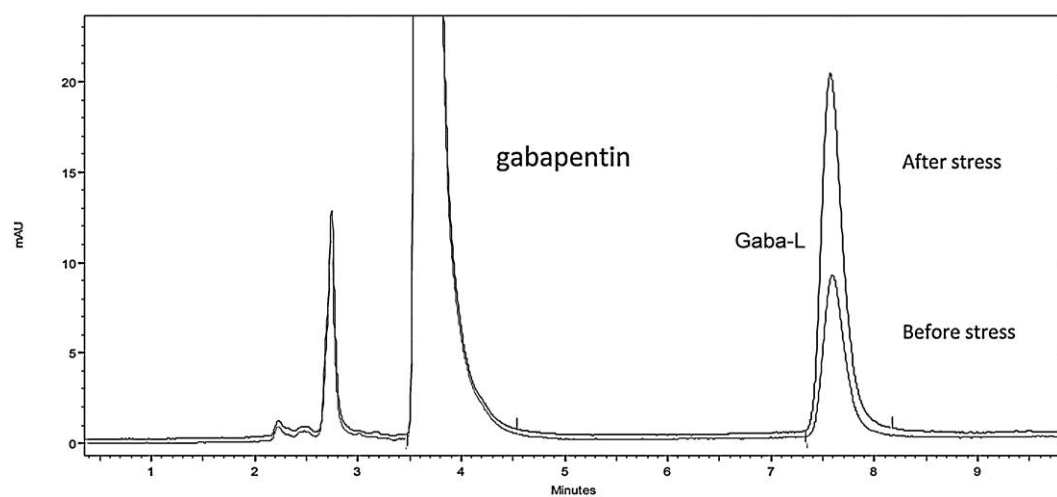


Figure IV-3. XRD patterns of unmilled and milled gabapentin samples.

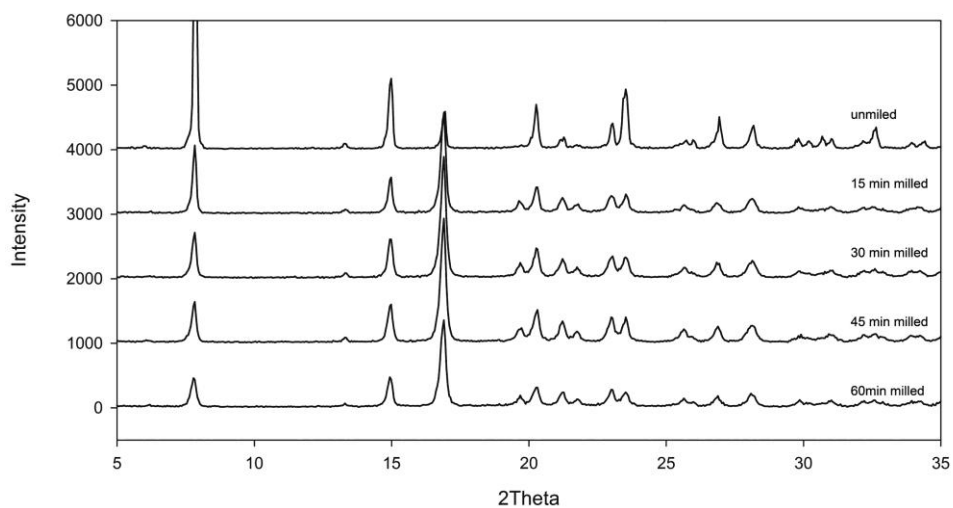


Figure IV-4. Solid State NMR spectrum of unmilled and milled gabapentin samples.

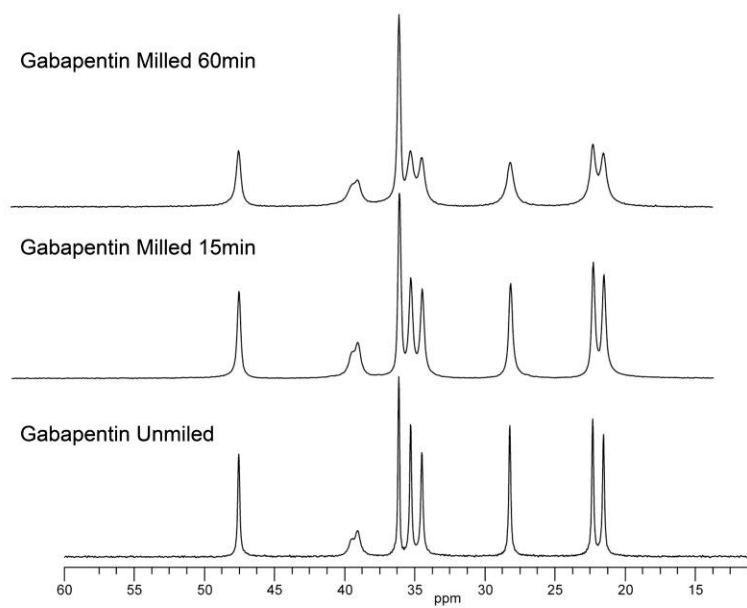


Figure IV-5. Gaba-L formation from 60 minutes milled gabapentin sample at 50 °C and different relative humidity.

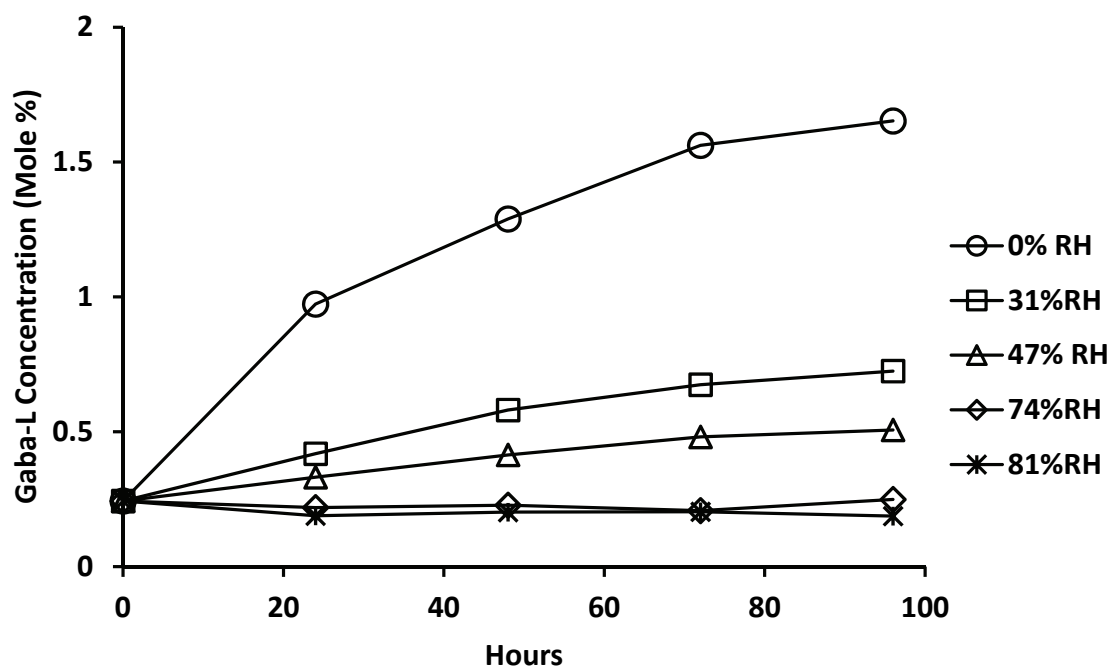


Figure IV-6. Lactamization rate (mole%/day at 5%RH and 50 °C) for gabapentin samples as a function of the measured specific surface area. *Empty square* sieved fractionated unmilled gabapentin, *empty triangle* sieved fractionated 10 min milled gabapentin, *filled circle* 15, 30, 45, and 60 min milled gabapentin samples.

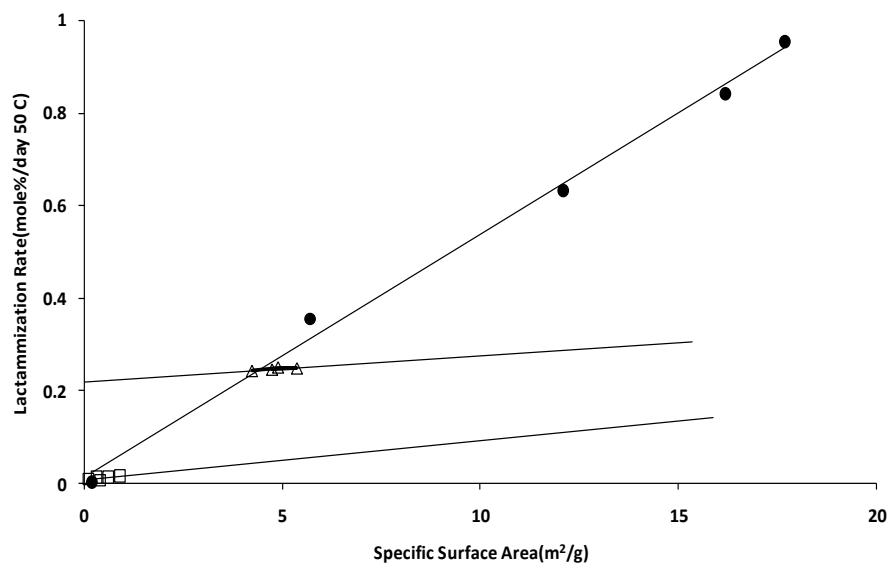


Figure IV-7. XRD patterns of moisture treated milled gabapentin sample and gabapentin monohydrate.

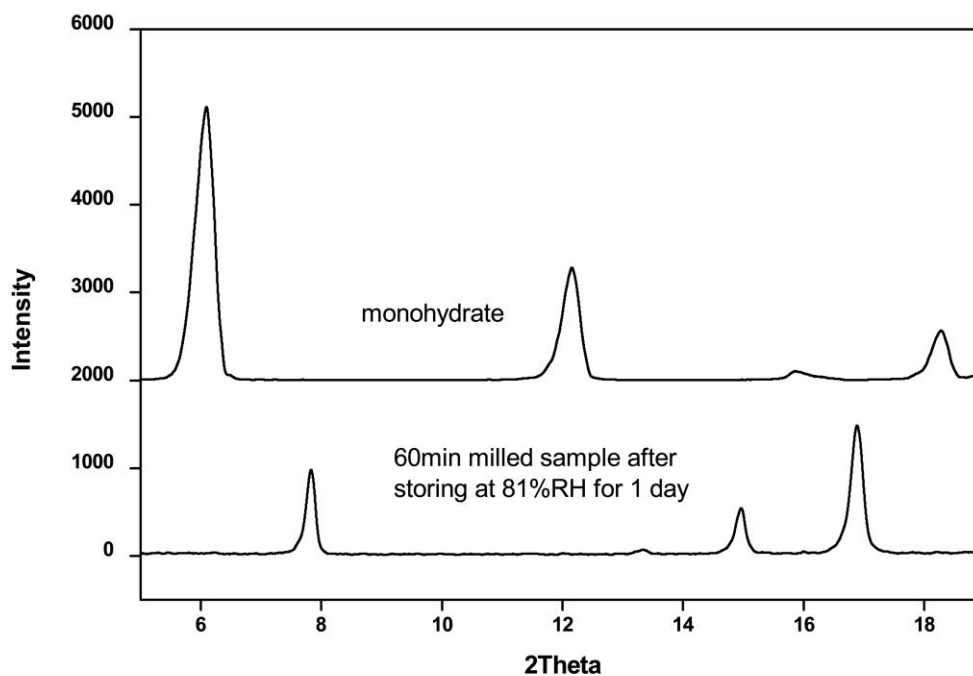
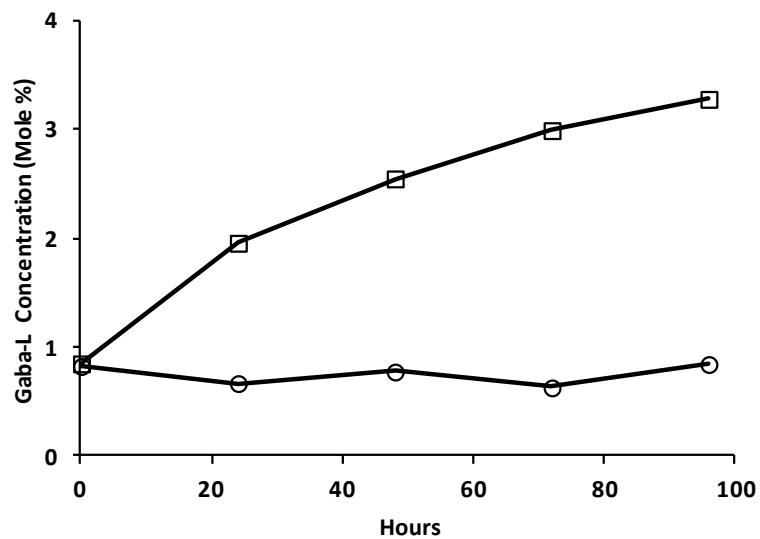




Figure IV-8. Gaba-L formation from moisture pretreated gabapentin sample. *Empty square* sample was stored at 25 °C 0% RH for 24 hours before thermal stress, *empty circle* sample was stored at 25 °C 81% RH for 24 hours before thermal stress.



CHAPTER V  
KINETIC MODEL FOR SOLID-STATE DEGRADATION OF  
GABAPENTIN

Introduction

The use of gabapentin as model for studying the connection between manufacturing-related stress and solid-state oral drug product has been the subject of an FDA-supported, multi-year project involving researchers at nine universities working collaboratively with industrial and governmental scientists under the leadership of the National Institute for Pharmaceutical Technology and Education.(58) The overarching objective of this research was aimed at incorporating stability and unit operation scaling issues into a Quality-by-Design paradigm for manufacturing quality control. Gabapentin is an ideal model compound for this project because of its proclivity to exist in various physical forms, its propensity to undergo structural disorder when subjected to mechanical stress and the susceptibility of the disordered material to chemical degradation by intramolecular cyclization.

As reported in Chapter IV, gabapentin, a  $\gamma$ -aminobutyric acid, was originally developed to treat epilepsy. Its major chemical degradation pathway is intramolecular cyclization to form gabapentin-lactam (gaba-L) by nucleophilic attack of the amine on the carboxylate carbonyl followed by dehydration. We have found that the formation of lactam is irreversible in solution and solid state under mild pH and temperature conditions associated with gabapentin formulations. Gaba-L has a reported toxicity of 300 mg/kg (DL<sub>50</sub>, mouse) compared to 8000 mg/kg for gabapentin.(59, 60) The US Pharmacopeia has a limit on gaba-L to be no more than 0.4% in gabapentin tablets.(61) Thus, minimizing lactamization is a critical product quality attribute.

Gabapentin has been reported to exist in three polymorphs (Forms II, III, and IV) and a monohydrate (Form I).(62, 63) All polymorphs are described by intermolecular

hydrogen bonds between amino and carboxyl groups from neighboring molecules, intramolecular hydrogen bonds have been reported for Form III. (63) Form II is the most physically-stable anhydrous form and is the predominant form present in solid pharmaceutical dosage forms. Forms III and IV have been reported to transform into Form II under a variety of conditions including exposure to elevated humidity (e.g. 50% RH).(64) Thermal treatment and mechanical stress (e.g. milling) has been reported to induce inter-conversion between the polymorphic forms.(64-66)

In Chapter IV, we have reported that gabapentin undergoes physical changes during milling and upon subsequent storage under various environmental conditions that can affect its degradation kinetics. We have hypothesized that milling induces crystal disorder which results in an observed increase in the rate of chemical degradation. Additionally we have reported that the subsequent exposure to high humidity decreases the apparent lactamization rate, and we have hypothesized that this apparent moisture “stabilization” is likely due to the competitive recovery of crystallinity wherein milling-induced crystal defects were lost upon exposure to high moisture thereby stabilizing the milling-damaged drug substance.

The objective of the work reported herein is to develop quantitative kinetic model that accounts for the effect of milling stress and environmental storage conditions on lactamization rate. This model forms the basis for connecting manufacturing-related effects on the physical integrity of the model drug substance to its subsequent chemical stability under a range of environmental conditions.

#### Materials and Methods

Gabapentin was obtained from Hangzhou Starshine Pharmaceutical Co. LTD (Hangzhou, China), and gaba-L was purchased from Sigma-Aldrich (St. Louis, MO). All other chemicals, solvents and water used were HPLC grade.

### X-Ray Powder Diffraction

X-Ray Powder Diffraction was used to identify polymorphic changes in gabapentin samples. The analysis was conducted as follows: samples were filled in a glass holder and exposed to Cu K $\alpha$  radiation (45 kV x 40 mA) in an X-Ray diffractometer (Shimadzu LabX XRD-6000) at ambient temperature. The instrument was operated in a step-scan mode, in 0.05  $^{\circ}2\theta$  increments, and counts were accumulated for 1.0 second at each step over the angular range of 5 to 40  $^{\circ}2\theta$ . Data analyses were performed with commercially available software (JADE, version 5.0).

### Chromatographic Methods

The mole fraction of gaba-L was determined by HPLC, as has been previously reported.<sup>1</sup> In brief, the HPLC system consisted of a Thermo SpectrumSystem P4000 pump, AS3000 auto injector, and UV 6000 LP photodiode array detector. The column was a 3.9x300mm  $\mu$ Bondapak Cyano column. Mobile phase composed with 95 parts buffer (10 mM KH<sub>2</sub>PO<sub>4</sub>/10 mM K<sub>2</sub>HPO<sub>4</sub>) and 5 parts acetonitrile. The mobile phase was filtered through 0.2  $\mu$ m filter before using. Analysis was carried out using an isocratic method with a flow rate of 1.0 mL/min, and an analytical wavelength of 210 nm. Retention volumes for gabapentin and gaba-L were 3.8 and 7.6 mL, respectively. As reported previously, limit of quantitation for gaba-L was 0.5  $\mu$ g/mL.

### Milling Stress

Aliquots (2.0 grams) of gabapentin were placed in 45 mL milling chamber with four stainless steel balls (25 mm), and milled in a planetary mill (Pulviserette 7, Planetary Micro Mill) for 0, 15, 45, 60 minutes and speed setting 5 or for 60 minutes using a speed setting of 7. XRD was used to confirm that the drug substance was form II upon receipt. Milled gabapentin samples were analyzed by XRD for crystal form changes and also assayed by HPLC to measure for chemical changes. At mill speed setting of 5 no polymorphic changes were observed, however using a speed setting of 7 and milling

duration of 60 minutes, XRD changes were observed that were consistent with the formation of Form III.

### Degradation Kinetics

Lactamization kinetics was determined using either aliquots of unmilled gabapentin or gabapentin that had been milled for 15, 45 or 60 minutes at a speed setting of 5. Gaba-L appearance profiles were measured by placing aliquots of milled gabapentin (15 mg) in glass vials, and then storing them in desiccators containing anhydrous calcium sulfate (Drierite®) or saturated salt solutions to control the relative humidity at the following values 5 (Drierite), 11 (LiCl), 31 (MgCl<sub>2</sub>), 50 (Mg[NO<sub>3</sub>]<sub>2</sub>) %RH at various isothermal conditions (40 - 60 °C) . Periodically samples were removed from stability chamber and dissolved in 1.0 mL 5% acetonitrile, and assayed for gaba-L and gabapentin. The gaba-L concentration was calculated as a molar percentage of the sum of gaba-L and gabapentin in the sample. Mass balance was 100%(±2%) of the initial amount of substrate at all time points.

Degradation kinetic models were parameterized using nonlinear regression (WinNonlin v. 5.2). A representative WinNonlin model file is shown in Appendix C.

### Long-term Stability Studies

Gabapentin drug substance (Form II) was blended with HPMC with 2.5-5.5% moisture content and median particle size from 160 µm to 270 µm. Then these initial blends were subjected to high shear wet granulation at various spray rates (12-18 g/min) and impeller speeds. These granules were put into fluidized bed for drying to different target moisture end point (0.5-1.0%) with various environmental equivalency factors. The granules then were milled, sieved and blended at low and high blending speed and different fill ratios (60 and 80%). The initial blends and final blends were compressed to tablets under different forces from 5 kN to 15 kN. These blends and tablets were prepared by collaborators at Duquesne University and University of Maryland.

Stability studies were conducted by the authors at the University of Iowa. The initial gaba-L and susceptibility to thermal stress (change of gaba-L mole % after 1 day 50 °C 5%RH stress) were estimated for these blends and tablet samples. Aliquots of blends and tablet samples (40 mg) were weighed and stored in type II glass vials at 22, 40, 50 °C and 11%RH for 3 months. Samples were pulled out after 0.5, 1, 2, 4, 8, 12 weeks of storage and gabapentin and gaba-L levels were immediately measured by HPLC. Gaba-L levels were calculated as mole percent based on the detected gaba-L and gabapentin amount.

### Results

Typical gaba-L formation profile obtained by storing aliquot of gabapentin at 40 °C and 5%RH for 25 days after drug had been milled for 60 minutes are depicted in Figure V-1. This profile can be described by the predominant degradation events occurring in two stages. Initially the lactamization rate is due to the rapid conversion of structurally-compromised substrate which was created during milling. Upon the nearly complete conversion of the structurally-disordered substrate crystal, the gaba-L appearance rate decreased and then accelerated as the kinetics was predominated by disorder propagation and chemical conversion to gaba-L as is typical of the Prout-Tompkins autocatalytic kinetics. Thus a simple model involving the consecutive irreversible processes of crystal defect propagation and spontaneous covalent dehydration is adequate to account for lactamization kinetics wherein the initial conditions are determined by the concentrations of intact gabapentin, disordered gabapentin and gaba-L.

As we have previously reported, the unexpected effect of increase humidity was to *decrease* the rate of lactam formation. We have presented empirical evidence that this effect is likely due to a humidity-induced *increase* in kinetics of recovery, that is the conversion of disordered-crystal back to structurally intact (or unreactive) substrate crystal. Thus a reasonable hypothetical model for lactamization (Figure V-2) includes

the physical transitions associated with crystal defect propagation and recovery followed by the subsequent the covalent conversion of reactive (disordered) gabapentin to gaba-L by intramolecular cyclization.

The quantitative effects of milling duration (at the lower speed setting) on lactam formation are depicted in Figure V-3. The gaba-L appearance profiles obtained after milling gabapentin aliquots for 15 to 60 minutes were largely parallel although the extent and rate of initial lactam formation increased for aliquots subjected to longer milling times.

The effects of humidity during storage of milled gabapentin samples are shown in two figures. In Figure V-4, the gaba-L appearance profiles resulting from the storage of aliquots of milled gabapentin (60 minute duration at speed setting 5) at 5, 11, 31 and 50 % relative humidity are compared. As the storage humidity increases, both the initial rate and (more profoundly) the autocatalytic second phase of lactam formation appear to be dramatically suppressed. In fact, at 50% relative humidity storage the appearance rate of lactam is almost absent.

Additional aliquots of gabapentin were milled under more rigorous conditions (60 minutes at a speed setting of 7). These samples were stored at 5% or 31 % RH (25 °C). The XRD patterns for these samples were measured periodically for two days (Figure V-5). In contrast to XRD spectra for gabapentin milled under more mild conditions, the initial XRD patterns for these samples indicated the present of two polymorphic forms: Form II and Form III. Upon storage, at 5% RH no detectable XRD changes were observed at 47 hours (Figure V-5a). However for the sample stored at 31%RH (Figure V-5b) the XRD peaks associated with Form II (stable API form) significantly increased over the same period of time. These results support our previous hypothesis that moisture accelerates the physical transitions resulting in the formation of relatively chemically-stable crystal Form II.

The temperature effect on the lactam formation is depicted in Figure V-6. Increased lactam formation in samples of 60-minute-milled gabapentin (milling speed setting 5) stored at 5%RH were observed with the increased temperature (40, 50 and 60 °C). At 60 °C storage conditions, the observation of two distinct stages in gaba-L is less obvious than at 50 °C. And at 40 °C storage, the second stage of gaba-L appearance is largely delayed beyond the range of observation.

### Discussion

#### Model Development

Historically, the kinetics of solid-state reactions has been described using various approaches. The Prout-Tompkins model is one of the most commonly used models in crystalline drug degradation.(67) Based on the assumptions of this model, the chemical reaction starts at crystal imperfection sites referred to as “nuclei”. Propagation (or branching) generates new nuclei at the interface between product and substrate. As reaction proceeds, the branching chains may be terminated when the reaction spreads to molecules have already reacted. In this model, the propagation rate is second-order: proportional to the concentrations of product (nuclei) and substrate, and the termination rate is second-order in product concentration.

A generalized Prout-Tompkins equation was derived by Jacobs that provides a description of reaction kinetics during the initiation stage.(68) A mathematically similar equation was developed by Skrdla using a two-step model, which separates nucleation as a non-catalytic reaction depending on the substrate and branching as an autocatalytic reaction depending on both product and substrate.(69)

Another approach that has been used to describe solid-state drug degradation is to treat the substrate as being composed of two distinct phases. One phase is an intact crystalline state, and the other phase is a disordered state that possesses greater mobility and therefore reactivity. A two-phase model was proposed by assuming parallel



degradation processes occur in two phases (i.e. in the intact crystalline and disordered state), and the degradation kinetics are zero-order (constant rate, independent of substrate or product concentrations) in both phases.(70) This model successfully described the initial rate degradation but is of limited value once non-linear product appearance profiles are observed. Moreover this model predicts infinite accumulation of product over time, which is physically incorrect.

From the studies of the effects of processing (manufacturing stress) on solid-state reactions, Zografi and co-investigators proposed that the mechanical stress creates a two phases system composed on crystalline and disordered substrate that degrade independently by parallel first order kinetics. (71) Waterman et al improved on this approach by proposing a model that treats crystalline and disordered substrate phases as inter-convertible forms wherein the degradant arises by an irreversible process from either form. However the kinetics of degradant formation from the disordered substrate predominates over direct formation from the crystalline substrate.(72) In the Waterman model, as in the Zografi model, all individual processes were described by first-order kinetics. Like the Zografi model, the Waterman model can account for an initial rapid rate of degradant formation. A steady state follows the initial rapid degradant formation as the initial amount of disordered-form is consumed. However the autocatalytic degradant formation profile, typical in Prout-Tompkins kinetics, is absent in the Waterman model because all processes are treated as first order reactions.

This inconsistency, as well as the inherent limitations of Prout-Tompkin kinetics and the Zografi model with respect to the observed gaba-L formation profiles, are depicted in Figure V-7. Both the Waterman and Zografi models account to the rapid initial gaba-L increase from crystal-disordered substrate formed during milling. However both of these models fail to account for the subsequent accelerated appearance of gaba-L. Contrariwise, Prout-Tompkins kinetics describes the accelerated appearance but fails to describe the initial formation of gaba-L.

A very important and interesting aspect of the Waterman model is the use of two consecutive steps to describe degradant formation. The first step describes a physical transition from intact crystal to disordered states. This process is reversible; thus, disordered crystal can recover to a largely unreactive form. The first reversible physical transformation is coupled to covalent conversion of the substrate to degradant via a first-order irreversible step. Thus, the Waterman model couples physical instability with chemical instability. This approach is fundamentally different than the usual presentation of Prout-Tompkins model wherein the conversion of the intact crystal combines both covalent and non-covalent processes into a single step. The Waterman model and the other two models have been developed largely to allow for quantitative description of the effects of mechanical (manufacturing) stress on the initial rates of degradant formation. Moreover they appear to be physically realistic in allowing for the existence of multiple forms of substrate with different reactivity. Where both the Waterman and Zografi models appear to fail is when autocatalytic processes become important in the appearance of degradant.

Thus, the direct application of these models is inadequate to describe the kinetics of gabapentin lactamization. As illustrate in Figure V-7, gaba-L appearance rate from milled gabapentin is initially rapid, followed by a notable deceleration and subsequent nonlinear acceleration. Direct use of Prout-Tompkins equation does not give an accurate prediction on gaba-L formation during the rapid accumulation initial stage (Figure V-7). The two-phase models of Waterman and Zografi fit the initial stage reaction, but fail to account for the non-linear acceleration at the second stage (Figure V-7). Thus, our approach has been to combine the useful elements of the two phase and Prout-Tompkins models into a more robust and physically-realistic form.

### Gabapentin Degradation Kinetics

Drug substances are often exposed to mechanical stresses during pharmaceutical manufacturing processes such as blending, roller compaction, milling and tablet compression. Numerous of studies have shown that milling process can induce polymorphic conversion or generation of amorphous materials.(73, 74) It has been known that part of active mechanical energy applied to solid can be stored in the form of lattice defects and this structural disordering state is a thermodynamically unstable state.(75)

As in the Zografi and Waterman models, we have described the effect of milling by a reactive component,  $Gaba^*$ , that represents chemically-intact gabapentin in a physical state capable of spontaneous formation of  $Gaba-L$ . In measuring  $Gaba-L$  formation kinetics from gabapentin samples that were milled under mild conditions ( $\leq 60$  minutes, speed setting 5), we did not observe detectable levels of polymorphic substrate other than Form II. Thus  $Gaba^*$  is meant to represent generally-disordered substrate and not a distinct polymorphic form. In our model, the kinetics formation of  $Gaba^*$  is an autocatalytic process, the rate is dependent on chemical intact but physically-disordered gabapentin, and also dependent on  $Gaba-L$  which is both physically- and chemically-changed form of gabapentin. The proposed reaction model is depicted in Figure V-2, and the kinetics can be described by Equations V-1, V-2 and V-3, wherein  $k_1$ ,  $k_2$  and  $k_3$  represent the rate constants for autocatalytic branching, spontaneous dehydration cyclization and recovery, respectively.

$$\frac{d[Gaba]}{dt} = -k_1[Gaba][Gaba^*] + [Gaba-L] + k_3[Gaba][Gaba^*] \quad \text{Equation V-1}$$

$$\frac{d[Gaba^*]}{dt} = k_1[Gaba]([Gaba^*] + [Gaba-L]) - k_2[Gaba^*] - k_3[Gaba][Gaba^*] \quad \text{Equation V-2}$$

$$\frac{d[Gaba-L]}{dt} = k_2[Gaba^*] \quad \text{Equation V-3}$$

The representative gaba-L formation data and predicted data based on Equations 1-3 are shown in Figure V-7. The observed data were also evaluated using Prout-Tompkin, Zografi, and Waterman models. The predicted kinetic curves shown in Figure V-7 were generated using the estimated values of  $k_1$ ,  $k_2$ ,  $k_3$  and  $\text{gaba}_0^*$  (initial concentration of gaba\*). As discussed earlier, the Prout-Tompkins model failed to predict the initial rapid generation of gaba-L, while the Zografi and Waterman models failed to describe the later autocatalytic stage. Our proposed model accounted for gaba-L formation over its entire time course.

#### Quantitative Effect of Milling Duration on Lactamization Kinetics

Kinetic differences due to different milling durations (at low milling speed) were described by our model as should in Figure V-3 wherein the model-predicted and observed data are compared. The estimated rates constant were not changed as a function of milling duration. However the estimated  $\text{gaba}_0^*$  values were 0.46, 0.92 and 1.04 mole% for gaba-L profiles generated from gabapentin samples milled for 15, 45 and 60 minutes, respectively.

#### Quantitative Effect of Temperature on Lactamization Kinetics

The effect of temperature on the estimated rate constants were contained using the data depicted in Figure V-6. The estimated rate constants at each temperature were used to compare model-predicted and observed gaba-L formation profiles at 5% RH and various temperatures (40, 50 and 60 °C). An Arrhenius plot for autocatalytic branching and spontaneous dehydration are shown in Figure V-8. The estimated activation enthalpy ( $\Delta H^\ddagger$ ) for the autocatalytic branching and spontaneous dehydration were 89 and 69 kJ/mol, respectively. Higher activation enthalpy for branching indicates that the degradation reaction is controlled by the growth and propagation of disordered region. The total activation enthalpy in the solid state is in similar magnitude with other solid-

state intramolecular cyclization reactions such as formation of diketopiperazine (DKP) from degradation of enalapril, aspartylphenylalanine or lisinopril.(76-78)

#### Quantitative Effect of Humidity on Lactamization Kinetics

The unexpected effect of humidity on decreasing the rate of gaba-L formation has been previously attributed to an increased rate of annealing of milling-induced crystal defects facilitated at high atmospheric moisture. This concept is consistent with the observed increase in XRPD peak intensity associated with crystal form II in samples of rigorously milled gabapentin exposed to 31% RH moisture (Figure V-5b). Although the possibility exists that moisture may affect all three processes depicted in the scheme shown in Figure V-2, empirical evidence suggests that the predominant effect of moisture is on recovery kinetics of gaba\*. The quantitative effect of moisture on lactamization kinetics is illustrated in Figure V-4. The model-predicted gaba-L profiles were obtained by fitting the rate constants described Equations 1-3 to the observed gaba-L data obtained from storing milled substrate at different RH levels and 40 °C. The effect of relative humidity on the estimated recovery rate constant ( $k_3$ ) was to cause a 100-fold increase over the humidity range of 11 to 50% whereas the estimated rate constants for spontaneous dehydration ( $k_2$ ) and autocatalytic branching ( $k_1$ ) largely unchanged. These results are consistent with our hypothesis that moisture facilitates the annealing of crystal defects generated by milling and stabilizes the solid-state degradation of gabapentin.

An empirical extended Arrhenius equation (Equation V-4) can be used to estimate the combined effects of temperature and relative humidity on reaction rates. (79, 80)

$$k = Ae^{-E_a/RT} (e^{c \times RH}) \quad \text{Equation V-4}$$

In this equation, k is the reaction rate constant; the frequency factor (A) and activation energy ( $E_a$ ) reflect the effect of temperature; c is the constant for the effect of relative humidity.

### Validation of Model

The ability of the kinetic model to predict drug product stability was demonstrated by comparing the predicted and observed gaba-L levels in representative tablets that had been prepared on conditions of variable manufacturing stress and then stored and analyzed at various temperatures for extended periods of time. In particular the blends used to make representative tablets were prepared under variable unit operations conditions. In particular, blends were prepared using high shear wet granulation operations with different initial water content (4, 5 and 6%), spray rates (12, 15 and 18 g/min) and fluidized bed drying conditions: drying cycle duration (208-2065 sec) at different temperature (19-45 °C). After granulation, post-granular excipient blending was performed at variable speeds (15-25 RPM) and filling ratios (60-80%). Then the blends were compressed into tablets using various compression different forces (4.88 -14.58 kN).

The initial levels of gaba-L and gaba\* (i.e. gaba-L<sub>0</sub> and gaba\*<sub>0</sub>) due to different levels of manufacturing processing stress were estimated either by direct HPLC analysis (gaba-L<sub>0</sub>) or from the initial rate of gaba-L formation (gaba\*<sub>0</sub>) under controlled accelerated conditions (24 hours @ 50 °C and 5% RH at which k<sub>2</sub> was determined to 0.37 day<sup>-1</sup>). These initial conditions and the rate constant estimates based on storage conditions (22, 40 and 50 °C at 11%RH) were used to predict gaba-L levels over a 3 month period. The rate constants were estimated based on Equations V-5, V-6 and V-7.

$$k_1 = 1.48 \times 10^{10} \times \exp(-10707/T) \quad \text{Equation V-5}$$

$$k_2 = 2.40 \times 10^9 \times \exp(-8295/T) \quad \text{Equation V-6}$$

$$k_3 = 2.15 \times 10^6 \times \exp(-8163/T) \times \exp(0.0923 \times \%RH) \quad \text{Equation V-7}$$

The predicted gaba-L values were compared to the measured levels (Figure V-9) The coefficient of determination (R<sup>2</sup>) of 0.95 indicated that the kinetic model appeared to describe drug stability with reasonable accuracy.

### Conclusion

A solid-state degradation model was developed to describe kinetics of gaba-L formation from milled gabapentin. The model connects the physical changes caused by the milling- and environmental-stress to chemical degradation. Specifically the model incorporates autocatalytic branching, spontaneous dehydration, and moisture-induced recovery steps. The model was shown to be robust enough to quantitatively account for the effects of various environmental storage conditions (temperature, relative humidity) on lactamization kinetics. Thus this post-manufacturing drug degradation model can act as a key linkage to establish the relationship between manufacturing variation and chemical stability of gabapentin. Along with compositional variation on lactamization kinetics, this model can be used to construct multidimensional design space models for specific unit operations and to develop risk-based stochastic models to link manufacturing variation with the likelihood of shelf-life failure.

Figure V-1. Typical gaba-L formation time profile from mechanically-stressed gabapentin Form II sample (60 min milled at speed setting 5) stored at 40 °C and 5%RH.

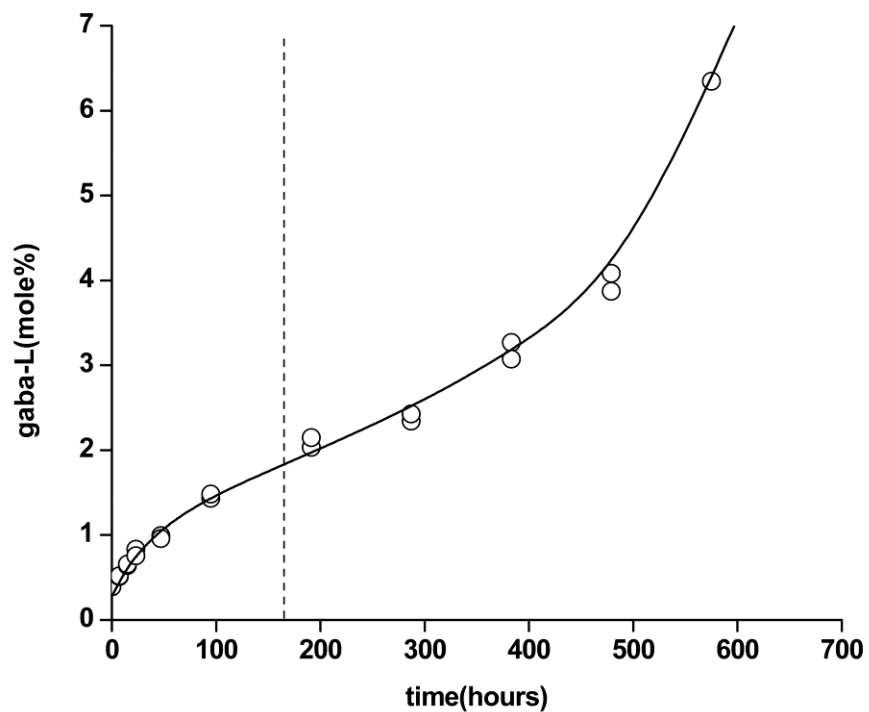




Figure V-2. Proposed solid-state gabapentin degradation model



Figure V-3. Effects of milling duration on gaba-L formation. Thermal stress: 50 °C, 11%RH.  $\diamond$ : unmilled,  $\square$ : 15 minutes milled,  $\Delta$ : 45 minutes milled,  $\circ$ : 60 minutes milled. Lines are predicted using least square estimated parameters based on proposed model.

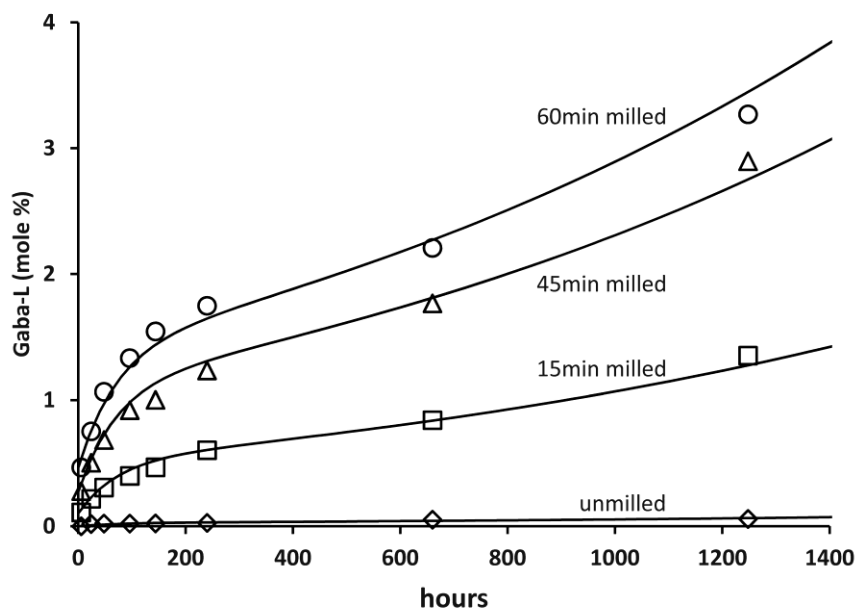


Figure V-4. Gaba-L formation from milled gabapentin samples (60 min at speed setting 5) stored at various relative humidity and 40 °C.  $\diamond$ : 5%RH,  $\square$ : 11%RH,  $\Delta$ : 31%RH,  $\circ$ : 50%RH. Lines are predicted using least square estimated parameters based on proposed model.

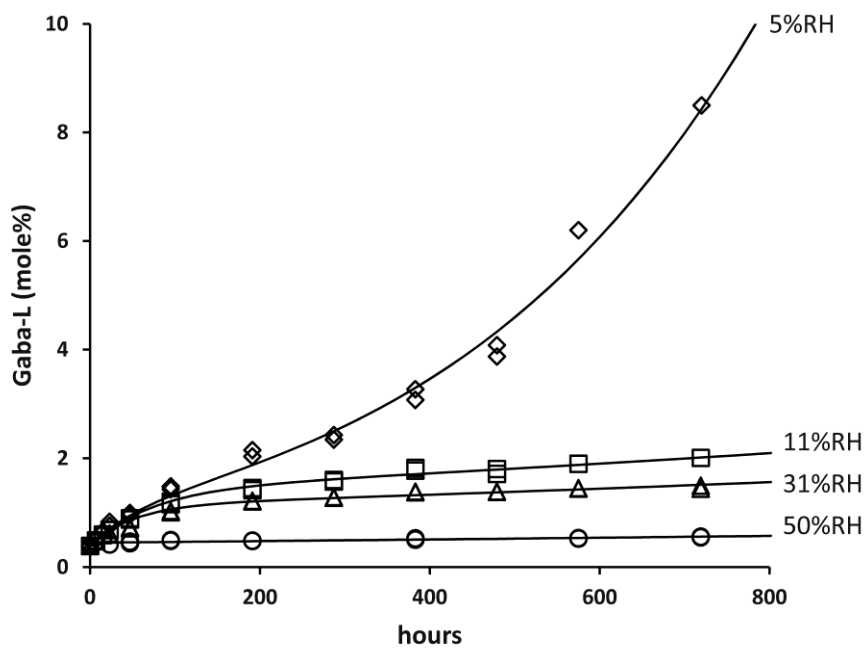


Figure V-5. XRD patterns of milled gabapentin sample (60 min at speed setting 7) stored at 25°C and various RH. (a) 5%RH, (b) 31%RH

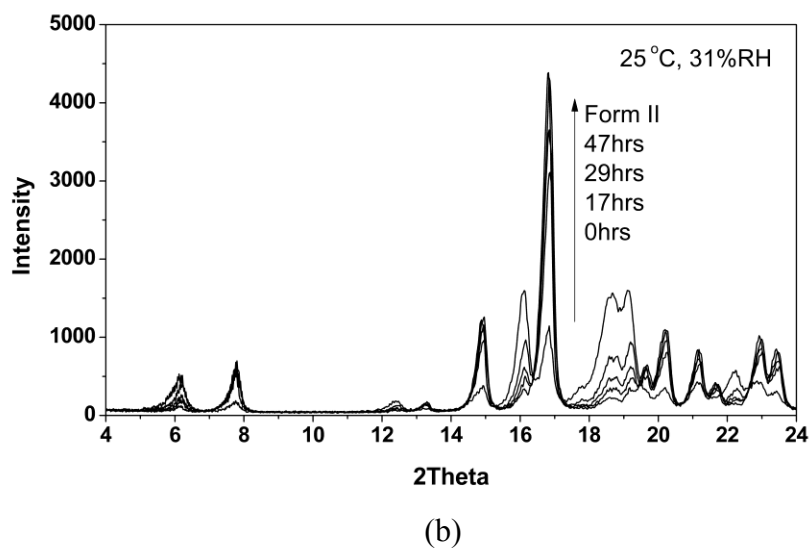
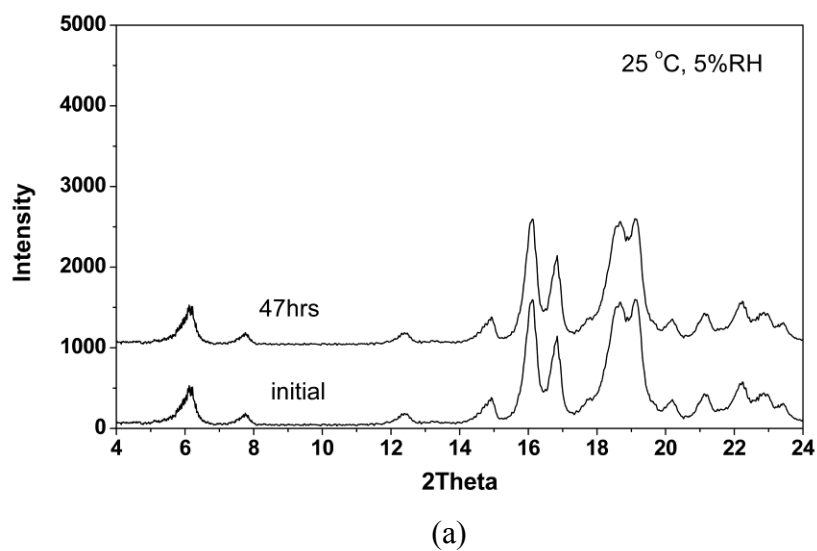


Figure V-6. Gaba-L formation from milled gabapentin samples (60 min at speed setting 5) stored at 5%RH and various temperatures.  $\Delta$ : 60 °C,  $\square$ : 50°C,  $\circ$ : 40°C. Lines are predicted using least square estimated parameters based on proposed model.

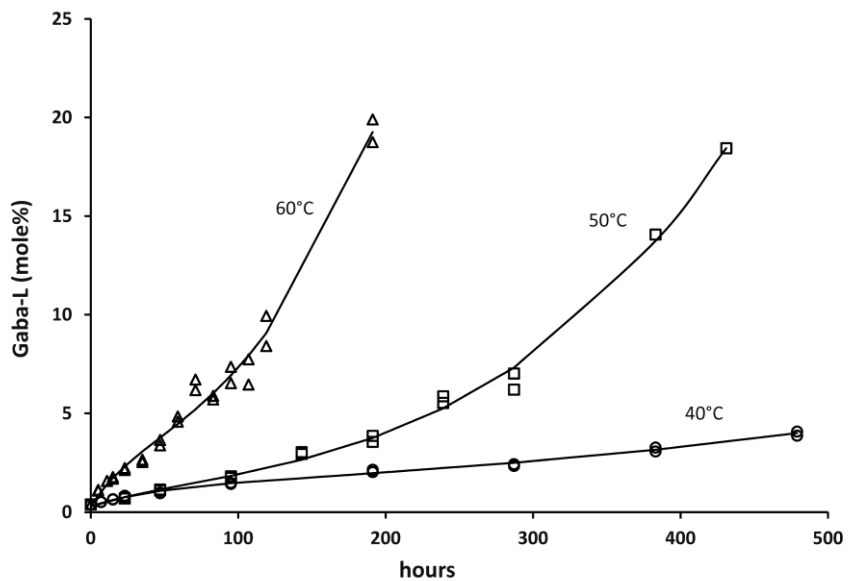


Figure V-7. Gaba-L formation and prediction based on different models. Open circles are observed gaba-L formation from milled gabapentin sample (60 min at speed setting 5) and stressed at 40 °C, 5%RH, lines are predicted data based on different kinetic models.

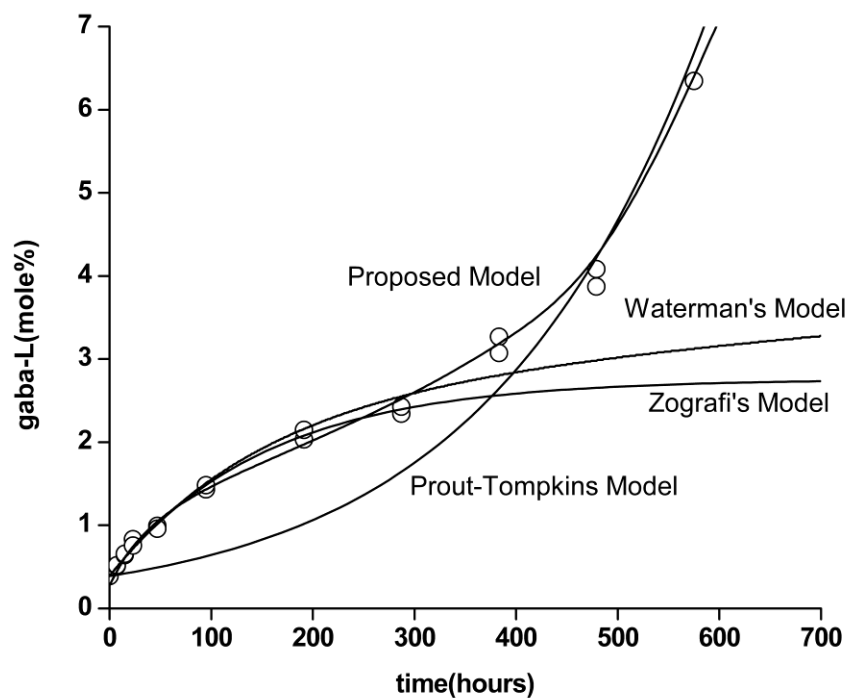


Figure V-8. Arrhenius plots for the estimated rate constants. *Open squares*,  $k_1$  [gaba], *open circles*,  $k_2$

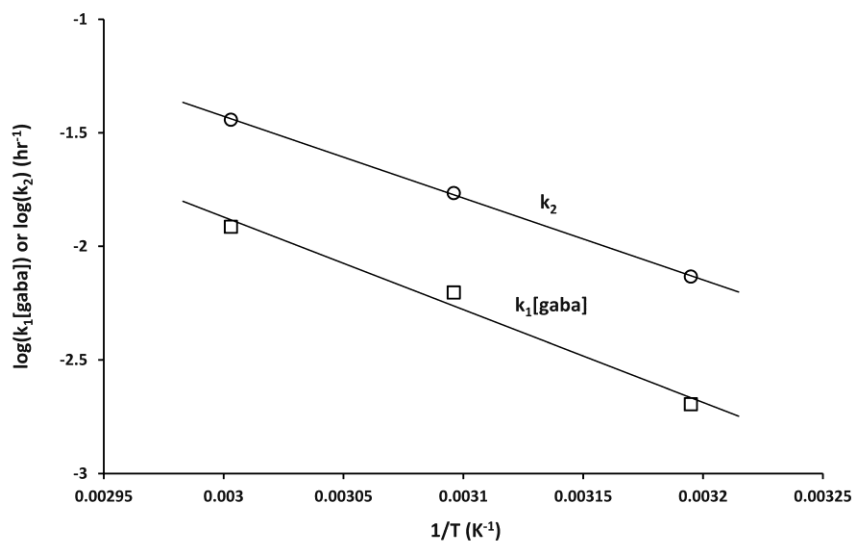
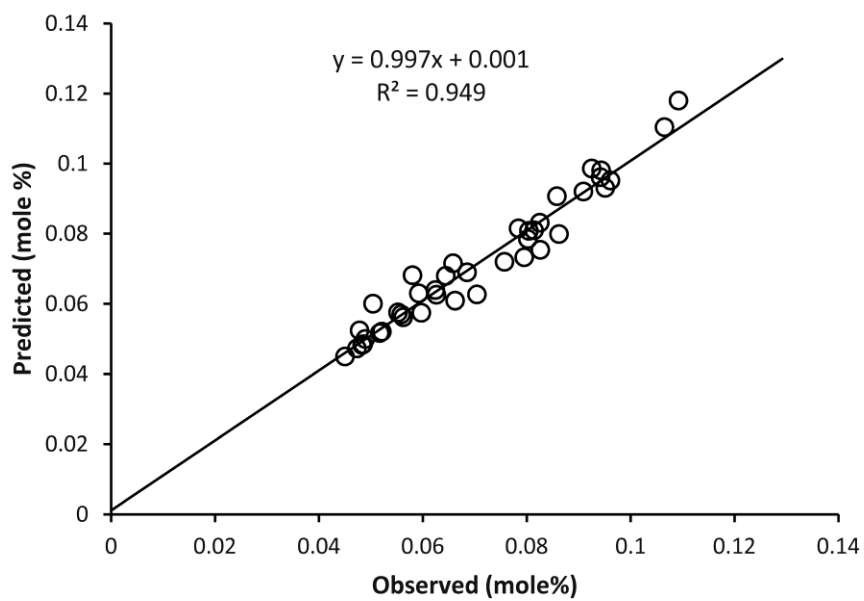


Figure V-9. Observed and predicted long term gaba-L formation from gabapentin tablets.





## APPENDIX A

## WINNONLIN MODEL FOR CHD ACIDIC HYDROLYSIS

MODEL

remark \*\*\*\*\*

remark Developer:

remark Model Date: 01-01-2007

remark Model Version: 1.0

remark \*\*\*\*\*

remark

remark - define model-specific commands

COMMANDS

NFUNCTIONS 6

NDERIVATIVES 8

NPARAMETERS 4

PNames 'kA', 'kD', 'kE', 'C0'

END

remark - define temporary variables

TEMPORARY

END

remark - define differential equations starting values

START

Z(1) = C0

Z(2) = 0

Z(3) = 0

Z(4) = 0

Z(5) = 0

$$Z(6) = 0$$

$$Z(7) = 0$$

$$Z(8) = 0$$

END

remark - define differential equations

DIFFERENTIAL

$$DZ(1) = -2*(kA+kD)*Z(1)$$

$$DZ(2) = 2*kD*Z(1)-(kA+kD+kE)*Z(2)$$

$$DZ(3) = kD*Z(2)-2*kE*Z(3)$$

$$DZ(4) = 2*kA*Z(1)-(kA+kD)*Z(4)$$

$$DZ(5) = kA*Z(3)+kD*Z(4)-kE*Z(5)$$

$$DZ(6) = kE*Z(3)-(kA+kD)*Z(6)$$

$$DZ(7) = 2*kE*Z(3)+kD*Z(6)-kE*Z(7)$$

$$DZ(8) = kA*(2*Z(1)+Z(2)+Z(4)+Z(6))+kE*(2*Z(3)+Z(2)+Z(5)+Z(6))$$

END

remark - define algebraic functions

FUNCTION 1

$$F = Z(1)$$

END

FUNCTION 2

$$F = Z(2)$$

END

FUNCTION 3

$$F = Z(3)$$

END

FUNCTION 4

$$F = Z(4)$$

END

FUNCTION 5

F= Z(5)

END

FUNCTION 6

F= Z(6)

END

remark - define any secondary parameters

remark - end of model

EOM

## APPENDIX B

## WINNONLIN MODEL FOR CHD ALKALINE HYDROLYSIS

MODEL

remark \*\*\*\*\*

remark Developer:

remark Model Date: 01-01-2007

remark Model Version: 1.0

remark \*\*\*\*\*

remark

remark - define model-specific commands

COMMANDS

NFUNCTIONS 4

NDERIVATIVES 4

NPARAMETERS 3

PNames 'kB', 'kF', 'C0'

END

remark - define temporary variables

TEMPORARY

END

remark - define differential equations starting values

START

Z(1) = C0

Z(2) = 0

Z(3) = 0

Z(4) = 0

END

remark - define differential equations

DIFFERENTIAL

$$DZ(1) = -2*kB*Z(1)$$

$$DZ(2) = 2*kB*Z(1)-kB*Z(2)$$

$$DZ(3) = 2*kB*Z(1)+kB*Z(2)-kF*Z(3)$$

$$DZ(4) = kF*Z(3)$$

END

remark - define algebraic functions

FUNCTION 1

$$F= Z(1)$$

END

FUNCTION 2

$$F= Z(2)$$

END

FUNCTION 3

$$F= Z(3)$$

END

FUNCTION 4

$$F= Z(4)$$

END

remark - define any secondary parameters

remark - end of model

EOM

## APPENDIX C

WINNONLIN MODEL USED TO ESTIMATE EFFECT OF MILLING  
ON GABA LACTAMIZATION

Model 1

remark \*\*\*\*\*

remark Developer:

remark Model Date: 2010-10-28

remark Model Version: 1.0

remark \*\*\*\*\*

remark

remark - define model-specific commands

COMMANDS

NFUNCTIONS 4

NDERIVATIVES 12

NPARAMETERS 7

PNAMES 'k1', 'k2', 'k3', 'D10', 'D20', 'D30', 'D40',

END

remark - define temporary variables

TEMPORARY

END

remark - define differential equations starting values

START

Z(1) = 100-D10

Z(2) = D10

Z(3) = 0

Z(4) = 100-D20

$$Z(5) = D20$$

$$Z(6) = 0$$

$$Z(7) = 100-D30$$

$$Z(8) = D30$$

$$Z(9) = 0$$

$$Z(10) = 100-D40$$

$$Z(11) = D40$$

$$Z(12) = 0$$

END

remark - define differential equations

DIFFERENTIAL

$$DZ(1) = -k1*Z(1)*(Z(2)+Z(3))+k3*Z(1)*Z(2)$$

$$DZ(2) = k1*Z(1)*(Z(2)+Z(3))-k2*Z(2)-k3*Z(1)*Z(2)$$

$$DZ(3) = k2*Z(2)$$

$$DZ(4) = -k1*Z(4)*(Z(5)+Z(6))+k3*Z(4)*Z(5)$$

$$DZ(5) = k1*Z(4)*(Z(5)+Z(6))-k2*Z(5)-k3*Z(4)*Z(5)$$

$$DZ(6) = k2*Z(5)$$

$$DZ(7) = -k1*Z(7)*(Z(8)+Z(9))+k3*Z(7)*Z(9)$$

$$DZ(8) = k1*Z(7)*(Z(8)+Z(9))-k2*Z(8)-k3*Z(7)*Z(8)$$

$$DZ(9) = k2*Z(8)$$

$$DZ(10) = -k1*Z(10)*(Z(11)+Z(12))+k3*Z(10)*Z(11)$$

$$DZ(11) = k1*Z(10)*(Z(11)+Z(12))-k2*Z(11)-k3*Z(10)*Z(11)$$

$$DZ(12) = k2*Z(11)$$

END

remark - define algebraic functions

FUNCTION 1

$$F = Z(3)$$

END

FUNCTION 2

F= Z(6)

END

FUNCTION 3

F= Z(9)

END

FUNCTION 4

F= Z(12)

END

remark - define any secondary parameters

remark - end of model

EOM



## REFERENCES

1. International Conference on Harmonisation of Technical Requirements for Registration of Pharmaceuticals for Human Use 2003. Stability Testing of New Drug Substances and Products. ICH Harmonised Tripartite Guideline Q1A(R2).
2. U.S. Food and Drug Administration 2000. Analytical Procedures and Methods Validation, Chemistry, Manufacturing, and Controls Documentation. FDA Draft Guidance.
3. International Conference on Harmonisation of Technical Requirements for Registration of Pharmaceuticals for Human Use 2005. Pharmaceutical Development. ICH Harmonised Tripartite Guideline Q8.
4. Charles AM, Callender M, Grosvenor T 1973. Efficacy of chemical asepticizing system for soft contact lenses. American journal of optometry and archives of American Academy of Optometry 50(10):777-781.
5. Denton GW. 2001. Chlorhexidine. In Block SS, editor Disinfection, Sterilization, and Preservation, 5th ed., Philadelphia, PA: Lippincott Williams & Wilkins. p 321-336.
6. Chhabra RS, Thompson M, Elwell MR, Gerken DK 1990. Toxicity of p-chloroaniline in rats and mice. Food Chem Toxicol 28(10):717-722.
7. Chhabra RS, Huff JE, Haseman JK, Elwell MR, Peters AC 1991. Carcinogenicity of p-chloroaniline in rats and mice. Food Chem Toxicol 29(2):119-124.
8. National Institutes of Health, 1979. Bioassay of 5-chloro-o-toluidine for possible carcinogenicity. National Cancer Institute Technical Report Series No 189.
9. World Health Organization, 2003. 4-Chloroaniline. Concise international chemical assessment document 48.
10. United State Pharmacopeial Convention, 2011. Chlorhexidine gluconate oral rinse. USP34: 2296-2297.
11. Dolby J, Gunnarsson B, Kronberg L, Wikner H 1972. Stability of chlorhexidine when autoclaving. Pharm Acta Helv 47(10):615-620.
12. Franck M, Schmidt PC 1993. Degradation of chlorhexidine in antacid suspensions - a novel approach to describe degradation kinetics. Eur J Pharm Biopharm 39(1):19-24.
13. Elpern B 1968. Chemistry of the biguanides. Ann N Y Acad Sci 148(3):577-586.
14. Ha Y, Cheung AP 1996. New stability-indicating high performance liquid chromatography assay and proposed hydrolytic pathways of chlorhexidine. J Pharm Biomed Anal 14(8-10):1327-1334.
15. Revelle LK, Doub WH, Wilson RT, Harris MH, Rutter AM 1993. Identification and isolation of chlorhexidine digluconate impurities. Pharm Res 10(12):1777-1784.

16. Szczepanik B, Latowski T 1997. The photoreactivity of p-chloroaniline. *Pol J Chem* 71(6):807-815.
17. Joshi AB, Kirsch LE 2004. The estimation of glutaminy deamidation and aspartyl cleavage rates in glucagon. *Int J Pharm* 273(1-2):213-219.
18. Notari RE, DeYoung JL 1975. Kinetics and mechanisms of degradation of the antileukemic agent 5-azacytidine in aqueous solutions. *J Pharm Sci* 64(7):1148-1157.
19. Clement B, Girreser U 1999. Characterization of biguanides by <sup>15</sup>N NMR spectroscopy. *Magn Reson Chem* 37(9):662-666.
20. Davies A 1973. The mode of action of chlorhexidine. *J Periodontal Res Suppl* 12:68-75.
21. Hjeljord LG, Rolla G, Bonesvoll P 1973. Chlorhexidine-protein interactions. *J Periodontal Res Suppl* 12:11-16.
22. Rolla G, Melsen B 1975. On the mechanism of the plaque inhibition by chlorhexidine. *J Dent Res* 54 Spec No B:B57-62.
23. Hauman CH, Love RM 2003. Biocompatibility of dental materials used in contemporary endodontic therapy: a review. Part 1. Intracanal drugs and substances. *Int Endod J* 36(2):75-85.
24. Denton GW. 2001. Chlorhexidine. In Block SS, editor *Disinfection, Sterilization, and Preservation*, 5th ed., Philadelphia, PA: Lippincott Williams & Wilkins. p 321-336.
25. Weinberg ED 1968. Antimicrobial activities of biguanides. *Ann N Y Acad Sci* 148(3):587-600.
26. Milstone AM, Passaretti CL, Perl TM 2008. Chlorhexidine: expanding the armamentarium for infection control and prevention. *Clin Infect Dis* 46(2):274-281.
27. McDonnell G, Russell AD 1999. Antiseptics and disinfectants: activity, action, and resistance. *Clin Microbiol Rev* 12(1):147-179.
28. Krithikadatta J, Indira R, Dorothykalyani AL 2007. Disinfection of dentinal tubules with 2% chlorhexidine, 2% metronidazole, bioactive glass when compared with calcium hydroxide as intracanal medicaments. *J Endod* 33(12):1473-1476.
29. Gomes BP, Souza SF, Ferraz CC, Teixeira FB, Zaia AA, Valdrighi L, Souza-Filho FJ 2003. Effectiveness of 2% chlorhexidine gel and calcium hydroxide against *Enterococcus faecalis* in bovine root dentine in vitro. *Int Endod J* 36(4):267-275.
30. Leonardo MR, Tanomaru Filho M, Silva LA, Nelson Filho P, Bonifacio KC, Ito IY 1999. In vivo antimicrobial activity of 2% chlorhexidine used as a root canal irrigating solution. *J Endod* 25(3):167-171.
31. Timmons SR, Harless JD, Hogan MM, Eckert GJ, Marek CL, Drake DR, Wefel JS 2007. Effect of an alcohol-free, 1% chlorhexidine gel as an adjunct to a fluoridated dentifrice using an intraoral crown model. *Caries Res* 41(3):190-197.

32. World Health Organization, 2003. 4-chloroaniline. Concise international chemical assessment document 48.
33. United State Pharmacopeial Convention, 2011. Chlorhexidine gluconate oral rinse. USP 34: 2296-2297.
34. Ibers JA 2001. Gabapentin and gabapentin monohydrate. Acta Crystallographica Section C Crystal Structure Communications 57(Pt 5):641-643.
35. Pesachovich M, Singer C, Pilarski G, inventors; Teva Pharmaceutical Industries Ltd., Israel; Teva Pharmaceuticals USA, Inc., assignee. Preparation of gabapentin. World patent 98/28255. 1998 July 2.
36. Reece HA, Levendis DC 2008. Polymorphs of gabapentin. Acta Crystallographica Section C Crystal Structure Communications 64(Pt 3):o105-108.
37. Hsu CH, Ke WT, Lin SY 2010. Progressive steps of polymorphic transformation of gabapentin polymorphs studied by hot-stage FTIR microspectroscopy. Journal of Pharmacy and Pharmaceutical Sciences 13(1):67-77.
38. Kearney AS, Mehta SC, Radebaugh GW 1992. The effect of cyclodextrins on the rate of intramolecular lactamization of gabapentin in aqueous solution. International Journal of Pharmaceutics 78(1):25-34.
39. Brago D, Grepioni F, Maini L, Brescello R, Cotarca L, Duarte MT, Andre V, Piedade MFM 2008. Polymorphic gabapentin thermal behavior, reactivity and interconversion of form in solution and solid-state. New Journal of Chemistry 32:1788-1795.
40. Lin SY, Hsu CH, Ke WT 2010. Solid-state transformation of different gabapentin polymorphs upon milling and co-milling. International Journal of Pharmaceutics 396(1-2):83-90.
41. Zambon E, Giovanetti R, Cotarca L, Pasquato L 2008. Mechanistic investigation on 2-aza-spiro[4,5]decan-3-one formation from 1-(aminomethyl)cyclohexylacetic acid (gabapentin). Tetrahedron 64(28):6739-6743.
42. Zour E, Lodhi SA, Nesbitt RU, Silbering SB, Chaturvedi PR 1992. Stability studies of gabapentin in aqueous solutions. Pharmaceutical Research 9(5):595-600.
43. Cutrignelli A, Denora N, Lopedota A, Trapani A, Laquintana V, Latrofa A, Trapani G, Liso G 2007. Comparative effects of some hydrophilic excipients on the rate of gabapentin and baclofen lactamization in lyophilized formulations. International Journal of Pharmaceutics 332(1-2):98-106.
44. Augart H, Gebhardt U, inventors; Godecke Aktiengesellschaft, Berlin, Germany, assignee. Lactam-Free Amino Acids. United States patent 6054482. 2000 Apr 25.
45. Chawla M, Raghuvanshi RS, Rampal A, inventors; Ranbaxy Laboratories Limited, India, assignee. Stable sustained-release oral dosage forms of gabapentin and process for their preparation. World patent 2005/077332. 2005 Aug 25.
46. Chawla M, Raghuvanshi RS, Rampal A, inventors; Ranbaxy Laboratories Limited, India, assignee. Sustained release tablets of gabapentin. World patent 2005020978. 2005 Mar 10..

47. Lloret Perez S, inventor Combino Pharm, S.L., Spain, assignee. Solid pharmaceutical composition of gabapentin of good stability and bioavailability. World patent 2007128495. 2007 Nov 15.
48. Manikandan R, Gogia A, Roy SB, Malik R, inventors; Ranbaxy Laboratories Limited, India, assignee. Gabapentin tablets and methods for their preparation. World patent 2004/032905. 2004 Apr 22.
49. Sherman BC, inventor Sherman, Bernard Charles, assignee. Solid pharmaceuticals comprising gabapentin having improved stability. World patent 2004/014356. 2004 Feb 19.
50. Singer C, Pilarski G, Pesachovich M, inventors; Teva Pharmaceutical Industries Ltd., Israel; Teva Pharmaceuticals USA, Inc., assignee. Stable gabapentin containing more than 20 ppm of chloride. World patent 2001/097612. 2001 Dec 27.
51. Yande V, Kulkarni S, Narasimharaghavan S, Meenakshisunderam S, inventors; Aurobindo Pharma Limited, India, assignee. Stable liquid formulations of antiepileptic agents. World patent 2007/107835. 2007 Sep 27.
52. Gupta A, Ciavarella AB, Sayeed VA, Khan MA, Faustino PJ 2008. Development and application of a validated HPLC method for the analysis of dissolution samples of gabapentin drug products. *Journal of Pharmaceutical and Biomedical Analysis* 46(1):181-186.
53. Volpe DA, Gupta A, Ciavarella AB, Faustino PJ, Sayeed VA, Khan MA 2008. Comparison of the stability of split and intact gabapentin tablets. *International Journal of Pharmaceutics* 350(1-2):65-69.
54. Inman EL, Tenbarger HJ 1988. High-low chromatography: estimating imprecision in HPLC using a pair of sample injections. *J Chromatogr Sci* 26:89-94.
55. Bryans JS, Morrell AI, inventors; Warner-Lambert Company, USA, assignee. Novel stereoselective processes for the preparation of gabapentin analogs. World patent 1999/14184. 1999 Mar 25.
56. Geibel W, Hartenstein J, Herrmann W, Witzke J, inventors; Goedecke A.-G., Germany, assignee. Process for the preparation of 1-aminomethyl-1-cyclohexaneacetic acid. European patent 414274. 1991 Feb 27.
57. Steiner K, Herrmann W, Crone G, Combs CS, inventors; Godecke Aktiengesellschaft, Berlin, Germany, assignee. Process For the Preparation of Cyclic Amino Acids and Intermediates Useful in the Process. United States patent 5068413. 1991 Nov 26.
58. Zong Z, Desai SD, Kaushal AM, Barich DH, Huang HS, Munson EJ, Suryanarayanan R, Kirsch LE 2011. The stabilizing effect of moisture on the solid-state degradation of gabapentin. *AAPS PharmSciTech* 12(3):924-931.
59. Augart H, Gebhardt U, Herrmann W. 2000. Lactam-free amino acids, US 6054482.
60. Coetzee JF, Mosher RA, Kohake LE, Cull CA, Kelly LL, Mueting SL, Kukanich B 2011. Pharmacokinetics of oral gabapentin alone or co-administered with meloxicam in ruminant beef calves. *Vet J* 190(1):98-102.

61. United State Pharmacopeia, 2007. Gabapentin. USP30-NF25.
62. Ibers JA 2001. Gabapentin and gabapentin monohydrate. *Acta Crystallogr C* 57(Pt 5):641-643.
63. Reece HA, Levendis DC 2008. Polymorphs of gabapentin. *Acta Crystallogr C* 64(Pt 3):o105-108.
64. Braga D, Grepioni F, Maini L, Rubini K, Polito M, Brescello R, Cotarca L, Duarte MT, Andre V, Piedade MFM 2008. Polymorphic gabapentin: thermal behaviour, reactivity and interconversion of forms in solution and solid-state. *New J Chem* 32(10):1788-1795.
65. Hsu CH, Ke WT, Lin SY 2010. Progressive steps of polymorphic transformation of gabapentin polymorphs studied by hot-stage FTIR microspectroscopy. *J Pharm Pharm Sci* 13(1):67-77.
66. Lin SY, Hsu CH, Ke WT 2010. Solid-state transformation of different gabapentin polymorphs upon milling and co-milling. *Int J Pharm* 396(1-2):83-90.
67. Prout EG, Tompkins FC 1944. Thermal decomposition of KMnO<sub>4</sub>. *Trans Faraday Soc* 40:488-498.
68. Jacobs PWM 1997. Formation and Growth of Nuclei and the Growth of Interfaces in the Chemical Decomposition of Solids: New Insights. *J Phys Chem B* 101(48):10086-10093.
69. Skrdla PJ 2004. Use of Coupled Rate Equations To Describe Nucleation-and-Branching Rate-Limited Solid-State Processes. *J Phys Chem A* 108(32):6709-6712.
70. Skwierczynski RD 1999. Disorder, molecular mobility, and solid-state kinetics: the two-environment model. *J Pharm Sci* 88(11):1234-1236.
71. Shalaev EY, Shalaeva M, Byrn SR, Zograf G 1997. Effects of processing on the solid-state methyl transfer of tetraglycine methyl ester. *Int J Pharm* 152(1):75-88.
72. Waterman KC, Carella AJ, Gumkowski MJ, Lukulay P, MacDonald BC, Roy MC, Shamblin SL 2007. Improved protocol and data analysis for accelerated shelf-life estimation of solid dosage forms. *Pharm Res* 24(4):780-790.
73. Brittain HG 2002. Effects of mechanical processing on phase composition. *J Pharm Sci* 91(7):1573-1580.
74. Brittain HG, Fiese EF 1999. Effects of pharmaceutical processing on drug polymorphs and solvates. *Drugs Pharm Sci* 95(Polymorphism in Pharmaceutical Solids):331-361.
75. Huettnerrauch R, Fricke S, Zielke P 1985. Mechanical activation of pharmaceutical systems. *Pharm Res* (6):302-306.
76. Leung SS, Grant DJ 1997. Solid state stability studies of model dipeptides: aspartame and aspartylphenylalanine. *J Pharm Sci* 86(1):64-71.

77. Wang SL, Lin SY, Chen TF 2001. Reaction kinetics of solid-state cyclization of enalapril maleate investigated by isothermal FT-IR microscopic system. *Chem Pharm Bull* 49(4):402-406.
78. Widjaja E, Tan WJ 2008. Kinetics of lisinopril intramolecular cyclization in solid phase monitored by Fourier transform infrared microscopy. *Appl Spectrosc* 62(8):889-894.
79. Genton D, Kesselring UW 1977. Effect of temperature and relative humidity on nitrazepam stability in solid state. *J Pharm Sci* 66(5):676-680.
80. Yoshioka S, Stella VJ. 2002. *Stability of Drugs and Dosage Forms*. Kluwer Academic Publishers, p 108-113.